Radiological Protection of the Public from Radioactive Particles

Corynne McGuire

January 2023

A thesis submitted for the degree

of Doctor of Philosophy

Declaration of Authorship

I hereby confirm that this PhD thesis is an original piece of work conducted independently by the undersigned, all work contained herein has not been submitted for any other degree, and all relevant literature has been duly acknowledged and cited.

Signed: Corynne McGuire

Date: 25th January 2023

Acknowledgements

Firstly, I would like to thank my supervisors Professor Andrew Tyler, Professor David Copplestone, and Dr Paul Dale. A part-time PhD is a lengthy commitment and I greatly appreciate you all sticking with me and for your encouragement and advice along the way. Special thanks go to Paul who initiated this research project and secured funding from the Scottish Environment Protection Agency (SEPA), and to Andrew for securing funding from the University of Stirling and agreeing for me to undertake my research part-time. And when my funding was all but spent, special thanks go to David for providing a bit extra to fund some additional analysis. I couldn't have hoped for a better supervisory team.

Throughout my research, the support I received from across the department was excellent. Special thanks go to Stuart Bradley for keeping me right in using the gamma spectrometers and the numerous laughs; George Macleod for help with using the optical macroscope and SEM-EDS, and his patience when the SEM filament needed changing (again!); Adam Varley for his indispensable wizardry with R; Ronnie Balfour for always being able to source the right resources no matter how obscure; James Weir for his valuable skills and always having the right materials and tools in his workshop for making bespoke items; Ian Washbourne for his expertise in the ICP-OES; and Pauline Blaikie for allowing me to borrow equipment from the teaching laboratories, without which my experiments would have been difficult (or expensive!).

Lastly, thanks to everyone named here and many others for always being available for giving advice, a general chat, or just a cup of tea; everything that everyone has done to help me get to the end of my PhD has been invaluable and greatly appreciated.

General Abstract

Radioactive particles are physically discrete sources of radioactivity that have been released into the environment as result of past accidents, incidents, and practices, and can present a hazard to members of the public by inadvertent contact with the skin and inadvertent ingestion. The historical use of radium in the luminising of aircraft components, and the subsequent decommissioning of those aircraft and associated waste disposal practices, has left a legacy of contamination, such as the radioactive particles containing Ra-226 at Dalgety Bay, Scotland. The overall aim of this thesis was to advance the current understanding of the characteristics of Ra-226 particles found in the environment and improve the assessment of radiation doses via inadvertent skin contact and inadvertent ingestion by members of the public.

Ra-226 particles were physically, chemically, and radiologically characterised using optical macroscopy, scanning election microscopy with energy dispersive X-ray spectroscopy, and gamma spectrometry. Particle characteristics showed wide variation for physical appearance, size, shape, mass, density, chemical composition, and radioactivity. The absorbed dose rate from inadvertent skin contact with Ra-226 particles was assessed using Radiochromic Film (RCF) dosimetry for different skin thicknesses and averaging areas. It was found that the ICRP reference 70 µm skin thickness and nominal 1 cm^2 skin averaging area are not appropriate for the assessment of Ra-226 particles. The committed effective dose from inadvertent ingestion of Ra-226 particles was assessed using the BARGE Unified Bioaccessibility Method. It was found that the nominal ICRP f_1 gastrointestinal absorption values are not appropriate for the assessment of committed effective dose from Ra-226 particles due to the wide range of bioaccessibility exhibited by the particles.

The research presented in this thesis characterised and assessed the greatest number of Ra-226 particles of any study and has found that many standard assumptions used in radiological protection may not be appropriate for Ra-226 particles. The diversity of Ra-226 particle characteristics and the wide range of potential radiation doses highlights the need for site-specific characterisation and assessment studies. The recommendations from this thesis will provide a valuable input into future studies, helping to improve the radiological protection of the public from radioactive particles.

Contents

Chapter 1

General Introduction

1 General Introduction

Since discovery in 1896, radioactive substances have found uses in energy generation, medical diagnostics and treatment, military applications, scientific research, and many industrial applications from food sterilisation to well-logging in oil and gas exploration. However, the historical use of radioactivity was not managed to the same standards that are in place today and in some cases has left a legacy of radioactive contamination in the environment. Such legacies require characterisation and assessment, followed by remediation where necessary, for the radiological protection of the public and the environment in line with contemporary standards.

1.1 Radioactive Particles: An Environmental Legacy

Part of the legacy contamination in the environment from past uses of radioactivity is in the form of radioactive particles. But what are radioactive particles? What are the sources of radioactive particles in the environment? And why are radioactive particles a problem?

1.1.1 What are radioactive particles?

Radioactive particles, also referred to as hot particles, are not universally defined, and there are several different definitions in use, such as:

- The International Atomic Energy Agency (IAEA) – *"Radioactive particles are a localised aggregation of radioactive atoms that give rise to an inhomogeneous distribution of radionuclides significantly different from that of the matrix background."* (IAEA, 2011).

- The International Commission on Radiological Protection (ICRP) – *"Hot particle exposures are spatially non-uniform exposures from discrete radioactive sources with dimensions of less than or about 1 mm."* (ICRP, 1992)

- The US Department of Energy (US DoE) – *"Hot particles are small, discrete, highly radioactive particles that can cause extremely high dose rates to a localised area."* (US DoE, 2011)

- The US National Council on Radiation Protection and Measurements (NCRP) – *"Hot particles are considered to be > 10 µm but < 3,000 µm in any dimension. Hot particles smaller than 10 µm may be treated as general contamination; exposures to hot particles larger than 3,000 µm do not exhibit the particular biological response characteristic of exposure from the smaller particles."* (NCRP, 1999)

- The US Nuclear Regulatory Commission (NRC) – *"Hot particle means a discrete radioactive fragment that is insoluble in water and is less than 1 mm in any dimension."* (US NRC, 1990)

The different definitions in use refer to different features of radioactive particles, which does not facilitate a common understanding of radioactive particles or allow for a consistent approach to radiological protection. The IAEA definition focuses on inhomogeneity from surrounding matter on the scale of atoms, the ICRP, US NCRP, and US NRC definitions focus on physical size much larger than the scale of atoms but specify different sizes, and the US DoE focuses on hazard but does not give an indication of what constitutes an extremely high dose rate. However, a common theme is that radioactive particles are discrete so in the absence of consensus and for the purposes of this thesis, radioactive particles are physically discrete sources of radioactivity that may be capable of delivering radiation doses to the public relevant to radiological protection.

1.1.2 What are the sources of radioactive particles in the environment?

Nuclear power reactor accidents have been a source of radioactive particles, such as the Chernobyl Nuclear Power Plant accident in 1986, that released about three tons of irradiated nuclear fuel particles into the atmosphere (Kashparov *et al.*, 2019). The Fukushima Daiichi Nuclear Power Plant accident in 2011 also released radioactive particles into the environment in the form of caesium-bearing micro-particles (Futagami *et al.*, 2020). Nuclear fuel reprocessing sites, such Dounreay in Scotland and Sellafield in England, have released a number of different radioactive particles into the local environment around these sites (Harrison *et al.*, 2005; Brown and Etherington, 2011).

Nuclear weapons testing carried out principally by the USA, USSR, UK, France, and China, and to a much lesser extent by India, Pakistan, and North Korea, has released radioactive particles into the environment. Tests were conducted in the atmosphere, underground, and underwater, the majority of which were atmospheric tests carried out between 1951 and 1980 (Prăvălie, 2014). Two accidents involving nuclear weapons have occurred where the aircraft carrying the weapons crashed, dispersing radioactive particles containing plutonium and uranium. The first of these happened in 1966 in Palomares, Spain followed by Thule, Greenland in 1968 (Lind *et al.*, 2007). Due to its high density, depleted uranium (DU) is used in military applications as ammunition and armour plating on military vehicles. Its use has resulted in the release of DU particles into the environment in areas that have experienced conflict using DU ammunition and

armour as well as on military land used for DU ammunition and armour testing (Handley-Sidhu *et al.*, 2010; Lind, Tschiersch and Salbu, 2020).

1.1.3 Why are radioactive particles a problem?

Radioactive particles are a problem as they can be capable of delivering radiation doses to the public relevant to radiological protection through skin contact, ingestion, and inhalation. The most extensive evaluations of public exposure pathways and the hazards from radioactive particles have been reported for the nuclear processing sites at Dounreay and Sellafield. The risk assessment for the Dounreay radioactive particles assessed the potential radiation doses from skin contact, ingestion, and inhalation. The Dounreay particles were found to be too large to enter the lung and would be deposited in the extrathoracic airways. The principal concern from Dounreay particles is the possibility of localised ulceration of the skin, the mucosal lining of the colon, and the extrathoracic airways (Harrison *et al.*, 2005). The risk assessment for Sellafield radioactive particles also assessed the potential radiation doses from skin contact, ingestion, and inhalation, but found that the principal concern was from the ingestion of alpha-rich particles dominated by Am-241 and the absorption of the radioactivity into circulation in the body (Brown and Etherington, 2011). The different pathways for public exposure and the potential for some to be more radiologically significant than others, highlights the need to characterise and assess the hazard from radioactive particles for the radiological protection of the public.

1.2 The System of Radiological Protection

Following the discovery of radioactivity, the expansion of its use, and the subsequent realisation of its hazards, the International X-ray and Radium Protection Committee (IXRPC) was formed, which issued its first recommendations on protection against X-rays and radium in 1928 (IXPRC, 1928). The IXRPC is now known as the International Commission on Radiological Protection (ICRP), and its 1928 recommendations have evolved significantly through several revisions into the current System of Radiological Protection as published in the 2007 Recommendations of the ICRP (ICRP, 2007), as well as a catalogue of supplementary guidance documents.

The Recommendations of the ICRP form the basis of national radiological protection frameworks in most countries worldwide. The IAEA incorporates the Recommendations of the ICRP into its Safety Standards (IAEA, 2014), which in turn are incorporated into the legislative and regulatory frameworks of the IAEA Member States. The European Union incorporates the Recommendations of the ICRP into legally binding Directives

(EU, 2013), which in turn impose a legal obligation for transposition into the legislative and regulatory frameworks of the EU Member States. A notable exception is the United States, which has its own National Council on Radiation Protection and Measurements (NCRP) that publishes its own recommendations and guidance (NCRP, 1999).

1.2.1 The Aim & Scope of the ICRP Recommendations

The aim of the system of radiological protection is to provide an appropriate level of protection for people and the environment against the detrimental effects of exposure to ionising radiation without unduly limiting its beneficial uses. Detrimental effects of radiation exposure can be deterministic where the effects only occur if the radiation dose exceeds a threshold, or they can be stochastic where the effects can occur at any radiation dose. Deterministic effects include harmful tissue reactions such as physical injury to the skin, whereas stochastic effects include cancer and heritable effects. One of the objectives of the system of protection is to control exposures to ionising radiation so that deterministic effects are prevented, and the risks of stochastic effects are reduced to as low as reasonably achievable (ICRP, 2007).

The system of radiological protection applies to all types of exposures to ionising radiation whether that be the occupational exposure of workers, medical exposure of patients, exposure of members of the public, or exposure of the environment. It applies to all circumstances where exposure to ionising radiation may occur, whether that be exposure during a planned use of ionising radiation, exposure when dealing with an emergency, or exposure from a source that already exists. Respectively, these are referred to as planned, emergency, and existing exposure situations. As legacy contamination by its nature already exists, it is commonly treated as an existing exposure situation (ICRP, 2007).

1.2.2 Radiological Protection of the Public in Existing Exposure Situations

Existing exposure situations include exposures due to past accidents, incidents, and practices as well as naturally occurring exposures that already exist when decisions on radiological protection must be taken. The level of radiological protection in existing exposure situations is defined by the reference level, which is the level of dose or risk, above which it is judged to be inappropriate to allow exposures to occur, and below which optimisation of protection should be implemented. The reference level is not prescribed by the ICRP but should be set by national regulatory authorities considering the prevailing circumstances of the existing exposure situation under consideration (ICRP, 2007). In deriving the reference level for a particular existing exposure situation, the

national regulatory authority needs to gather data on the characteristics of the contamination and assess the potential radiation doses to the public.

1.2.3 Assessment of Radiation Dose

For the assessment of radiation dose, the ICRP publishes standard approaches for common public exposure pathways. For example, the ICRP recommends assessing radiation doses to the skin using a reference skin thickness of 70 µm and a nominal skin averaging area of 1 cm^2, regardless of the actual area exposed (ICRP, 2007). For assessing ingestion dose, the ICRP maintains a set of ingestion dose coefficients that describe how many sieverts would be received per becquerel of a given radionuclide. The dose coefficients incorporate a fractional absorption (f_1) value, which takes into account the fraction of an ingested radionuclide that is released from the ingested material into the gastrointestinal fluids (i.e., the fraction that is bioaccessible) and absorbed across the gastrointestinal wall into systemic circulation (i.e., the fraction that is bioavailable) (ICRP, 1995, 2012). However, radioactive particles are not common public exposures, and these standard approaches may not necessarily applicable, as exemplified by the historical use of radium in past military applications and the existing exposure situation at Dalgety Bay, Scotland.

1.3 Radium Contamination from Past Military Applications

A lesser studied source of radioactive particles is the historical use of radium-226 in military applications. Ra-226 was formerly used to luminise aircraft components such as dials, gauges, and switches in the cockpits of military aircraft so that they would glow in the dark for the pilots to read them at night. The subsequent decommissioning of those aircraft and associated waste disposal practices has left a legacy of contamination on former military sites. One such site is Dalgety Bay in Scotland (Dale, 2013).

1.3.1 Ra-226 and its daughter radionuclides

Ra-226 is a long-lived radionuclide with a physical half-life of 1,600 years that decays via a chain of daughter radionuclides to end as Pb-208, which is stable. Ra-226 itself is a daughter radionuclide as part of a longer radioactive decay chain starting with U-238, but as the Ra-226 was chemically isolated for use in its historical military applications, its parent radionuclides are not present in the subsequent legacy contamination. Figure 1.1 shows the Ra-226 decay chain, which consists of nine different radionuclides of five different elements that decay by either alpha or beta emission, with physical half-lives ranging from microseconds to years. Additionally, Ra-226, Pb-214, Bi-214, and Pb-210 decays are accompanied by the emission of significant gamma photons.

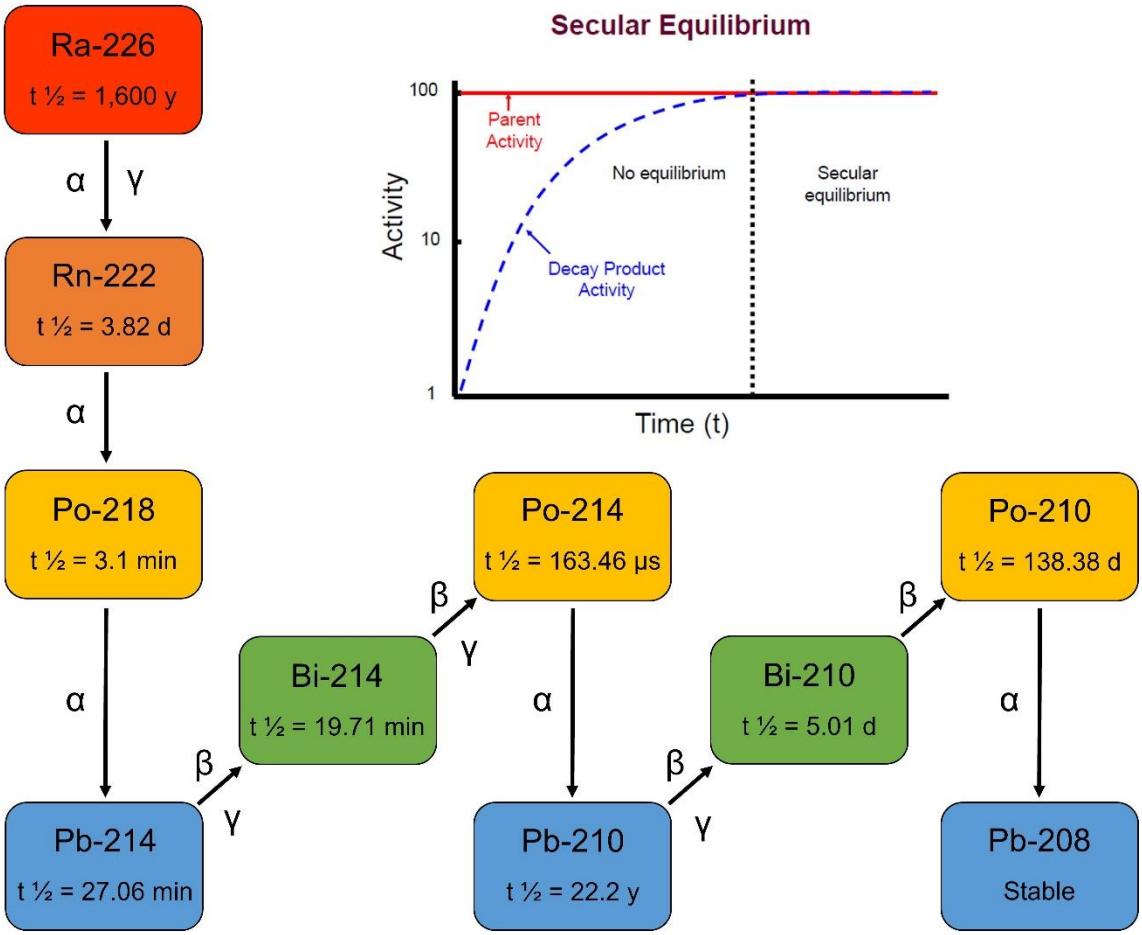

Figure 1.1 The Ra-226 decay chain and secular equilibrium

Due to the long half-life of Ra-226 and the comparatively shorter half-lives of the daughter radionuclides, the Ra-226 decay chain can reach a point where secular equilibrium is achieved (Figure 1.1). Secular equilibrium is when all the radionuclides in a decay chain decay at the same rate (i.e., have the same activity (Bq)). The time it takes for daughter radionuclides to reach secular equilibrium with their parent is proportional to their half-lives, and as a general rule it takes ~ 6 half-lives to reach secular equilibrium. The first daughter radionuclide is Rn-222 with a half-life of 3.82 days, meaning it will reach secular equilibrium with Ra-226 within ~ 3 weeks. The four subsequent radionuclides in the decay chain all have very short half-lives and will achieve secular equilibrium with Rn-222 within a few hours but will be in deficit relative to Ra-226 until Rn-222 reaches its secular equilibrium. However, the next radionuclide is Pb-210 with a half-life of 22.3 years and will take considerably longer, ~ 134 years, to reach secular equilibrium. Bi-210 will reach secular equilibrium with Pb-210 within a few weeks and Po-210 within a few years but both will be in deficit relative to Ra-226 until Pb-210

reaches its secular equilibrium. It is important to note that this is the idealised scenario in which the in-growth of daughter radionuclides is undisturbed. However, Rn-222 is gaseous so achieving full secular equilibrium requires that no Rn-222 escapes. If some Rn-222 is escaping, the rest of the decay chain will be in deficit relative to Ra-226.

In the assessment of the hazard to the public from Ra-226 particles, it is important to consider Ra-226 and all its daughter radionuclides, as well as the extent to which secular equilibrium has been achieved, to properly assess potential radiation doses.

1.3.2 Ra-226 Particles at Dalgety Bay, Scotland

One existing exposure situation with legacy contamination from historical military practices using Ra-226 is found at Dalgety Bay, which is an estuarine bay located on the north bank of the Firth of Forth estuary in Scotland (Figure 1.2).

Figure 1.2 Location of Dalgety Bay, Scotland, and the stretch of coastline where Ra-226 particles have been found (red line = ~ 850m)

Ra-226 particles were first discovered on the beach at Dalgety Bay in 1990 and originate from past military practices undertaken on the adjacent land by the United Kingdom Ministry of Defence (UK MoD). The land was host to UK MoD air force activities (RNAS Donibristle and HMS Merlin) between 1917 and 1959, a time when Ra-226 was used in paint to luminise aircraft components (Patton, 2013). Activities on the land left a legacy of radioactive contamination that has been present in the environment for at least 60 years. The Scottish Environment Protection Agency (SEPA) undertook regular

radiological monitoring surveys that collectively recovered > 1000 Ra-226 particles, varying greatly in physical size and Ra-226 activity (~ 1 kBq – 76 MBq).

The risk to members of the public from the Ra-226 particles at Dalgety Bay was assessed by SEPA in 2013 (Dale, 2013). The assessment concluded there is a significant possibility of members of the public receiving radiation doses via inadvertent skin contact and inadvertent ingestion that exceed the relevant radiation dose criteria as defined in The Radioactive Contaminated Land (Scotland) Regulations 2007 Statutory Guidance (Scottish Government, 2010). Consequently, the site is in the process of being remediated by the UK MoD against reference levels as advised from Public Health England (now the UK Health Security Agency). However, the SEPA risk assessment highlighted some challenges in the radiological protection of the public from Ra-226 particles that would benefit from further research.

1.3.3 Challenges in Radiological Protection of the Public from Ra-226 Particles

The existing exposure situation at Dalgety Bay has highlighted three key challenges in the radiological protection of the public from Ra-226 particles, which are largely applicable to radioactive particles in general:

I. Radioactive particle characterisation

Unlike planned exposure situations where the radiation source is already characterised, and the potential radiation doses prospectively assessed, the radiation source in an existing exposure situation is often not well characterised and the potential radiation doses unknown (Dale, Robertson and Toner, 2008). In these circumstances, data on the radiation source characteristics, including any radioactive particles present, need to be obtained to undertake an assessment of radiation doses. There are limited data available on the characteristics of Ra-226 particles as the only study to characterise Ra- 226 particles from legacy contamination studied nine Ra-226 particles from Dalgety Bay to investigate their origin, deposition, and transport within the local environment (Wilson et al., 2013). This study was commissioned by SEPA to provide data to underpin its risk assessment and remains the only published study on Ra-226 characteristics. Further research is required for a larger number of Ra- 226 particles to gain a better understanding of their characteristics to better inform dose assessment.

II. Assessment of absorbed dose due to inadvertent skin contact

The ICRP standard approach to the assessment of skin dose may not be appropriate for Ra-226 particles. Typically, the exposure of the skin would be over areas greater than 1 cm^2, meaning the nominal 1 cm^2 averaging area would result in a conservative assessment. However, as radioactive particles are discrete sources of radiation, they may only irradiate an area much smaller than 1 cm^2. It is also known that the skin cells involved in injury from radiation exposure are not necessarily located at the reference 70 µm skin thickness (Hopewell, 2000). There are limited data available on the dosimetry of Ra-226 particles as the only study to measure the absorbed dose rate to skin from Ra-226 particles was undertaken using Ra-226 particles from Dalgety Bay and reported to the Scottish Environment Protection Agency (SEPA) (Charles and Gow, 2010). This study was commissioned by SEPA to provide data to underpin its risk assessment and remains the only study on Ra-226 particle dosimetry. The SEPA risk assessment used the ICRP reference skin depth of 70 µm and the 1 cm^2 nominal averaging area given they are the current standards but acknowledged that further research was required to establish whether this was appropriate. Furthermore, the UK Government Committee on the Medical Aspects of Radiation in the Environment (COMARE) recommended that further research should be undertaken regarding skin doses from radioactive particles, with particular reference to young children (COMARE, 2014). Further research is required to establish whether the ICRP reference skin depth of 70 µm and the 1 cm^2 nominal averaging area are appropriate for the assessment of skin dose from Ra-226 particles.

III. Assessment of committed effective dose due to inadvertent ingestion

The ICRP standard approach to the assessment of ingestion dose may not be appropriate for Ra-226 particles. Typically, members of the public would ingest radioactivity from the environment that has, for example, been incorporated into foodstuffs. The ICRP ingestion dose coefficients were derived for such typical exposures, not for the ingestion of radioactive particles. Depending on their characteristics, radionuclides contained within radioactive particles could be more, or less, bioaccessible during digestion than if the same radionuclides were incorporated into food. There are limited data available on the bioaccessibility of Ra-226 particles as only one study has been published on the *in vitro* bioaccessibility of Ra-226 particles (Tyler *et al.*, 2013). This study was commissioned by SEPA to provide data to underpin its risk assessment and remains the only published study on Ra-226 particle bioaccessibility. Further

research is required on the bioaccessibility of Ra-226 particles to improve ingestion dose assessment.

1.4 Thesis Aim and Structure

The widespread historical use of Ra-226 in military applications raises the possibility of a similar contaminant profile as at Dalgety Bay being present at many other sites, but the paucity of data on Ra-226 particles has limited our understanding of the hazard to members of the public. The overall aim of this thesis was to advance the current understanding of the characteristics of Ra-226 particles found in the environment and improve the assessment of radiation doses via inadvertent skin contact and inadvertent ingestion by members of the public. An introduction to my research, as well as some preliminary data, has been published as part of a special issue on radioactive particles in the Journal of Environmental Radioactivity (McGuire *et al.*, 2020).

Chapter 1 has provided a general introduction to radioactive particles, the system of radiological protection, and highlighted the specific case of radium contamination from past military practices. From the work undertaken by SEPA to address the Ra-226 particles at Dalgety Bay, three key challenges in the radiological protection of the public were identified. Ra-226 particles from Dalgety Bay were studied in this thesis to address these challenges, the results of which are presented in Chapters 2, 3, and 4 in the form of research papers for publication.

Chapter 2 addresses the first challenge regarding Ra-226 particle characterisation. The aim of this research was to physically, chemically, and radiologically characterise Ra-226 particles from legacy contamination to provide the necessary data for informing dose assessment.

Chapter 3 addresses the second challenge regarding the assessment of absorbed dose from inadvertent skin contact with Ra-226 particles. The aim of this research was to investigate whether the reference 70 µm skin thickness and nominal 1 cm^2 skin averaging area are appropriate for the assessment of absorbed dose to the skin from inadvertent contact with Ra-226 particles by the public.

Chapter 4 addresses the third challenge regarding the assessment of committed effective dose from inadvertent ingestion of Ra-226 particles. The aim of this research was to investigate whether the nominal f_1 values are appropriate for the assessment of committed effective dose from inadvertent ingestion of Ra-226 particles by the public and investigate the particle characteristics that influence bioaccessibility.

Chapter 5 provides a general discussion of the results and provides recommendations for how this work can be used to improve the characterisation and assessment of Ra-226 particles, as well as radioactive particles in general, in the radiological protection of the public. Further research in support of radioactive particle characterisation and assessment is identified, and Chapter 6 presents the key conclusions from this research.

Chapter 2

Characteristics of Ra-226 Particles from Legacy Contamination and Implications for Radiological Protection

2 Characteristics of Ra-226 Particles from Legacy Contamination and Implications for Radiological Protection

2.1 Introduction

Radioactive particles are physically discrete sources of radioactivity that have been released into the environment as result of past accidents, incidents, and practices (IAEA, 2011), the characteristics of which are often unknown due to the unplanned nature of the releases (Dale, Robertson and Toner, 2008). The historical use of radium in the luminising of aircraft components, and the subsequent decommissioning of those aircraft and associated waste disposal practices, has left a legacy of contamination on former military sites. One such site is Dalgety Bay in Scotland, which was host to United Kingdom Ministry of Defence air force activities between 1917 and 1959, leaving behind legacy contamination in the form of Ra-226 radioactive particles (Dale, 2013). One of the challenges for radiological protection of the public is in the characterisation of radioactive particles found in the environment to provide the necessary data to inform the assessment of potential radiation doses (McGuire *et al.*, 2020).

2.1.1 Radiological protection from legacy contamination

The system of radiological protection, as published and maintained by the International Commission on Radiological Protection (ICRP), considers three different types of radiation exposure situation intended to encompass all possible circumstances where radiation exposure could occur: planned, emergency and existing. Existing exposure situations involve exposures that already exist when decisions on radiological protection must be taken, such as legacy contamination due to past emergencies, events, or practices as well as naturally occurring exposures. The level of radiological protection in existing exposures situations is the reference level, which is the level of dose or risk, above which it is judged to be inappropriate to allow exposures to occur, and below which optimisation of protection should be implemented. The reference level is not prescribed by the ICRP but should be set by national regulatory authorities considering the prevailing circumstances of the existing exposure situation being assessed (ICRP, 2007). In deriving the reference level for a particular existing exposure situation, the national regulatory authority needs to gather data on the characteristics of the contamination and assess the potential radiation doses to the public.

Unlike planned exposure situations where the radiation source is already characterised, and the potential radiation doses prospectively assessed, the radiation source in an existing exposure situation is often not well characterised and the potential radiation

doses unknown (Dale, Robertson and Toner, 2008). In these circumstances, data on the radiation source characteristics, including any radioactive particles present, need to be obtained to undertake an assessment of potential radiation doses to the public.

2.1.2 Characteristics of Radioactive Particles

Several studies have been published that characterised radioactive particles found in the environment. Physical characteristics, such as size, shape, and density, are important for understanding the hazard from radioactive particles. Particles of different sizes can pose different hazards to members of the public depending on, for example, whether their size makes them amenable to inhalation, inadvertent ingestion, and/or prolonged contact with the skin. Radioactive particles have been shown to vary greatly in size, such as the Cs-137 particles released during the accident at the Fukushima Daiichi nuclear power plant, which range from 3 µm to 1.6 mm (Futagami *et al.*, 2020).

Chemical characteristics, such as elemental composition, can provide insights into the source of radioactive particles and how they were formed (Salbu *et al.*, 2018). Characterisation of six plutonium-containing particles from the US nuclear weapons testing site in the Republic of the Marshall Islands revealed there to be two different types of particles (Jernström *et al.*, 2006). The first type consisted of a plain plutonium matrix with no evidence of fission, indicating that these particles may have formed from a safety test. The second type was rich in silicon and oxygen with traces of Cs-137, an indication of minor fission of the plutonium, perhaps formed from a low yield test.

Radiological characteristics, such as the radionuclides present and their activities, are essential characteristics to measure for informing the assessment of potential radiation doses. The radioactive particles released from Sellafield contain different radionuclides, where particles classified as alpha-rich are dominated by Am-241, beta-rich particles are dominated by Cs-137, and Co-60 rich particles are dominated by Co-60 (Cowper, 2009; Clacher, 2010, 2011). Alpha, beta, and gamma radiation present different hazards so it is important to identify the radionuclides present in radioactive particles for correctly assessing the potential radiation doses. The radioactive particles released from Dounreay contain different amounts of Cs-137 and Sr-90 activity and have been classified according to their ability to cause harm based on their Cs-137 activity as the relationship between Cs-137 and Sr-90 has been established. Particles with a Cs-137 activity $> 10^6$ Bq are classed as *significant* in terms of implications for public health, $> 10^5$ Bq but $< 10^6$ Bq as *relevant*, and $< 10^5$ Bq as *minor* (DPAG, 2006). The higher activity particles can present a greater hazard, so it is important to quantify the amount

of activity present in radioactive particles for ensuring any radiological protective actions taken are proportionate.

Similarities between particles from different contaminated sites may be revealed by studying particle characteristics, facilitating the use of knowledge and experience across multiple contaminated sites with similar contaminant profiles. Three particles originating from the Thule nuclear weapons accident have been characterised in terms of size, activity, morphology, elemental distribution, and oxidation states (Lind *et al.*, 2005). Another study, characterising six Thule particles, utilised a similar suite of techniques with the addition of 3D visualisation of elemental distribution and structure (Eriksson *et al.*, 2005). A similar suite of analyses has been applied to particles originating from the Palomares nuclear weapons accident in several studies and these have revealed them to be very similar to the Thule particles despite having been isolated from quite different environments (Jiménez-Ramos *et al.*, 2006; Lind *et al.*, 2007; Aragón *et al.*, 2008).

Conversely, differences between particles from the same contaminated site may also be revealed by studying particle characteristics, providing valuable data for informing dose assessment if different particles present different hazards. Several studies have characterised depleted uranium (DU) particles from Kosovo and Kuwait that found DU particles can have different characteristics depending on their mode of formation (Danesi *et al.*, 2003; Salbu *et al.*, 2003, 2005; Török *et al.*, 2004). Furthermore, these differences have been shown to affect the potential bioaccessibility in the human gastrointestinal tract (Lind *et al.*, 2009). DU particles from a military testing ground in the UK also exhibited different characteristics depending on whether the particles were formed by the impact of DU ammunitions on targets during testing, or corrosion of DU buried within the soil (Sajih *et al.*, 2010). Different types of radioactive particles have been identified at nuclear weapons testing sites, such as the USSR test site at Semipalatinsk in Kazakhstan, which has been shown to be contaminated with at least four different types of radioactive particle varying in size, morphology, and topography (Lukashenko *et al.*, 2020).

Characteristics of Ra-226 Particles

There are limited data available on the characteristics of Ra-226 particles as the only study to physically, chemically, and radiologically characterise Ra-226 particles from legacy contamination studied nine Ra-226 particles from Dalgety Bay (Wilson et al., 2013). This study was undertaken to investigate their origin, deposition, and transport within the local environment. Gamma spectrometry, optical macroscopy, and scanning electron microscopy with energy dispersive X-ray spectroscopy (SEM-EDS) were used

to characterise the particles. The analyses reported a wide range of activities, sizes, shapes, and surface elemental compositions despite the small sample size. However, given the general lack of data available on the characteristics of Ra-226 particles, this study provided a valuable insight into the source of the particles and their deposition and potential transport within the local environment.

2.1.3 Aim and Objectives

The paucity of data on the characteristics of Ra-226 particles has limited the understanding of legacy contamination from the historical use of Ra-226 in luminous paint and its hazard to the public. As Ra-226 was widely used across military sites the absence of such data may mean that assessments undertaken for the protection of the public lack relevant information that may result in an inaccurate assessment. The aim of this research was to physically, chemically, and radiologically characterise Ra-226 particles from legacy contamination to provide the necessary data for informing dose assessment. This aim was achieved through the following objectives:

I. Physically characterise Ra-226 particles using optical macroscopy with image analysis to measure particle size and shape, measure particle mass, and calculate particle density, as well as general observations on their physical appearance.

II. Chemically characterise Ra-226 particles using SEM-EDS to measure surface elemental composition.

III. Radiologically characterise Ra-226 particles using gamma spectrometry to measure the activities of Ra-226 and its gamma-emitting daughter radionuclides.

2.2 Materials and Methods

2.2.1 Sample Selection

The Ra-226 sample inventory from Dalgety Bay collected by SEPA was made available for this research. A total of 162 samples (~ 10 % of the inventory) were selected comprising 160 Ra-226 particles (P1 – P160) and two Ra-226 artefacts (A1 and A2). The artefacts were identifiable aircraft components, where A1 was a partially intact dial and A2 was a flick switch. The Ra-226 particles were selected to represent a range of activities and physical sizes based on the SEPA in-field estimates of Ra-226 activity and physical size.

2.2.2 Optical Macroscopy

Particle size and shape were measured by optical macroscopy using a Leica M420 optical macroscope fitted with an Olympus ColourView III digital camera linked to the Olympus Stream Image Analysis Software for image acquisition, processing, and measurement. The macroscope was calibrated for a series of magnifications (5.8x, 8x, 10x, 12.5x, 16x, 20x, 25x, and 35x) to analyse a range of particle sizes. Each magnification was calibrated using a stage micrometer and the calibration was checked before and after each use using a reference object, the dimensions of which were independently measured using a set of calibrated Vernier callipers.

Each particle was placed on the macroscope stage beneath the objective lens under oblique incident illumination from two opposing directions to minimise shadows. The most appropriate magnification was selected, and adjustments made to the white balance and exposure. Images were captured using the manual extended focal imaging (EFI) function in Stream, which captures a single image that is built pixel-wise to ensure the whole object is in focus even when parts of the object are in different focal planes. Once the EFI was captured, the image was segmented using HSV thresholding to separate the sample from the image background, allowing the software to make size and shape measurements on the particle.

For size, the equivalent circular diameter (ECD) was measured, which is the diameter of a circle with the same area as the measured object and provides a means to estimate and compare the size of irregular objects. For shape, two measurements were made, sphericity and shape factor. Sphericity takes a value from 0 to 1 and is the squared quotient of the width and length of the object, providing an indication of how much the body of the measured object deviates from a circle. Shape factor takes a value from 0 to 1 and is the area of the object relative to the area of a circle with an equal perimeter, providing an indication of how much the surface of the measured object deviates from a circle.

Each particle was imaged in as many different orientations as possible to calculate the mean ECD, sphericity, and shape factor. It was noted if a particle could not have its smallest dimension imaged due to either being ‘flat’ or ‘elongated’ and classified accordingly, otherwise the sample was classed as ‘volume’. Qualitative observations were made regarding the amount of visible void space within the particles. If only a few small voids were visible the particle was classed as ‘few’, if many small voids were visible and/or there was a large void(s) it was classed as ‘many’, otherwise the particle was classed as ‘none’. The artefacts were photographed on 1 mm ^{2} graph paper for scale as

they were too big to be imaged by the optical macroscope, and did not have their ECD, sphericity, or shape factor measured.

2.2.3 Mass and Density

Particle mass was measured using an Oxford GM-2505D 5-figure laboratory balance. The balance was calibrated annually by a UKAS accredited calibration service, and the calibration was checked before and after use using a set of calibration weights (1, 10, and 100 mg; Kern & Sohn) manufactured to International Organisation of Legal Metrology (OIML) standards. The mass of each sample was measured once, and the result recorded when the balance had stabilised.

Particle density was estimated by using the sample mass and the equivalent spherical volume (ESV), calculated using the ECD from the optical macroscopy data. This method was tested using a distortable material, in this case plasticine, to establish if the ECD can provide a reasonable estimate of density. The density of the plasticine was established by measuring its mass and its volumetric displacement in water. The plasticine was then imaged and analysed by optical macroscopy, first as a sphere to see if the ECD can provide a reasonable estimate of density under optimal conditions, followed by a cylinder, prism, cone, and disk to see the effect of deviations from a sphere.

2.2.4 SEM-EDS

Particle surface elemental composition was measured by SEM-EDS. The analysis used a Zeiss EVO MA-15 variable pressure SEM fitted with a backscattered electron (BSE) detector, installed above the microscope stage, and an Oxford Instruments X-Max 80 mm^2 EDS detector, installed to the left at an angle (approx. 30 °) relative to the microscope stage. The SEM-EDS was also fitted with a secondary electron (SE) detector and a variable pressure secondary electron (VPSE) detector, but these were not used in this analysis. The SEM used Zeiss SmartSEM Software for BSE image acquisition and Oxford Instruments AZtec Software for EDS spectrum analysis. The SEM-EDS was calibrated annually by the manufacturer using a multi-element standard, and the calibration was checked before and after use using a cobalt standard.

The BSE detector was used to gather qualitative information on surface elemental composition in terms of atomic number (Z), where areas composed of high-Z elements appear brighter in the BSE image than areas composed of low-Z elements. The EDS detector was used to gather semi-quantitative information on surface elemental composition by identifying individual elements to produce element distribution maps and calculating the relative element abundance (weight %). All analyses were performed with

a 25 kV accelerating voltage, 100 µA beam current, 447 pA Iprobe current, 2.75 A filament current, 60 Pa chamber pressure, and a working distance of 8.5 mm.

Each sample was analysed in a single orientation mounted on a standard 12.5 mm diameter aluminium SEM pin stub using a carbon adhesive disk. The samples were not subject to any preparation, such as the application of a conductive coating or polishing, to preserve their original characteristics. As the samples were uncoated, the analysis was performed under low vacuum conditions to help prevent the accumulation of electrostatic charge on the sample surface (Wilson *et al.*, 2013). Spectra were acquired from the surface of the sample facing the detector using a freehand area drawn around the sample. Tungsten was excluded from the analysis due to contribution from the SEM tungsten filament, as was carbon due to contribution from the adhesive disks.

2.2.5 Gamma Spectrometry

Particle activity was measured by gamma spectrometry using Ortec Gamma-X (GMX) N-Type High Purity Germanium (HPGe) Coaxial Photon Detectors linked to Ortec Gamma Vision Software for spectrum analysis. A custom efficiency calibration was developed as efficiency calibrations associated with standard sample geometries were not appropriate due to the varying size and irregular shape of the samples. To minimise the impact of sample geometry, an efficiency calibration was required that was as independent from sample geometry as possible (Tyler *et al.*, 2013). Using two gamma reference point sources, efficiency calibrations were established at distance from the detectors. The reference sources used in the calibrations were Ra-226 (100 kBq with 3 % relative uncertainty, UR-371, Eckert & Ziegler, including Pb-214 and Bi-214 in equilibrium) and Pb-210 (231 kBq with 4 % relative uncertainty, KU-654, AEA Technology). The incidence angle of photons on a detector will vary for samples of different shapes and sizes, particularly when they are close to the detector, which is why samples are usually analysed in standard geometries. However, with increasing distance this becomes less significant and will eventually reach a distance at which the differences in incidence angle become insignificant.

To optimise the distance from the detectors, efficiency calibrations were established at 10, 15, and 20 cm from the detectors using the Ra-226 and Pb-210 reference sources. The distances were not extended further as beyond 20 cm the lead shielding of the gamma spectrometers could not be closed. At each distance, the activity of the physically largest sample (equivalent circular diameter = 12.34 mm), and therefore the one that deviated the most from the geometry of the calibration sources, was measured to establish the distance at which it effectively appears the same as the calibration sources.

There were no significant differences in measured activities for any of the radionuclides across the three distances, indicating that for samples up to this physical size, the impact of sample geometry is mitigated at a distance of at least 10 cm. For the measurement of the samples, a distance of 20 cm was chosen as it offered the advantage of minimising detector deadtime for the higher activity samples. The efficiency calibration was quality checked using a different gamma reference point source, Eu-152 (43.8 kBq with 3 % relative uncertainty, AF4331, Eckert & Ziegler).

Each sample was placed in the centre of a plastic pot, which was closed with a lid but not hermetically sealed, allowing any emanating Rn-222 to escape. The pots were placed 20 cm from the detectors to measure the activity of Ra-226 and its gamma-emitting daughter radionuclides Pb-214, Bi-214, and Pb-210. The measurements were stopped once the measurement uncertainty was ~ 5 % or lower for all four radionuclides. Spectra were analysed using the custom efficiency calibrations and internal energy calibrations to report activities (Bq) for Ra-226, Pb-214, Bi-214, and Pb-210 with 2-sigma total uncertainty.

Each sample was analysed in a single physical orientation, but preliminary analysis of these data showed that in many cases the Pb-210 activity was lower than what would be expected based on secular equilibrium and the approximate age of the samples. This apparent lack of equilibrium could indicate that self-absorption of radiation within some of the particles may be significant for Pb-210 with its relatively low energy 46.54 keV gamma photon, compared to the calibration source. Self-absorption could be due to physical properties of the particles, such as size or density, where physically large or dense particles could absorb a greater proportion of the 46.54 keV gamma photons, never allowing them to reach the detector. Self-absorption could be exacerbated if the activity was heterogeneously distributed within the particle and was on the side facing away from the detector during measurement. To investigate this, a selection of samples (n = 41) with low Pb-210 activities were re-analysed in two different orientations.

2.3 Results

2.3.1 Size, Shape, Mass, and Density

The optical macroscopy analysis revealed a physically diverse population exhibiting wide ranges for size, shape, mass, and density, as well as physical appearance. Figure **2.1** provides examples of the diversity in physical appearance observed across the samples, which can be qualitatively classified into five groups. The first row shows examples of the ‘rocky’ group (n = 90) that can be described as resembling rocks or stones.

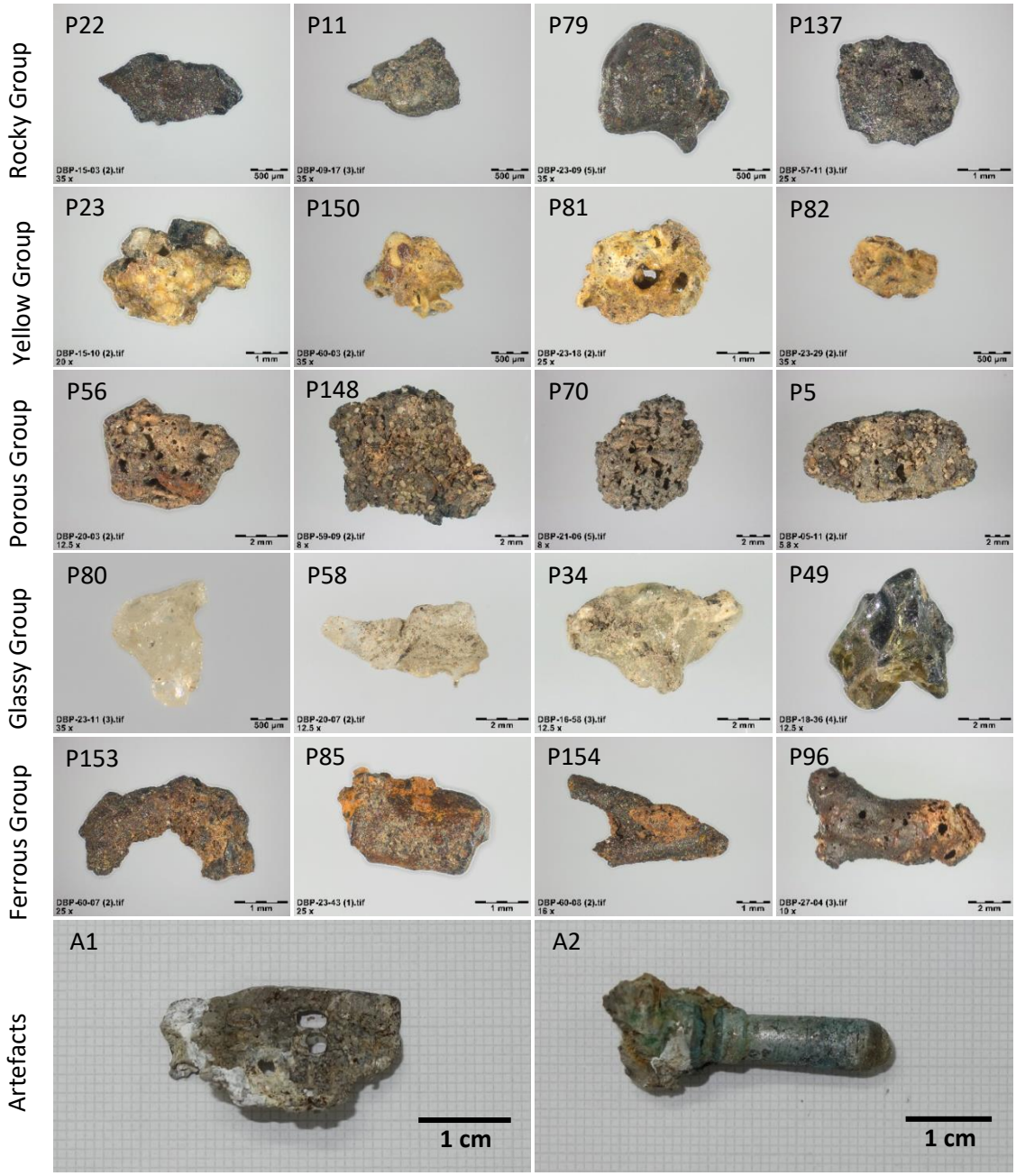

Figure 2.1 Optical macroscopy images of 20 particles and photographs of the 2 artefacts

The second row shows the 'yellow' group (n = 37) that exhibited a characteristic yellow colour, followed by the 'porous' group (n = 22) where samples tended to be physically large often with significant void space, and with what appeared to be sand grains adhered to the surface and/or embedded in the void spaces. The remaining two groups were smaller but had their own distinctive qualities. In the fourth row there are examples of samples that appear to be made of a glassy material (n = 7), followed by samples in the fifth row that appear to have iron oxide on their surfaces, suggesting they might be

made of ferrous metal (n = 4). The last row shows the two artefacts, where the first photograph shows the dial (A1), and the second photograph shows the switch (A2).

Qualitative observations of particle shape classed particles as ‘flat’ (n = 22) or ‘elongated’ (n = 37) if it was not possible to image the smallest dimension, otherwise the particle was classed as ‘volume’ (n = 101). These observations are important as without the smallest dimension, the ECD will be overestimated and consequently density will be underestimated. P150 is an example of a ‘flat’ sample that could only be imaged in two orientations, but this is difficult to see from the optical macroscopy image. More obvious are the ‘elongated’ samples such as P22, P5, P58, and all the members of the ‘ferrous’ group. Qualitative observations of visible void space classed particles as ‘many’ (n = 44) if many small voids were visible and/or there was a large void(s), ‘few’ (n = 63) if only a few small voids were visible, or ‘none’ (n = 53) if there were no visible voids. These observations are important as significant void space will result in an underestimation of density. For example, many small voids can be seen in P56, and a few large voids can clearly be seen in P81, whereas samples such as P137 have only a few small voids and some do not have any visible voids such as P22, P80, and P153.

Size varies across the samples with ECDs ranging from 0.44 to 12.34 mm, with a median of 2.65 mm (IQR = 3.08 mm). However, the ECD for some samples will be overestimated if their smallest dimension could not be imaged. Excluding samples classed as ‘flat’ or ‘elongated’, the ECD still showed considerable variation ranging from 0.44 to 11.44 mm, with a median of 2.50 mm (IQR = 3.16 mm). Shape varies across the samples for both sphericity and shape factor. Sphericity values ranged from a very low sphericity value of 0.11 to close to a perfect sphere at 0.93, with a median of 0.5 (IQR = 0.27). Excluding samples classed as ‘flat’ or ‘elongated’, the sphericity values still showed considerable variation ranging from 0.29 to 0.84 with a median of 0.54 (IQR = 0.19). Shape factor tended to be low across all the samples ranging from 0.092 to 0.58 with a median of 0.24 (IQR = 0.11). Excluding samples classed as ‘flat’ or ‘elongated’, shape factor still showed considerable variation ranging from 0.11 to 0.58 with a median of 0.25 (IQR = 0.11).

Mass ranged across five orders of magnitude from 0.00009 to 1.07 g with a median of 0.011 g (IQR = 0.066 g). Using the mass and the ECD, the density of each sample was calculated, which ranged from 0.30 to 2.96 g/cm^3 with a median of 1.12 g/cm^3 (IQR = 0.52 g/cm^3). Excluding the samples classed as ‘flat’ or ‘elongated’, the density range narrowed to between 0.65 and 2.96 g/cm^3, with a median of 1.24 g/cm^3 (IQR = 0.51 g/cm^3). Also excluding the samples that had a ‘few’ or ‘many’ visible void spaces,

the density range narrowed further to between 1.063 and 2.96 g/cm^3, with a median of 1.57 g/cm^3 (IQR = 0.48 g/cm^3).

The use of the ECD to estimate density was tested using plasticine, the density of which was established to be 1.61 g/cm^3 by measuring its mass and volumetric displacement in water. Using the ECD, the density of the plasticine sphere was in close agreement at 1.62 g/cm^3. For the cylinder, the ECD gave an underestimated density of 1.38 g/cm^3, as would be the case for samples classed as 'elongated'. For the prism, the ECD gave an underestimated density of 1.15 g/cm^3 as did the cone at 1.37 g/cm^3. The greatest underestimation of density was for the disk, as would be the case for the samples classed as 'flat', with a density of 0.65 g/cm^3.

2.3.2 Surface Elemental Composition

The SEM-EDS analysis revealed a diversity of surface elemental compositions with 23 different elements detected across the samples. Table 2.1 shows a summary of the weight % for each element across the 162 samples. Some elements were ubiquitous (Ca, Fe, O, and Si), some were detected in most samples (Al, Cl, K, Mg, Na, Ti, and Zn), some in around half of the samples (Cu, P, and S), and some in a minority of samples (Ba, Co, Cr, Mn, Mo, Ni, Pb, Sn, and Sr). Oxygen was the element with the highest weight % for most samples (n = 149). After oxygen, the most abundant elements were Si (n = 71), Fe (n = 54), Zn (n = 12), Cu (n = 11), Al (n = 10), Pb (n = 3), and Ba (n = 1). Elements detected in only a minority of samples are not necessarily insignificant. For example, Pb is only detected in 12 samples, but its weight % ranges between 2.21 and 35.18 and is the most abundant element in 3 samples. Conversely, elements detected in most samples are not necessarily significant. For example, K is present in 148 samples but its weight % ranges between 0.24 and 2.54, and it is always one of the least abundant elements in the samples. None of the samples had all 23 detected elements present, instead ranging between 8 and 18, with a median of 12, elements detected in individual samples.

Table 2.1 Summary of the weight % of the 23 elements detected in the EDS analysis

Element	No. of samples it is detected	Minimum (weight %)	Median (weight %)	IQR (weight %)	Maximum (weight %)
Aluminium (Al)	160	1.64	8.85	4.02	26.49
Barium (Ba)	17	0.32	1.69	2.47	16.88
Calcium (Ca)	162	0.28	2.6	2.06	9.39
Chlorine (Cl)	127	0.14	1.3	1.61	9.9
Chromium (Cr)	7	0.19	0.49	2.41	5.24
Cobalt (Co)	1	1.63	1.63	*NA*	1.63
Copper (Cu)	80	0.3	1.4	3.71	33.71
Iron (Fe)	162	0.52	11.22	9.78	48.45
Lead (Pb)	12	2.21	2.9	5.34	35.18
Magnesium (Mg)	157	0.37	2.08	1.18	6.56
Manganese (Mn)	21	0.23	0.47	0.26	1.35
Molybdenum (Mo)	1	0.73	0.73	*NA*	0.73
Nickel (Ni)	8	0.19	0.53	2.37	5.74
Oxygen (O)	162	25.5	41.74	7.76	52.46
Phosphorous (P)	85	0.26	0.45	0.23	2.77
Potassium (K)	148	0.24	0.8	0.6	2.54
Silicon (Si)	162	0.4	14.25	7.1	41.85
Sodium (Na)	149	0.89	2.8	2.21	15.59
Strontium (Sr)	1	0.94	0.94	*NA*	0.94
Sulphur (S)	84	0.19	0.44	0.39	3.92
Tin (Sn)	4	1.75	2.68	1.47	6.11
Titanium (Ti)	138	0.17	0.66	0.41	8.2
Zinc (Zn)	115	0.48	4.82	8.01	33.85

The SEM images and EDS element maps provide qualitative spatial information about element distribution and surface features. Figure 2.2 presents examples of the particles plus the two artefacts. For each sample, the first image is the BSE image, followed by three element maps. Element distribution varied greatly across the particles, with some appearing to be completely homogenous like P22, whilst others exhibiting varying degrees of heterogeneity.

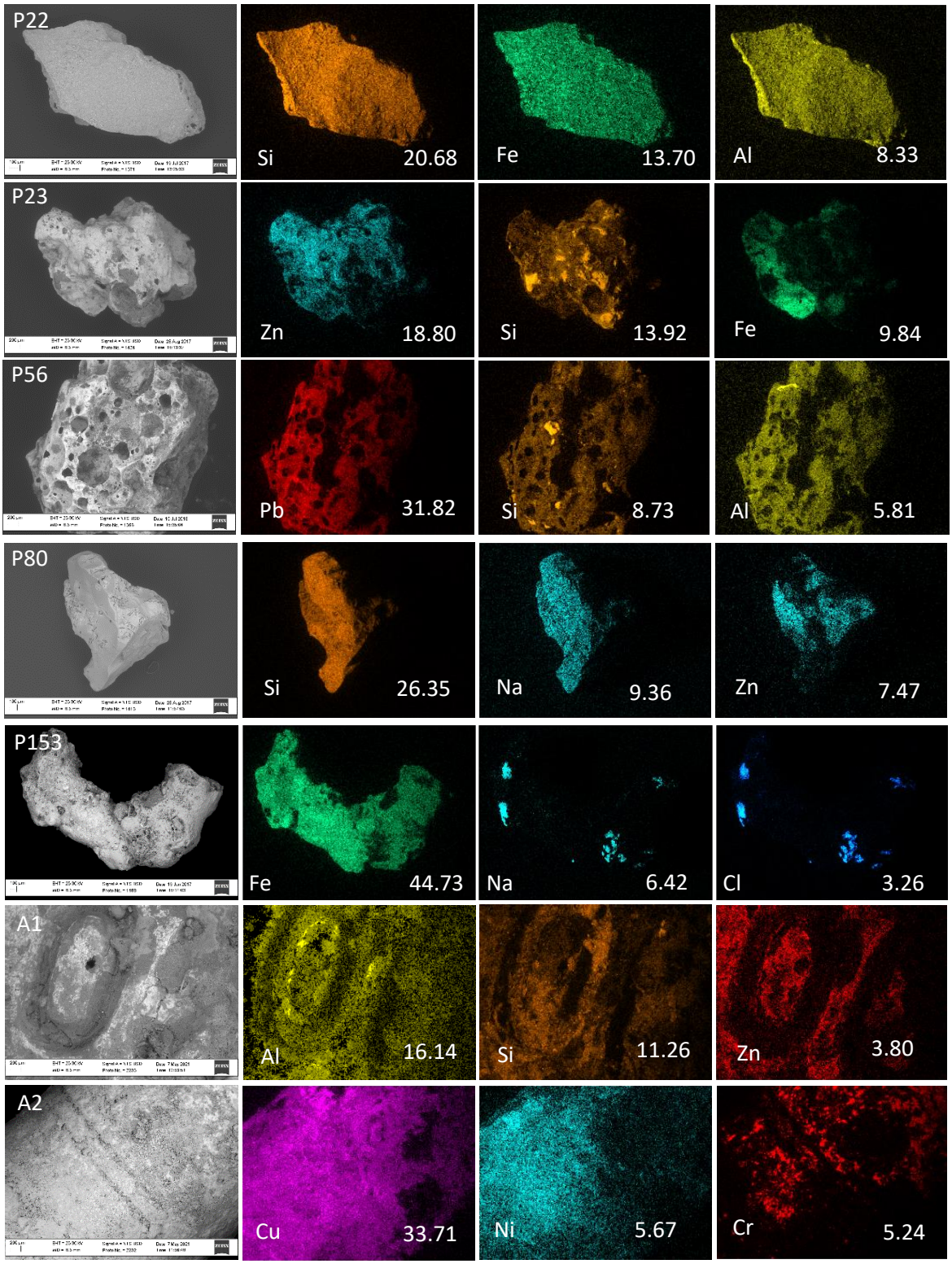

Figure 2.2 BSE images and EDS element distribution maps for five particles and the two artefacts

As can be seen for P23, Zn was widely distributed, whereas Si was displaying some heterogeneity, and Fe was very heterogeneous. The heterogeneity is reflected in the BSE image, where the Zn aligns with the brighter areas, and the Si aligns with the darker areas. Conversely, Zn was heterogeneously distributed in P80, whereas Si and Na were largely homogeneous. As observed in the optical macroscopy analysis, many particles contained visible void spaces, as exemplified by the BSE image of P56.

Some samples show evidence of the estuarine environment from which they were recovered. For example, bright spots can be seen embedded in the void spaces of P56 on the Si map. Point spectra were acquired that revealed these bright spots to be almost exclusively composed of Si and O, suggesting they are grains of sand. Furthermore, bright spots can be seen on the surface of P153 on the Na and Cl maps. Point spectra were acquired that revealed these bright spots to be almost exclusively composed of Na and Cl, suggesting they are salt deposits.

The SEM-EDS analysis of the dial (A1) focused on an area of its surface that appeared to feature the number zero. It contained one of the highest weight % for Al at 16.14 and a weight % for Ba of 2.30, despite Ba being relatively uncommon across the particles. In contrast, it had one of the lowest weight % for Fe at 2.77 and a relatively low weight % for Si at 11.26, despite Fe and Si being the most abundant elements in most particles. The analysis of the switch (A2) focused on the main shaft of the switch. It contained the highest weight % for Cu of all samples at 33.71 and amongst the highest weight % for Ni and Cr at 5.67 and 5.24 respectively, despite Ni and Cr being relatively uncommon across the particles. In contrast, it had one of the lowest weight % for Fe at 2.4 and the lowest weight % of all samples for Si at 0.4, despite Fe and Si being the most abundant elements in most particles. Interestingly, the switch did not contain any detectable Al, despite Al being almost ubiquitous across the particles.

A notable observation made during this analysis was the structural integrity of the samples. Part of the analytical procedure was to adhere the samples to aluminium pin stubs using carbon adhesive disks for mounting onto the SEM-EDS microscope stage. To ensure the sample was securely attached, a small amount of pressure was applied using forceps which, on several occasions, caused samples to fracture. Figure 2.3 shows examples of the fracturing in the BSE images of P47 and P120. Additionally, some samples exhibited friability, as shown by the crumbly nature of PX. It was not possible to fully remove this sample from the carbon adhesive disk to undertake any further analysis therefore it was excluded from this study and does not have a sample number, hence its designation as PX.

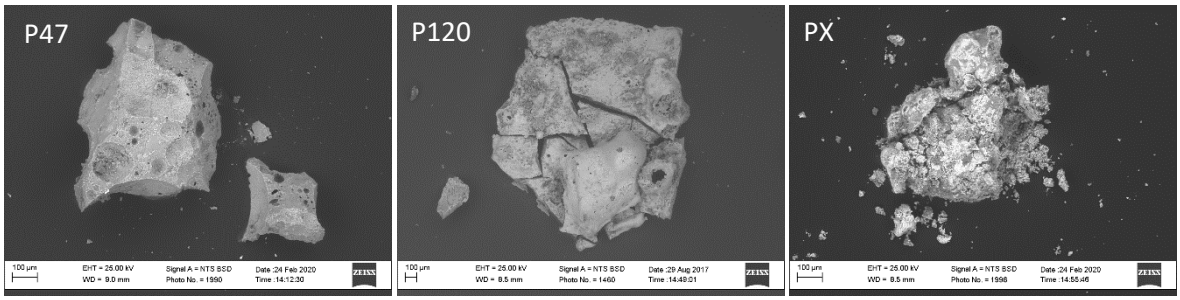

Figure 2.3 BSE images should particle fracturing and intrinsic friability

2.3.3 Activity of Ra-226 and its daughter radionuclides

The gamma spectrometry analysis confirmed the presence of Ra-226 and its gamma-emitting daughter radionuclides Pb-214, Bi-214, and Pb-210 in all the particles and the two artefacts. Figure 2.4 shows the range of activities for each of the radionuclides. Activities were skewed to the right with several higher activity outliers and spanned several orders of magnitude. Outliers are data points that fall outside 1.5 times the interquartile range (IQR). Mean 2-sigma total measurement uncertainties for Ra-226, Pb- 214, Bi-214, and Pb-210 were 6.99 %, 6.06 %, 6.10 %, and 8.58 % respectively.

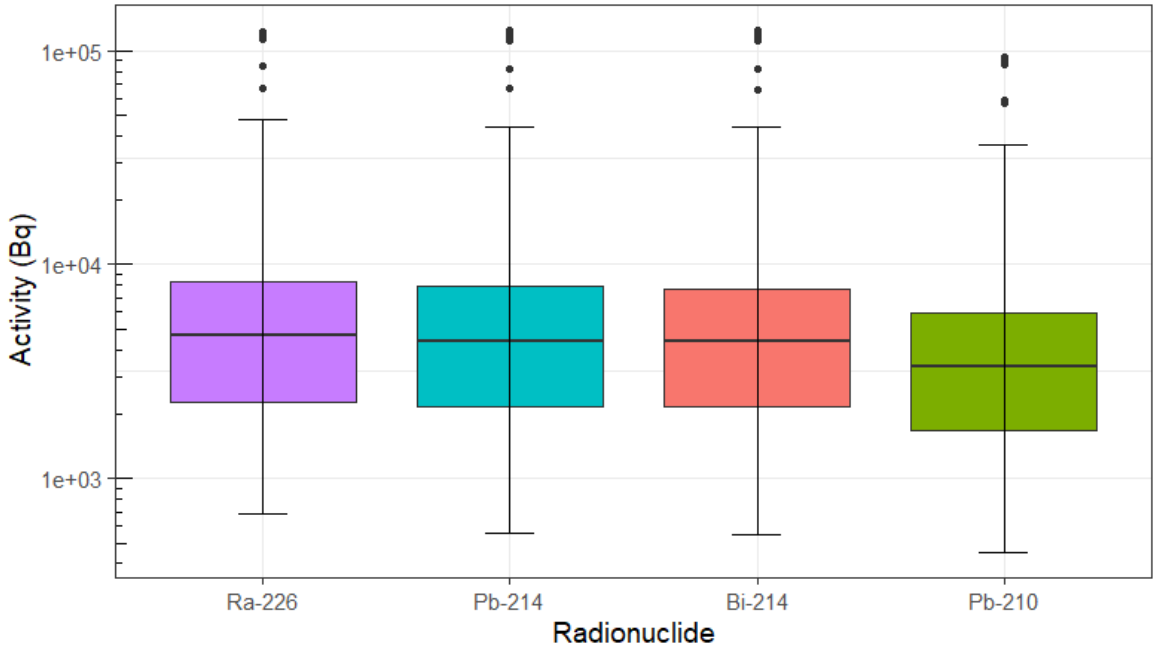

Figure 2.4 Activities (Bq) of Ra-226 and its gamma-emitting daughter radionuclides in radioactive particles (n = 160) and artefacts (n = 2)

Ra-226 activities ranged from 683 to 122,530 Bq with a median of 4,635 Bq (IQR = 6,009 Bq). Activities of the first gamma-emitting daughter radionuclide in the decay chain, Pb-214, were slightly lower and ranged from 556 to 123,490 Bq with a median of 4,414 Bq (IQR = 5,720 Bq). Similarly, activities of the second gamma-emitting daughter radionuclide, Bi-214, ranged from 548 Bq to 123,750 Bq with a median of 4,365 Bq (IQR = 5,575 Bq). However, activities were considerably lower for the last gamma-emitting daughter radionuclide, Pb-210, which ranged from 453 Bq to 93,964 Bq with a median of 3,314 Bq (IQR = 4,279 Bq).

Given the potential age of the particles and artefacts, it is reasonable to expect the full decay chain to be reaching secular equilibrium, but the lower Pb-210 activities suggests this might not be the case. To test this, the percentage difference was calculated between each parent radionuclide and its nearest gamma-emitting daughter radionuclide. Figure 2.5 shows the percentage difference between the parent-daughter radionuclide pairs: Ra-226 and Pb-214, Pb-214 and Bi-214, and Bi-214 and Pb-210. The smallest percentage difference was seen between Pb-214 and Bi-214 and ranged from -1.35 to 3.92 %, which is less than the measurement uncertainties for these radionuclides. Ra-226 and Pb-214 exhibited a wider range from -2.26 to 21.65 %, but with a 75th percentile percentage difference of 6.71 %, only a minority of values were greater than the measurement uncertainties. However, there was a greater range between Bi-214 and Pb-210 (excluding one outlier) from 4.95 to 84.58 %, and with a 25th percentile percentage difference of 16.94 %, the majority of values were greater than the measurement uncertainties. The outlier was significantly different with a percentage difference between Bi-214 and Pb-210 of -19.99 %, making the Pb-210 activity the highest of all radionuclides in this particle.

The percentage difference between Pb-214 and Bi-214 for the two artefacts, A1 and A2, was very low and similar to each other at 0.47 and -0.019 %, respectively. Between Ra- 226 and Pb-214 it was relatively high and again, similar to each other, at 8.93 and 9.61 %. However, the percentage difference between Bi-214 and Pb-210 was very different with A1 exhibiting one of the lowest at 11.16 % and A2 exhibiting one of the highest at 55.03 %.

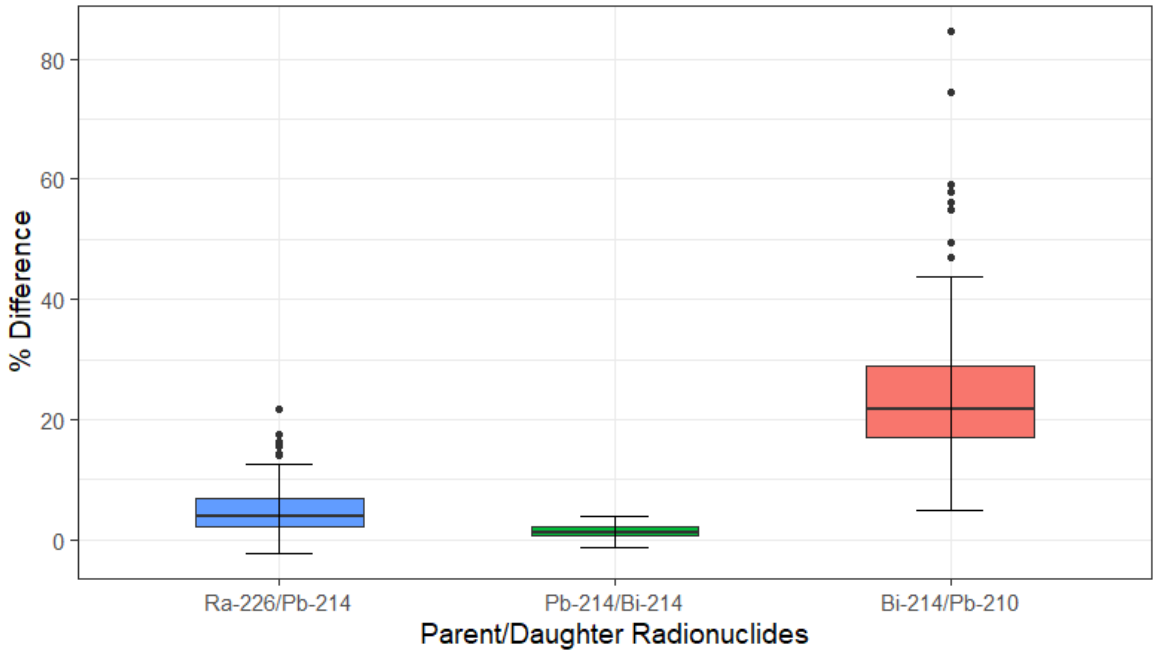

Figure 2.5 Percentage difference between the activities of parent radionuclides and their nearest gamma-emitting daughter radionuclide in radioactive particles (n = 159, one outlier has been excluded) and artefacts (n = 2)

To investigate whether the variability of the Pb-210 activities was due to heterogeneity, a selection of samples with the highest percentage difference between Bi-214 and Pb- 210 (n = 41) were reanalysed in two different orientations. Figure 2.6 shows the percentage difference between activities of each radionuclide when the particles are analysed in two different orientations. The percentage difference for Pb-210 activities between the two orientations ranged from 0.35 to 69.70 % with a median of 7.88 % (IQR = 12.37 %). With a mean 2-sigma measurement uncertainty of 8.58 %, these data show that changing orientation resulted in a significant change to the reported Pb-210 activity for roughly half of particles, whereas for the others the difference was within measurement uncertainty. Changing particle orientation did not affect the other radionuclides to the same extent. The percentage difference for Ra-226 activities ranged from 0.14 to 16.31 % with a median of 2.06 % (IQR = 2.24 %) so changing orientation only significantly affected a few particles. Pb-214 and Bi-214 were relatively unaffected by the change in orientation with maximum percentage differences of 7.37 % and 5.96 %, respectively.

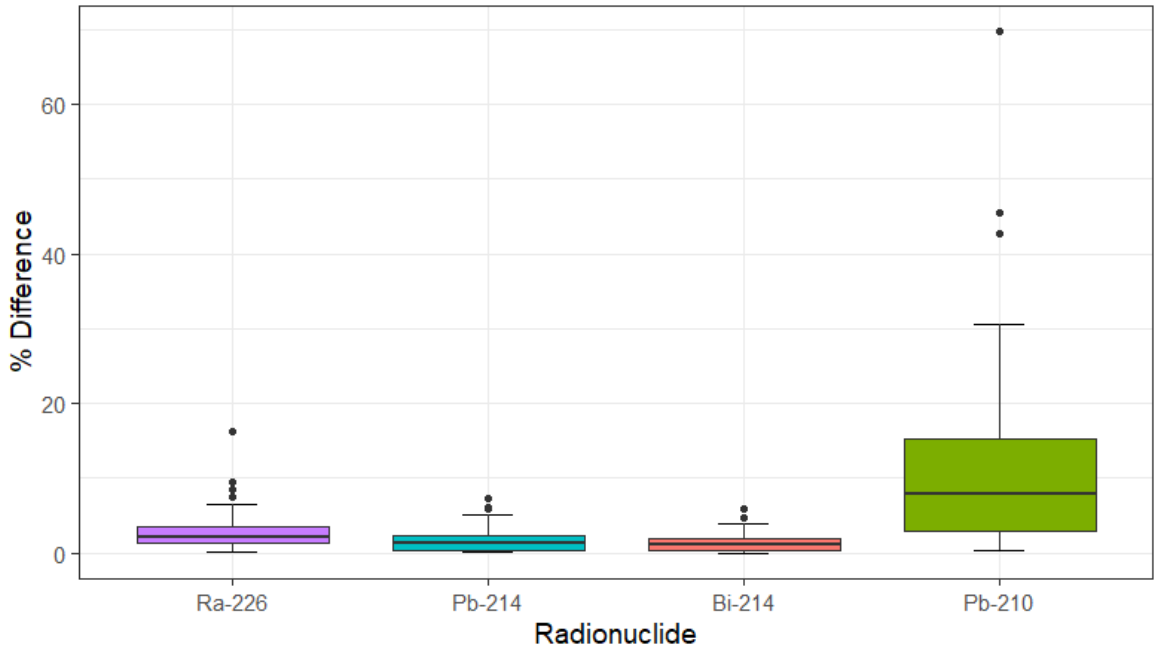

Figure 2.6 Percentage difference between the activities of each radionuclide when Ra-226 particles are analysed in two different orientations

2.4 Discussion

2.4.1 Physical characteristics of Ra-226 particles

All particles were significantly smaller than the artefacts and bear little physical resemblance to them, except perhaps the ferrous group as they all have distinctive shapes that could indicate they are degraded artefacts, or parts of degraded artefacts given they are much smaller than the dial and switch. Given that these particles were recovered from an estuarine environment in which they have been subject to the forces of weathering and abrasion for several decades, it is perhaps to be expected that they will no longer resemble the original artefacts from which they derived.

The highly irregular shape of the Ra-226 particles made physical characterisation challenging. Optical macroscopy was a suitable analytical technique for revealing different types of particles based on physical appearance but presented challenges estimating size, shape, and density for some samples. The ECD provided a good estimate of density for the plasticine sphere, suggesting this method is suitable for estimating density under optimal conditions. However, the ECD is less reliable for objects that deviate from a sphere, as demonstrated by the underestimated density of the plasticine cylinder (- 15.4 %), prism (- 33.3 %), cone (- 16.1 %), and disk (- 85 %). Many particles exhibited irregular shape, in some cases inhibiting the imaging of their smallest

dimension, as well as containing visible void spaces. However, even the sub-set of samples with no visible void spaces and classed as “volume” exhibited wide ranges for sphericity and shape factor, making it very challenging to estimate density. The most appropriate use of these data would be as an indicative density range, but it is highly likely to be an underestimate.

The calculation of density of the Dounreay MTR particles using 3-dimensional images of the particles constructed through microscope photography from different angles reported lower than expected densities for the most irregularly shaped particles (DPAG, 2006). Other methods involved measuring particle mass and estimating particle dimensions from SEM images for calculating volume based on cuboid or ovoid geometries (Cowper, 2009). Another involved sequential immersion in a series of haloalkanes or sodium tungstate solutions of known densities where the density of the sample was assumed to be between the densities of the liquids in which it changed from floating to sinking (Clacher, 2010). Using cuboid and ovoid geometries is an oversimplification of the complex shape of radioactive particles, and using sequential immersion risks the radioactive particles reacting with the solutions in which they are being immersed, so the estimation of radioactive particle density remains challenging.

2.4.2 Chemical characteristics of Ra-226 particles

The study by Wilson et.al. (2013) on nine particles from Dalgety Bay found a similar suite of elements but the weight % showed less variation. For example, Pb was only found in trace amounts whereas the analysis reported here found up to 35.18 weight % for Pb. Also, the wide range of weight % for many other elements reported here, such as Fe for example, was not found by Wilson et.al. (2013), although this could be partly due to the inclusion of carbon in the results of the study. Carbon was the element with the highest weight % for each of the nine particles, which will have had a significant influence on the proportions of the other elements in the samples. The analysis reported here excluded carbon due to the contribution from the carbon adhesive disk used to mount the samples, making direct comparisons with the previous study difficult. However, it is clear the analysis of the larger sample size here has enabled the identification of greater diversity in surface elemental composition.

It is important to note that the SEM-EDS analysis did not detect radium or the elements of its daughter radionuclides, except for the 12 particles in which Pb was detected. The study by Wilson et.al. (2013) did not detect radium or any of its daughter elements either, citing that the limit of detection of this method was too high, which is typically 0.01 weight %. It is likely to be the case here too, particularly as neither radium nor any of its

daughter elements were detected in either of the artefacts. The artefacts were likely to have offered the most favourable conditions for the detection of radium and its daughter elements given they would have been painted with radium paint on their surface and the radionuclides are presumably still located on the surface. Nevertheless, Ra-226 and its daughter radionuclides were detected using gamma spectrometry, highlighting the importance of using different analytical techniques to gather complementary datasets on radioactive particle characteristics.

The lead detected in 12 of the particles is more likely to be from a non-radioactive source, rather than being the Pb-214 and Pb-210 present from the radium paint. As the weight % for lead in these samples is relatively high and none of the other elements in the radium decay chain were detected, the lead in these samples must be from a non-radioactive source. It is not unreasonable for lead to have been present at Dalgety Bay given the site was used for luminising aircraft components using radium paint, and lead is commonly used as a shielding material to reduce radiation exposure of workers.

2.4.3 Radiological characteristics of Ra-226 particles

Although Ra-226 and its gamma-emitting daughter radionuclides were detected in all the particles and the two artefacts, their radiological characteristics were variable, particularly for Pb-210. The small percentage difference between the Pb-214 and Bi-214 activities suggests these radionuclides were in secular equilibrium. However, the percentage difference between Ra-226 and Pb-214 exhibited a larger range with the values above the 75th percentile greater than measurement uncertainty, suggesting that for a minority of particles these radionuclides were not in secular equilibrium. Given the gaseous alpha-emitting Rn-222 is between Ra-226 and Pb-214 in the decay chain, this disequilibrium was likely due to some emanation of Rn-222 from these particles. Furthermore, the percentage difference between Bi-214 and Pb-210 exhibited an even larger range with the values above the 25th percentile greater than measurement uncertainty, suggesting that for the majority of particles these radionuclides were not in secular equilibrium.

One reason for this could be that Pb-210 has not yet had sufficient time to reach secular equilibrium. For instance, assuming the Ra-226 was chemically pure when used to make the radium paint, the time taken for the daughter radionuclides to reach secular equilibrium is proportional to their half-lives and, with a half-life of 22.3 years, Pb-210 may not yet have reached secular equilibrium. The amount of Pb-210 that has grown-in depends on when the Ra-226 was chemically isolated for making the paint, which is not known. However, as an illustration, after 120 years (the approximate time since Ra-226

was first isolated) the percentage difference between Bi-214 and Pb-210 would be 1.18 %, whereas after only 60 years (the approximate time since military activities at Dalgety Bay ceased) it would be 15.90 %. Some particles (n = 36) had percentage differences that fall between these values, but most particles (n = 123) had percentage differences that were greater suggesting the age of the Ra-226 is not the only factor contributing to the low Pb-210 activities.

Another reason for the low Pb-210 activities could be that the 46.54 keV photon of Pb-210 is being impacted by self-absorption and heterogeneity. The analysis of particles in two different orientations has shown that changing particle orientation has the greatest impact on the Pb-210 activities, with minimal impact on the other radionuclides. Roughly half of the particles were affected by the change in orientation suggesting that heterogeneously distributed activity is contributing to the low Pb-210 activities. For the particles that were not significantly affected by the change in orientation, it is likely that their low Pb-210 activities were mostly due to self-absorption of homogeneously distributed activity. It is notable that the Pb-210 activity of the dial was much closer to what would be expected presumably due to the radioactive side of the dial facing the detector and its flat geometry providing minimal self-absorption. In contrast, the Pb-210 activity for the switch was much lower than expected, presumably due to the activity being present around the cylindrical surface, meaning that approximately half of the activity was facing away from the detector and was being absorbed within the switch itself. Furthermore, the percentage difference between the other radionuclides were very similar between the two artefacts, providing compelling evidence that self-absorption and heterogeneity are only affecting the low energy photon of Pb-210, and not the higher energy photons of the other radionuclides.

Gamma spectrometry detected the gamma-emitting radionuclides in the samples, but the Ra-226 decay chain has five daughter radionuclides that are alpha or beta emitters: Rn-222, Po-218, Po-214, Bi-210, and Po-210. Fortunately, their activities can be estimated from the gamma-emitting radionuclides. Due to the possibility of Rn-222 emanation, the activity of Ra-226 should not be used to determine the activities of daughter radionuclides. However, the short half-lives of all daughter radionuclides from Rn-222 to Po-214 means that secular equilibrium will be established in this section of the decay chain, as evidenced by the measurable equilibrium between Pb-214 and Bi- 214, therefore the activities of Rn-222, Po-218, and Po-214 can be inferred from the Pb-214 and Bi-214 activities. Beyond Po-214, secular equilibrium may not yet be achieved due to the potential age of the radium and the relatively long half-life of Pb-210.

The activities of Bi-210 and Po-210 will be in secular equilibrium with the Pb-210 therefore the inference of their activities is subject to the same sensitivities associated with self-absorption and heterogeneity. It may be appropriate to infer the activities of Pb- 210, Bi-210, and Po-210 from Bi-214, acknowledging it is a conservative approach and likely an overestimate.

2.4.4 Particle characteristics and implications for radiological protection

The main public exposure pathways for radioactive particles are inhalation, ingestion, and skin contact, therefore it is important to consider particle characteristics and their implications for radiological protection. However, none of the particles in this study were small enough to be inhaled and the inhalation pathway is not considered further.

During skin contact with a radioactive particle, the amount of energy released from the particle and its deposition in the skin determines the absorbed dose. Particle characteristics revealed by this research may influence energy deposition and could be important considerations when assessing the absorbed dose. For example, the observation that the Pb-210 46.54 keV photon is being subject to varying degrees of self-absorption indicates that the alpha and beta emissions will also be subject to self- absorption. Measurement of the absorbed dose from Ra-226 particles of a range of characteristics is important to adequately inform the assessment of skin dose.

During ingestion of a radioactive particle, the amount of radioactivity released from the particle into the gastrointestinal tract (i.e., bioaccessibility), and subsequently absorbed into the body (i.e., bioavailability) determines the committed effective dose. Particle characteristics revealed by this research may influence bioaccessibility and could be important considerations when assessing the committed effective dose. For example, the variety of different surface elemental compositions could indicate that their chemistry may also differ greatly, which may influence their behaviour in the gastrointestinal tract. Measurement of the bioaccessibility of Ra-226 particles of a range of characteristics is important to adequately inform the assessment of ingestion dose.

More generally, heterogeneity and friability may have implications for longevity in the environment and the viability of exposure pathways. If radioactive particles are left to persist in the environment there could be an increased likelihood of the particles breaking down into smaller pieces, particularly in an environment like Dalgety Bay where the particles are subject to movement within sediment due to tidal forces. The breakdown of physically larger particles may increase the number of particles more amenable to inhalation, inadvertent ingestion, and/or prolonged contact with the skin. Of particular

importance is the case of particles with heterogeneously distributed activity, where there is the possibility of some breakdown products containing most of the activity whereas others may contain significantly less, or even be inert.

Lastly, the observation that the particles are physically, chemically, and radiologically diverse, and divergent from the two artefacts, could be an indication that the original source of the contamination has undergone significant alteration. Waste treatment and disposal practices were known to be diverse at Dalgety Bay including burning at incineration temperatures and incomplete burning at lower temperatures under uncontrolled conditions, as well as direct disposal into pits (Patton, 2013). It could be that these waste treatment and disposal practices transformed the original material into different forms, therefore it is important to characterise a sufficient sample size to capture the full range of particle characteristics to adequately inform dose assessment.

2.5 Conclusions

This research was the first to study a large sample of Ra-226 particles from legacy contamination and has revealed a population that is physically, chemically, and radiologically diverse. The widespread use of Ra-226 in military applications raises the possibility of a similar contaminant profile as at Dalgety Bay being present at many other sites. The analytical techniques used in this study are equally applicable to Ra-226 particles from other sites, and the insights provided by this research may help with future Ra-226 particle characterisation. It is important to use a suite of analytical techniques to gather complimentary datasets and analyse a sufficiently large sample size to capture the potential variety of particles that may be present on a Ra-226 legacy site. The highly heterogeneous characteristics of the particles may have implications for the assessment of doses due to skin contact and inadvertent ingestion. Comparisons of the particles with the two artefacts potentially indicates that the original material has undergone significant alteration, meaning it may not be appropriate to make assumptions during dose assessment based on knowledge of the original material, if available. Due to the general lack of data available on Ra-226 particles from legacy contamination it is not possible to say whether the characteristics and diversity seen in the Dalgety Bay particles is typical of Ra-226 contamination from past military applications. Until data from other sites become available, site-specific characterisation studies will be required to understand the hazard from Ra-226 particles for the radiological protection of the public.

Chapter 3

Dosimetry of Ra-226 Particles from Legacy Contamination and Assessment Skin Dose

3 Dosimetry of Ra-226 Particles from Legacy Contamination and Assessment of Skin Dose

3.1 Introduction

Radioactive particles are physically discrete sources of radioactivity that have been released into the environment as result of past accidents, incidents, and practices (IAEA, 2011), and can present a hazard to members of the public by inadvertent skin contact. The historical use of radium in the luminising of aircraft components, and the subsequent decommissioning of those aircraft and associated waste disposal practices, has left a legacy of contamination on former military sites. One such site is Dalgety Bay in Scotland, which was host to United Kingdom Ministry of Defence air force activities between 1917 and 1959, leaving behind legacy contamination in the form of Ra-226 radioactive particles (Dale, 2013). One of the challenges for radiological protection of the public is in the assessment of absorbed doses from the inadvertent skin contact with radioactive particles found in the environment (McGuire *et al.*, 2020).

3.1.1 Skin in Radiological Protection

The objective of radiological protection is to control exposures to ionising radiation so that harmful tissue reactions are prevented, and the risks of stochastic effects are reduced to as low as reasonably achievable. Generally, the limiting of stochastic effects will also prevent the occurrence of harmful tissue reactions, but there are a few exceptions where this may not be the case. One such exception is the exposure of widely distributed tissues, such as the skin. If the skin is heterogeneously exposed, the absorbed dose to a small area may be sufficient to cause a harmful tissue reaction, even if the stochastic risk to the skin is reduced to as low as reasonably achievable. Recognising this, the ICRP recommends averaging absorbed dose to the skin over a nominal 1 cm^2, regardless of the actual area exposed, at a reference skin thickness of 70 µm (ICRP, 2007).

The primary harmful tissue reaction for large areas of skin is moist desquamation (MD) resulting from damage to the basal cells of the epidermis. However, when small areas of skin are irradiated, such as during exposure to radioactive particles, the reaction of the skin is different. The primary reaction is acute dermal ulceration (ADU) resulting from damage to fibroblasts and endothelial cells of the papillary dermis. Acute epidermal necrosis (AEN) is another harmful tissue reaction resulting from damage to suprabasal cells of the epidermis, but this is of secondary concern as it is regarded as clinically less severe (ICRP, 1992).

Studies have been undertaken on the skin of pigs using beta-emitting sources of different energies and different physical sizes to establish dose-response relationships for these reactions (Peel *et al.*, 1984; Kaurin, D G; Baum, 1997). The studies found that the type of reaction depends on the beta energy and the physical size of the source. ADU was seen when irradiation involved sources of high and intermediate beta energy, such as Sr-90/Y-90 and Tm-170, and of a size < 2 mm in diameter. MD was seen when these sources had a diameter > 5 mm. An area effect was observed for both reactions where the smaller the area, the higher the dose required to elicit the reaction. AEN was seen when irradiation involved sources of low beta energy, such as Pm-147 and Yb-125, regardless of the size of the irradiated area. Threshold doses[a] were reported for these reactions for a 16 µm skin thickness averaged over 1.1 mm^2 due to the specification of the extrapolation chamber used for the dosimetry. For practical radiological protection purposes, a threshold dose for the ICRP reference 70 µm skin thickness and nominal 1 cm^2 averaging area was approximated from these studies by calculation to give a threshold of 1 Gy (70 µm, 1 cm^2) for the prevention of ADU and AEN (Hopewell, 2000).

However, the ICRP reference skin thickness of 70 µm can be considered arbitrary in the context of radiological protection of the public from radioactive particles as the depth of the skin cells associated with harmful tissue reactions depends on age. The 70 µm skin thickness refers to the average depth of the epidermal basal cells in adults. However, skin thickness is known to vary with age and the ICRP provides reference values for the average depth of the epidermal basal cells in other age groups: 45 µm for new-born up to 5 years, 50 µm for 10 years, and 60 µm for 15 years (ICRP, 2002). These reference values are biologically relevant to MD as the target cells for this reaction are the epidermal basal cells, but the target cells for ADU and AEN are located at different depths in skin. Fibroblasts and endothelial cells involved in ADU are found at ~ 100 – 150 µm in adults and the suprabasal cells involved in AEN are found at ~ 50 µm. For children, this would equate to ~ 64 – 96 µm and ~ 32 µm based on a reference skin thickness of 45 µm. As the depth of the target cells for harmful tissue reactions depends on age, it is important to consider whether the reference 70 µm skin thickness is appropriate for assessing exposures of the skin from radioactive particles of a mixed-age population, such as the public.

The ICRP nominal 1 cm^2 averaging area can also be considered arbitrary in the context of radioactive particle exposure as the irradiated area may be smaller than 1 cm^2 and

[a] The ICRP defines a threshold dose as the dose at which it is estimated there would be a 1 % incidence of a harmful tissue reaction.

vary depending on the physical size of the particle. As the threshold dose over 1 cm^2 was approximated from the small sources (< 2 mm in diameter) used in the pig skin exposure studies averaged over 1.1 mm^2, it is important to consider whether the nominal 1 cm^2 averaging area is appropriate for assessing exposures of the skin from radioactive particles that are a different physical size. Radioactive particles isolated from the environment can exhibit a wide range for physical size, as reported in Chapter 2, which may impact the dose distribution and consequently the dose averaging, in ways that may not be reflected in threshold dose.

3.1.2 Dosimetry of Radioactive Particles

A few studies have been published that have measured absorbed doses to the skin from radioactive particles found in the environment. The absorbed doses from radioactive particles from Dounreay have been measured using radiochromic film (RCF) dosimetry (Aydarous, Charles and Darley, 2008). RCF dosimetry provides data on dose distribution with high spatial resolution down to tens of micrometres and can be tailored to study different skin thicknesses and averaging areas. The study measured 37 radioactive particles ranging from a few hundred micrometres to ~ 6 mm in length and reported absorbed dose rates ranging from 0.3 to 140 Gy hr^{-1} (70 µm, 1 cm^2). An assessment of the hazard to the public from skin contact with Dounreay particles estimated that the exposure time required to reach the threshold dose for ADU ranged from a few days to a few minutes depending on particle activity, based on the reference 70 µm skin thickness and the nominal 1 cm^2 averaging area (Harrison *et al.*, 2005).

Different techniques were used in the dosimetry of radioactive particles from Sellafield using an ion chamber contact dose rate meter and thermoluninescent dosimeters (TLD) (Clacher, 2010, 2011). Unlike RCF dosimetry, these techniques cannot provide data on the spatial distribution of the dose as ion chambers are of a fixed volume and TLD are of a fixed area. Consequently, the measurement of dose from radioactive particles using these techniques requires the application of significant correction factors. For beta-rich particles, the main contribution to skin dose was from Cs-137 and Sr-90 with absorbed dose rates up to 29.7 mGy hr^{-1}, which would take ~ 67 hours to reach the threshold. For alpha-rich particles, the main contribution to skin dose was the gamma emissions from Am-241 with absorbed dose rates up to 8 mGy hr^{-1}, which would take ~ 250 hours to reach the threshold. The assessment assumed that alpha emissions were not expected to irradiate skin cells relevant to radiological protection as the alpha emissions cannot reach the reference 70 µm skin thickness (Brown and Etherington, 2011).

Dosimetry of Ra-226 particles

There are limited data available on the dosimetry of Ra-226 particles as the only study to measure the absorbed dose rate to skin from Ra-226 particles was undertaken using Ra-226 particles from Dalgety Bay and reported to the Scottish Environment Protection Agency (SEPA) (Charles and Gow, 2010). Measurements of absorbed dose rate were undertaken using RCF dosimetry for ten particles over a range of skin depths from 15 to 351 µm averaged over 1 cm^2. The beta emissions were the dominant contributor to the absorbed dose, with an indication of a small contribution from the alpha emissions at 15 µm. The next skin depth used in this study was 51 µm, which gave no indication of any contribution from alpha emissions, but measurements using a count rate meter gave an alpha emission range in tissue of ~ 25 µm. An assessment of the hazard to the public from skin contact with Dalgety Bay particles estimated that the exposure time required to reach the threshold dose for ADU ranged from ~ 2 months for the lowest activity particles to ~ 12 minutes for the highest activity particles (Dale, 2013). Similar to the assessments for other particles, this assessment was based on the reference 70 µm skin thickness and the nominal 1 cm^2 averaging area but acknowledged that further work was required to establish whether this was appropriate. Furthermore, the UK Government Committee on the Medical Aspects of Radiation in the Environment (COMARE) recommended that further research should be undertaken regarding skin doses from radioactive particles, with particular reference to young children (COMARE, 2014).

3.1.3 Radiochromic Film Dosimetry

RCF was originally developed as an alternative to the traditional silver-halide radiographic films used in medial dosimetry. It undergoes an automatic, permanent colour change upon exposure to ionising radiation. A polymerisation reaction occurs in the active layer of the film that causes the development of a blue colour, the intensity of which can be related to absorbed dose after suitable calibration (Devic, Tomic and Lewis, 2016). Furthermore, it can be scanned using readily available document scanners. The RCF manufacturer recommends using the Epson Expression 11000XL Scanner, but other models are also suitable. A study has compared its predecessor, the Epson 10000XL Scanner, and the Epson Perfection V700 (both now superseded) and found them to be of comparable performance (Alnawaf, Yu and Butson, 2012).

At the time of the RCF dosimetry undertaken on the Dounreay and Dalgety Bay particles, the active layer of most RCF products was bound between two layers of PET, but it was necessary for the RCF to be supplied without a PET top layer (i.e., unlaminated) to

investigate the absorbed dose for a range of skin thicknesses. HD-810 (now superseded) was the only form of RCF available unlaminated, but it required a minimum absorbed dose of 10 Gy resulting in exposure times that were very long, up to 18 weeks for the lowest activity Dalgety Bay particles (Charles and Gow, 2010). A newer version of RCF has since become available that has a much lower dose range and is available unlaminated. The EBT3 is a form of RCF designed for the measurement of absorbed doses from 0.2 to 10 Gy. The standard product consists of a 125µm polyethylene terephthalate (PET) base layer, a 28µm active layer, and a 125µm PET top layer. However, it can be supplied unlaminated where it is simply half of the standard product; the 125 µm PET base layer and a 14 µm active layer.

3.1.4 Aim and Objectives

The variation in skin thickness with age, as well as the potential contribution from alpha emissions, may have implications for the use of the reference 70 µm skin thickness in the assessment of skin dose from Ra-226 particles. Furthermore, the wide range of particle physical size may have implications for the use of the nominal 1 cm^2 averaging area. The aim of this research was to investigate whether the reference 70 µm skin thickness and nominal 1 cm^2 skin averaging area are appropriate for the assessment of absorbed dose to the skin from inadvertent contact with Ra-226 particles by the public. This aim was achieved through the following objectives:

I. Develop a dosimetry technique using GafChromic™ EBT3 RCF for the measurement of absorbed dose rate from Ra-226 particles, including alpha emissions.

II. Measure the absorbed dose rate over a range of skin thicknesses and skin averaging areas to determine the depth-dose and lateral-dose distributions.

III. Assess whether the reference 70 µm skin thickness and nominal 1 cm^2 averaging area are sufficient to prevent harmful tissue reactions from inadvertent skin contact with Ra-226 particles by the public.

3.2 Materials and Methods

3.2.1 Sample Selection

The Ra-226 sample inventory from Dalgety Bay collected by SEPA was made available for this research. Figure 3.1 shows the nine particles selected for this study. These particles have been physically, chemically, and radiologically characterised as reported in Chapter 2 and were selected to represent a range of activities and physical sizes.

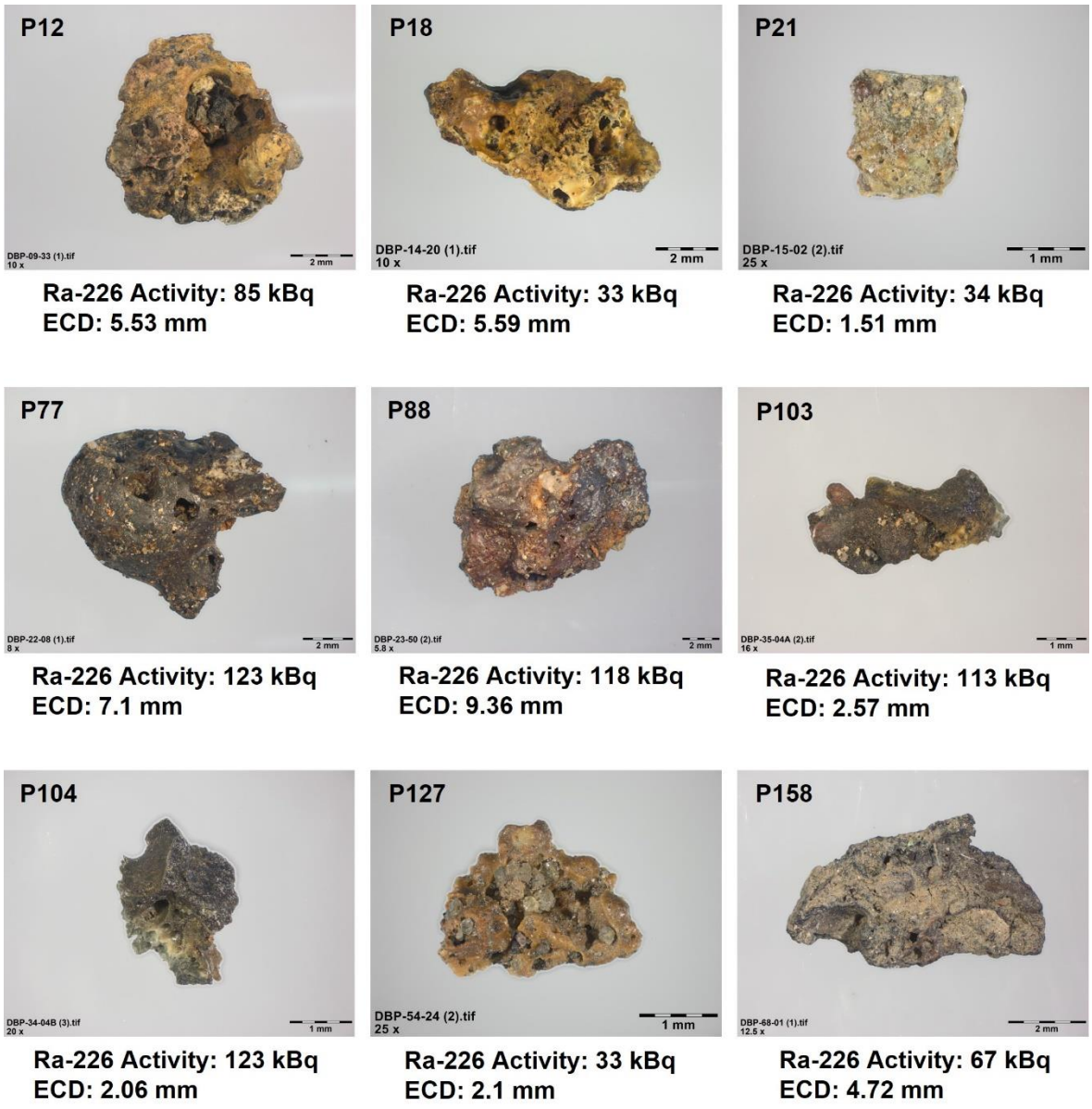

Figure 3.1 Ra-226 particles, their activity, and equivalent circular diameter (ECD)

3.2.2 RCF Dosimetry

The RCF used in this study was the unlaminated version of GafChromic™ EBT3 manufactured by Ashland, USA and supplied by Vertec, UK, consisting of a 125 µm PET base layer and a 14 µm active layer. The thickness of the RCF PET base layer and active layer was checked using a Wiha digital calliper. The RCF was measured with and without the active layer, which was removed from a section of RCF using a scalpel and was found to be in accordance with the manufacturer specifications. To simulate different skin thicknesses, PET sheets of different thicknesses were used to act as absorbers. The PET used was Hostaphan® RNK (12 and 23 µm) and Hostaphan® RN (36, 50, 75, 100, 125, and 350 µm) manufactured by Mitsubishi Polyester Film GmbH, Germany and supplied by UK Insulations Ltd, UK. The thickness of the PET was checked using a Wiha digital calliper and was found to be in accordance with the manufacturer specifications.

RCF & PET Preparation

The RCF was supplied as sheets each measuring 20.32 by 25.4 cm (i.e., 8" by 10"), which were equally divided into 25 rectangular pieces (4.06 cm by 5.08 cm). Using a cutting board and ruler, the RCF was scored using a scalpel on the side with the active layer. Each piece was labelled with a unique identifier to ensure traceability. The RCF pieces were cut from the sheets using dissection scissors for use in exposures, as required. The top right-hand corner of each piece was cut off as an intrinsic means to ensure that each RCF piece was exposed and scanned in the same orientation. As RCF acts as a polariser, it is critical to maintain the same orientation across all exposures (Devic, Tomic and Lewis, 2016). The PET was supplied as sheets each measuring 21.0 by 29.7 cm (i.e., A4), which were equally divided into 25 rectangular pieces (5.25 by 5.94 cm) and labelled with the relevant thickness. All handling of the RCF and PET was done wearing gloves and the RCF was stored in the manufacturers packaging, and inside a light-proof black bag, when not in use.

RCF Calibration Exposures

The RCF was calibrated using a Sr/Y-90 source within a Risø TL/OSL Reader by the UK Health Security Agency (Eakins, Hager and Tanner, 2016). Small samples of the RCF (25 mm^2) were exposed to known doses of radiation from the Sr/Y-90 source at a distance sufficient to provide a uniform exposure. The optimum dose range specified by the manufacturer for EBT3 is 0.2 to 10 Gy so a series of 12 calibration exposures at different doses within this range was obtained. The manufacturer specifies that the uniformity of response from EBT3 is ± 3 %, but as the pieces of RCF used in the calibration exposures were small relative to the size of the sheets, multiple sets of

calibration exposures were obtained. Five sets were obtained from different areas of the same RCF sheet to account for any intra-sheet variability, and a further 4 were taken from different RCF sheets to account for any inter-sheet variability.

RCF Ra-226 Particle Exposures

Exposures were undertaken at 12 simulated skin thicknesses with the Ra-226 particles in two different physical orientations (A and B), giving a total of 24 exposures per sample. For the surface exposures, one RCF piece was simply placed on a polymethyl methacrylate (PMMA) block, to simulate backscatter from underlying body tissues. For exposures using 12, 23, 36, 75, 100, or 350 µm PET, one RCF piece was placed on a PMMA block and covered with one of the corresponding PET pieces. For exposures using 50 or 125 µm PET, two or three RCF pieces were stacked directly on top of each other respectively, placed on a PMMA block, and covered with one of the corresponding PET pieces. Figure 3.2 shows the different configurations of RCF and PET to achieve the different skin thicknesses. For each exposure, in addition to the unique identifier, each piece of RCF was labelled with the sample name, exposure date and start time, PET thickness, sample orientation (A or B), and position in the stack, where applicable.

Although RCF and PET exhibit near-tissue equivalence, a correction is needed to account for the slightly lower density of skin. The density of skin is 1.1 g cm^{-3} whereas the density of the RCF and PET is specified by the manufacturers to be 1.35 and 1.4 g cm^{-3}, respectively. Figure 3.2 shows the tissue-equivalence of the 12 simulated skin depths. The values were calculated for the middle of the active layer, shown using a dashed line, as energy is deposited throughout the 14 µm active layer.

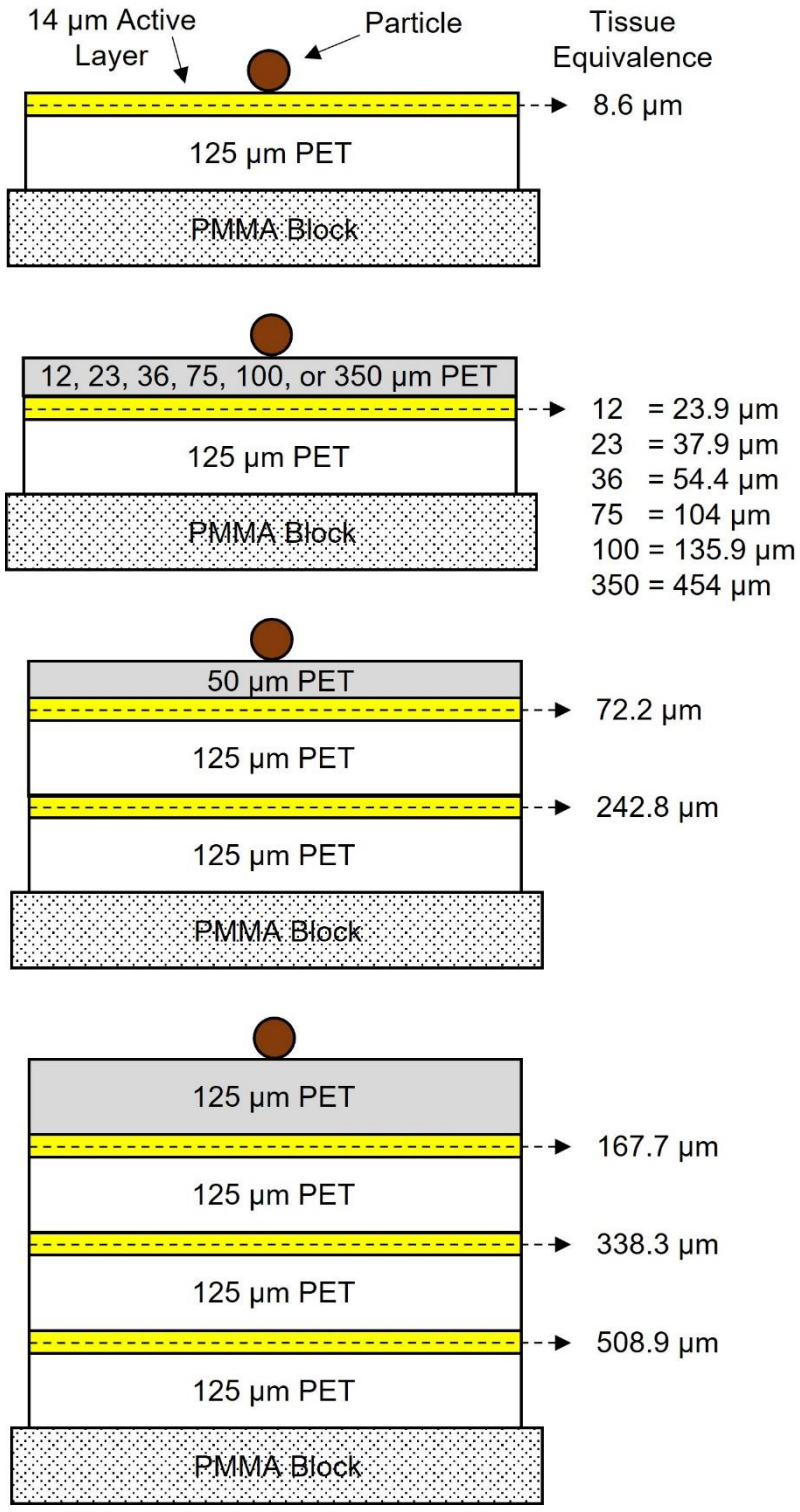

Figure 3.2 The four different configurations of RCF and PET to measure the absorbed dose rate at different simulated skin thicknesses and their tissue equivalance (NB: not to scale)

Due to the different characteristics of the samples, the exposure times required to deliver a dose within the optimum dose range of the film were different for each sample. The exposure times for each sample were optimised through a series of test exposures to deliver peak absorbed doses towards the upper end of the optimum dose range, allowing for as much of the lower doses areas to fall within the range as possible.

The exposures were conducted in MDF boxes lined with lead sheet, with three samples per box, shielded from each other using PMMA blocks. The samples were placed on top of the exposure stacks, firstly in orientation A for all skin depths, followed by orientation B. The samples were stored in their respective orientations between exposures and photographed *in-situ* to provide a reference should the orientation needed to be reset. During the exposures, each stack was covered with a black cardboard box to block out light, and each MDF box covered with a piece of lead sheet to provide shielding. At the end of each exposure, the samples were removed from the exposure stacks and the RCF pieces were stored in a light-proof black bag for a post-exposure development period of 1 week prior to scanning, consistent with the calibration exposures.

RCF Am-241 Source Exposures

To investigate a potential contribution to skin dose from alpha particles, an alpha reference source was used to expose the RCF at the thinner simulated skin thicknesses using the 12, 23, 36 and 50 µm PET, as well as a surface exposure. The source was an Am-241 source (40.1 kBq with 3.5 % relative uncertainty, S3-214, Eckert & Ziegler) that was electrodeposited as a diffusion bonded oxide onto a platinum surface and fixed into an aluminium holder. As it is essentially an unsealed source, it is recessed into the aluminium holder preventing direct contact to maintain its integrity. The recess is 380 µm deep, creating an air gap between the source and the RCF, which contributes negligible additional absorption with a tissue equivalent thickness of 0.42 µm. The active area of the source is 5 mm in diameter and was manufactured and calibrated to NIST and DAKKS standards, respectively.

RCF Scanning & Image Processing

The RCF was scanned using an Epson Perfection V800 Film and Photo Flatbed Scanner. The scanner was used in Reflection Mode with all the image correction features turned off. All scans were performed using the Positive Film type, in 48-bit RGB colour, at a resolution of 1200 dpi (i.e., 1 pixel = 0.0004 mm ^{2}), and saved in Tagged Image File Format (TIFF). The RCF pieces were scanned individually so they could be placed on the same area of the scanner and were all scanned in the same orientation. A median filter (radius = 20 pixels) was applied to the values to smooth out any speckles present

in the images that would have otherwise contributed to the results or affected the positioning of the averaging areas. The images were processed to extract the red pixel values for each individual pixel as these exhibit the greatest degree of change per unit dose.

For the calibration exposures, image analysis was done manually using Fiji, an open-source software package specialising in biological image analysis (Schindelin *et al.*, 2012). Red pixel values were extracted from each calibration exposure from a square area consisting of 10,000 pixels. Additionally, red pixel values for zero dose were obtained from unexposed film. As the calibration exposures were uniform, the mean red pixel value for each dose point across the 9 exposure sets were plotted against the known doses and fitted with a local polynomial regression (loess) model to form the calibration curve as shown in Figure 3.3. The intensity of the colour change of the RCF is related to the dose, where higher doses cause a change to a darker blue, which results in lower red pixel values.

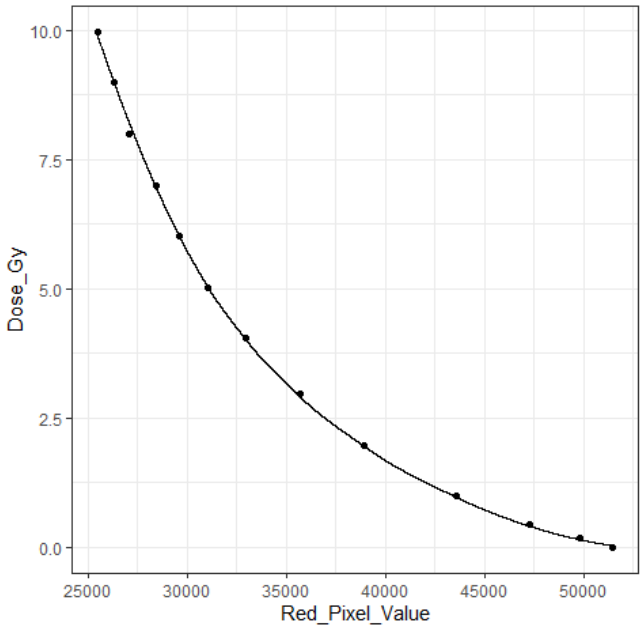

Figure 3.3 Calibration curve for RCF exposed to known doses from a Sr/Y-90 source

For the Am-241 exposures, image analysis was also done manually using Fiji (Schindelin *et al.*, 2012). Red pixel values were extracted from each exposure from a circular area of 5 mm in diameter. As the Am-241 exposures were uniform, the mean red pixel value from each exposure was converted to absorbed dose (Gy) using the calibration curve and subsequently converted to absorbed dose rate (Gy hr^{-1}) using the exposure times.

For the Ra-226 particle exposures, image analysis was automated using R, a language and environment for statistical computing (R Core Team, 2022) to give the absorbed dose rate averaged over a range of circular areas (1, 2, 5, 10, 20, 35, 50, 75, and 100 mm ^{2}) centred on the peak absorbed dose rate. Figure 3.4 shows the averaging areas used in this study. As the exposures from the Ra-226 particles were non-uniform, the red pixel values for each individual pixel were converted to absorbed dose (Gy) using the calibration curve and subsequently converted to absorbed dose rate (Gy hr $^{-1}$) using the exposure times. Absorbed dose rate maps were plotted showing the lateral dose distribution at each skin thickness for all particles in both orientations. From each map, the mean absorbed dose rate was calculated for the 9 averaging areas.

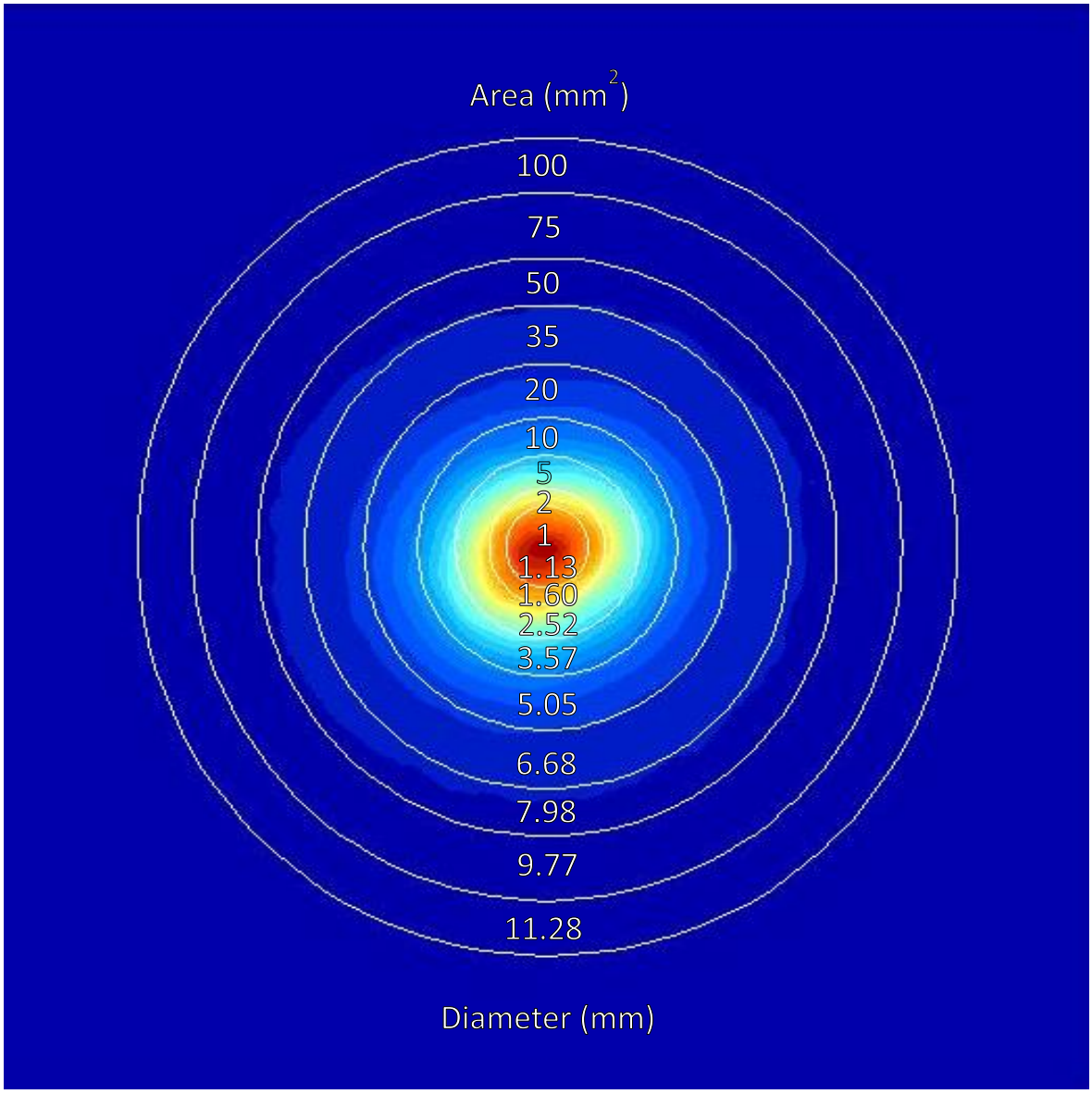

Figure 3.4 The circular averaging areas (mm ^{2}) and their corresponding diameter (mm)

3.3 Results

3.3.1 Absorbed dose rate from Ra-226 Particles

The RCF dosimetry has shown that the absorbed dose rate from Ra-226 particles exhibited inter- and intra-particle variation. Figure 3.5 shows an absorbed dose rate map for each particle in the orientation (A or B) that gave the highest dose rate at a simulated skin thickness of 72.2 µm over a 1 cm ^{2} averaging area.

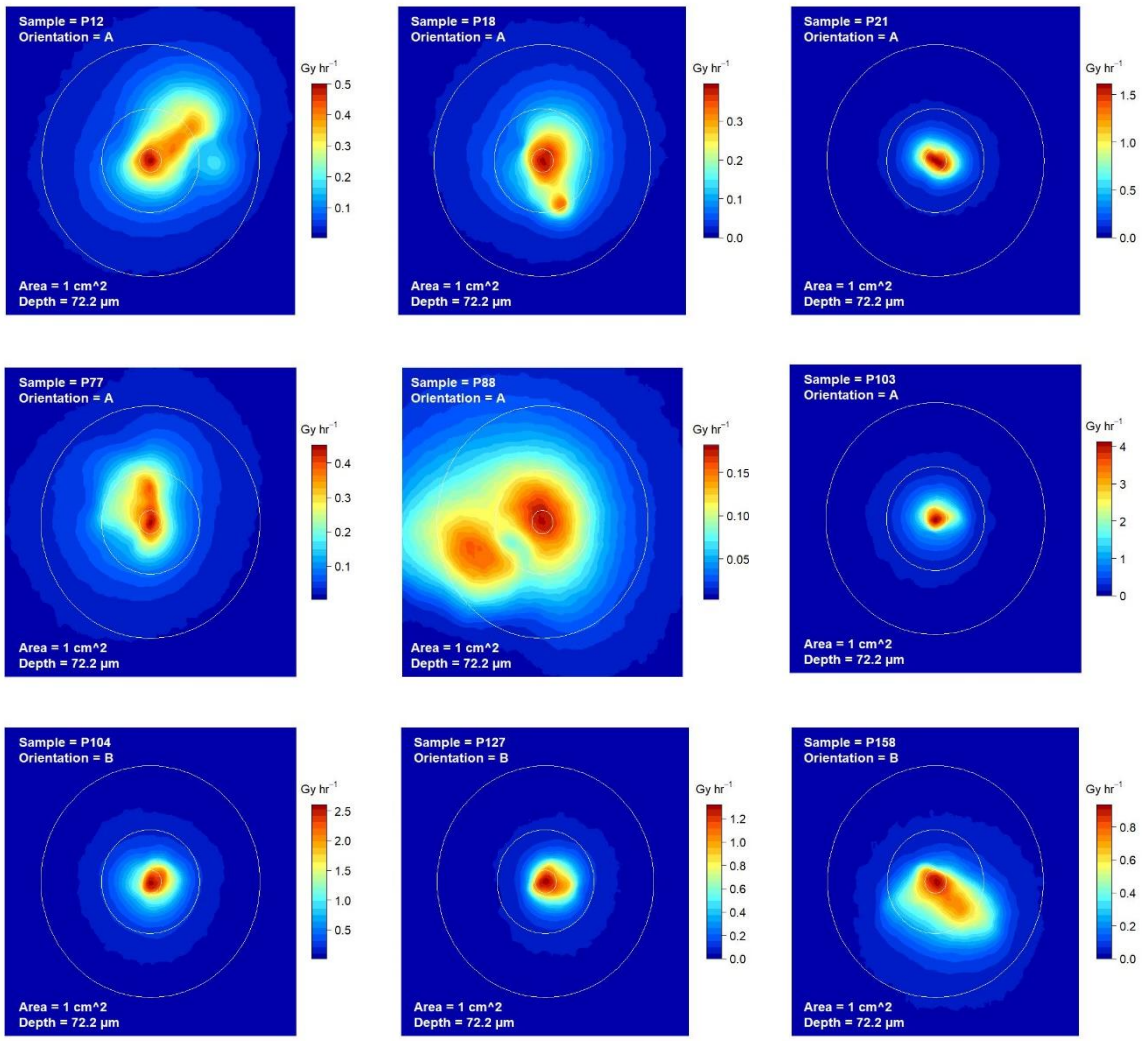

Figure 3.5 Absorbed dose rate maps for each particle in the orientation that gave the highest dose rate at a simulated skin thickness of 72.2 µm over a 1 cm ^{2} averaging area (circles marked are for 1 mm ^{2}, 20 mm ^{2}, and 1 cm ^{2})

The highest absorbed dose rate (72.2 µm, 1 cm ^{2}) was from P103 at 0.2 Gy hr $^{-1}$, which would reach the 1 Gy threshold dose in ~ 5 hours. The lowest absorbed dose rate was from P18 at 0.06 Gy hr $^{-1}$, which would take > 16 hours to reach the threshold. However,

it can be seen in Figure 3.5 that the peak absorbed dose rates (72.2 µm, 0.0004 mm^2, i.e., 1 pixel) were significantly higher than the absorbed dose rates averaged over 1 cm^2. For comparison, the peak absorbed dose rate for P103 was 4.1 Gy hr^{-1} and 0.4 Gy hr^{-1} for P18, which were greater than the absorbed dose rates averaged over 1 cm^2 by factors of 20 and 6.5, respectively. For inter-particle comparison, the absorbed dose rate per unit of activity was calculated using the Ra-226 activities reported in Chapter 2. The highest absorbed dose rate (72.2 µm, 1 cm^2) per unit activity (MBq) was from P127 at 2.5 Gy hr^{-1} MBq^{-1} and the lowest was from P77 at 0.6 Gy hr^{-1} MBq^{-1}. Interestingly, P127 was the particle with the lowest Ra-226 activity and was one of the physically smallest, whereas P77 was the particle with the highest Ra-226 activity and was one of the physically largest.

The absorbed dose rate measurements in the two different orientations have shown there was also intra-particle variability. The largest difference was seen from P18 where the absorbed dose rate (72.2 µm, 1 cm^2) in Orientation A was higher than Orientation B by a factor of 3.4, suggesting the activity is heterogeneously distributed within the particle. In contrast, the smallest difference was seen from P127 where Orientation B was higher than Orientation A by a factor of 1.02, suggesting the activity distribution is effectively homogeneous. Additionally, Figure 3.5 shows that the absorbed dose rate exhibits heterogeneity within a single orientation and that the peak absorbed dose rate is not necessarily at the centre of the dose distribution. The physically smaller particles P21, P103, P104, and P127 had peak absorbed dose rates close to the centre of their lateral dose distributions, which radiated out fairly evenly in all directions. In contrast, the physically larger particles P12, P18, P77, P88, and P158 had peak absorbed dose rates that were offset from the centre of fairly uneven lateral dose distributions.

The size of the irradiated area varied considerably between the particles. The particle that irradiated the largest area was P88 as can be seen in Figure 3.5 where the lateral dose distribution was over a large proportion of the 1 cm^2 averaging area. P88 was the physically largest particle in this study with an ECD of 9.36 mm, whereas some of the other particles were significantly smaller, such as P21, P103, P104, and P127. The irradiated area from these particles was significantly smaller where a large proportion of the 1 cm^2 averaging area was effectively unexposed. Between these two extremes was the irradiated areas from P12, P18, P77, and P158, which had a higher proportion of low dose rate areas, rather than unexposed areas.

3.3.2 Depth-dose and lateral-dose distributions

The absorbed dose rate decreased with increasing skin thickness for all particles, rapidly at first followed by a more gradual decline. Figure 3.6 shows the absorbed dose rate for a range of skin thicknesses from 8.6 to 508.9 µm averaged over 1 cm ^{2}.

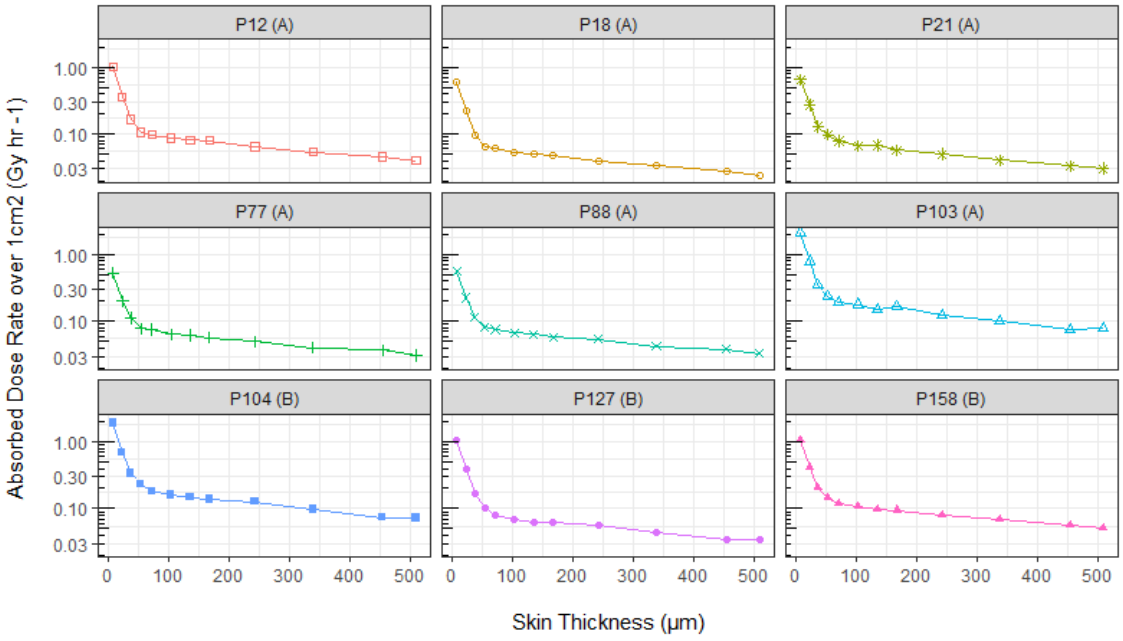

Figure 3.6 Absorbed dose rate (Gy hr $^{-1}$) for a range of skin thicknesses from 8.6 to 508.9 µm averaged over 1 cm ^{2}

The highest absorbed dose rates were at 8.6 µm and ranged from 0.53 to 2.06 Gy hr^{-1} averaged over 1 cm ^{2}. The absorbed dose rates decreased rapidly over the thinner skin thicknesses, with the curve changing slope after 37.9 µm for P12, P18, P77, P88, and P158, and 54.4 µm for P21, P103, P104, and P127. The absorbed dose rates continued to decrease, but with a shallower slope, to reach the lowest absorbed dose rates at 508.9 µm ranging from 0.01 to 0.08 Gy hr^{-1}. The abrupt change in slope provides evidence that alpha particles were contributing to the absorbed dose rate at thinner simulated skin thicknesses. The exposures using the Am-241 source exhibited a similar range in skin for alpha particles. The reduction in the absorbed dose rate with depth from alpha particles was rapid, where the absorbed dose rates at 23.9 and 37.9 µm were 40.7 and 7.1 % of the dose rate at 8.6 µm, respectively. Beyond 37.9 µm, the absorbed dose rate from alpha particles was effectively zero where the dose rates at 54.4 and 72.2 µm were respectively 0.009 and 0.004 % of the dose rate at 8.6 µm.

The absorbed dose rate decreased with increasing skin averaging area for all particles, but for some the decrease was more pronounced than others. Figure 3.7 shows the absorbed dose rate for a range of skin averaging areas from 1 mm ^{2} to 1 cm ^{2} at a skin thickness of 72.2 µm.

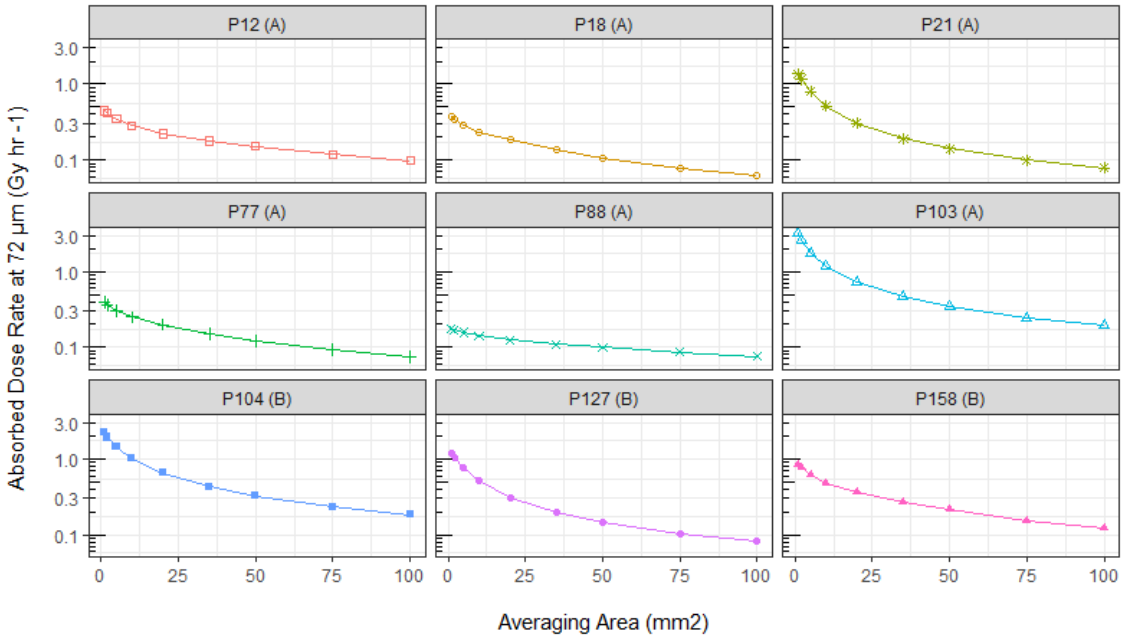

Figure 3.7 Absorbed dose rate (Gy hr $^{-1}$) for a range of skin averaging areas from 1 mm ^{2} to 1 cm ^{2} at a skin thickness of 72.2 µm

The highest dose rates were over 1 mm ^{2} and ranged from 0.2 to 3.2 Gy hr^{-1} at 72.2 µm, which decreased to 0.06 to 0.2 Gy hr^{-1} over 1 cm ^{2}, but the rate at which the absorbed dose rates decreased was dependent on the size of the particle. The physically smaller particles P21, P103, P104, and P127, irradiated a relatively small area confined to 1 or 2 mm ^{2} as shown in Figure 3.5. As the absorbed dose rate was averaged over increasingly larger areas, the absorbed dose rates for the smaller particles quickly started incorporating a high proportion of low dose or zero dose areas, rapidly reducing their mean absorbed dose rates. In contrast, the physically larger particles P12, P18, P77, P88, and P158 irradiated larger areas as shown in Figure 3.5, which had smaller proportions of low dose or zero dose areas. This is reflected in the lateral-dose distribution curves where they are noticeably steeper for the physically smaller particles compared to the physically larger particles.

3.3.3 Absorbed dose rate relative to 70 µm, 1 cm ^{2}

To understand whether the reference 70 µm skin thickness and the nominal 1 cm ^{2} averaging area are appropriate for radioactive particles, it is necessary to compare the absorbed dose rates for different skin thicknesses and averaging areas relative to the 70 µm and 1 cm ^{2} used for radiological protection. Figure 3.8 shows the absorbed dose rate for all skin thicknesses and averaging areas relative to the absorbed dose rate at 72.2 µm averaged over 1 cm ^{2} for the nine particles.

The skin depths from 104 to 167.7 µm approximate to the depth of fibroblasts and endothelial cells in adults, which are the target cells in ADU. The relative absorbed dose rate at these depths ranged from 0.73 to 0.92 Gy hr $^{-1}$ averaged over 1 cm ^{2}. The skin depths from 54.4 to 104 µm approximate to the depth of fibroblasts and endothelial cells in children. The relative absorbed dose rate was slightly higher at these depths and ranged from 0.85 to 1.2 Gy hr $^{-1}$ averaged over 1 cm ^{2}. The skin depth of 54.4 µm approximates to the depth of suprabasal cells in adults, which are the target cells in AEN. The relative absorbed dose rate at this depth ranged from 1 to 1.2 Gy hr $^{-1}$ averaged over 1 cm ^{2}. The skin depth of 37.9 µm approximates to the depth of suprabasal cells in children. The relative absorbed dose rate at these depths was higher and ranged from 1.5 to 2 Gy hr $^{-1}$ averaged over 1 cm ^{2}.

The varying effect of dose averaging can be seen across the particles where the relative absorbed dose rate at 72.2 µm averaged over 1 mm ^{2} ranges from 2.3 to 17 Gy hr $^{-1}$. The physically smaller particles, P21, P103, P104, and P127, had higher relative absorbed dose rates of 17, 16, 12, and 15 Gy hr $^{-1}$ respectively, whereas for the physically larger particles, P12, P18, P77, P88, and P158 it was 4.6, 6.0, 5.3, 2.3, and 7.0 Gy hr $^{-1}$. As can be seen from Figure 3.5, the larger particles irradiated a larger area and are therefore less sensitive to averaging compared to the smaller particles. For comparison, the study on the skin of pigs by Baum and Kaurin derived absorbed doses averaged over 1.1 mm ^{2} relative to 1 Gy (70 µm, 1 cm ^{2}). The relative absorbed doses at 70 µm averaged over 1.1 mm ^{2} where higher and ranged from 42 to 80 Gy hr^{-1} across the UC_2, Tm-170, Yb- 125, and Sc-46 sources used in the study (Kaurin, D G; Baum, 1997).

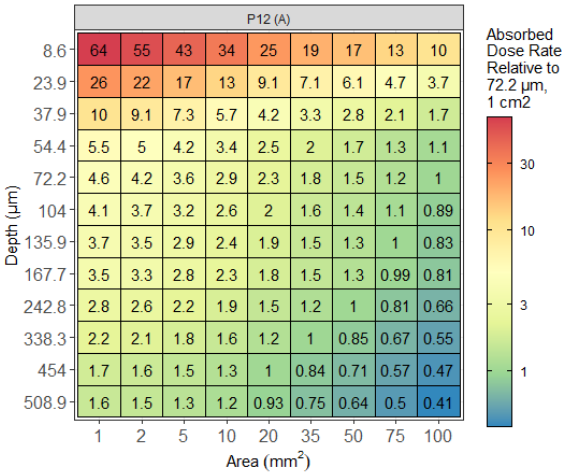
P12 (A)
Depth (µm)
8.6 64 55 43 34 25 19 17 13 10
23.9 26 22 17 13 9.1 7.1 6.1 4.7 3.7
37.9 10 9.1 7.3 5.7 4.2 3.3 2.8 2.1 1.7
54.4 5.5 5 4.2 3.4 2.5 2 1.7 1.3 1.1
72.2 4.6 4.2 3.6 2.9 2.3 1.8 1.5 1.2 1
104 4.1 3.7 3.2 2.6 2 1.6 1.4 1.1 0.89
135.9 3.7 3.5 2.9 2.4 1.9 1.5 1.3 1 0.83
167.7 3.5 3.3 2.8 2.3 1.8 1.5 1.3 0.99 0.81
242.8 2.8 2.6 2.2 1.9 1.5 1.2 1 0.81 0.66
338.3 2.2 2.1 1.8 1.6 1.2 1 0.85 0.67 0.55
454 1.7 1.6 1.5 1.3 1 0.84 0.71 0.57 0.47
508.9 1.6 1.5 1.3 1.2 0.93 0.75 0.64 0.5 0.41
1 2 5 10 20 35 50 75 100
Area (mm2)
Absorbed Dose Rate Relative to 72.2 µm, 1 cm2
30
10
3
1

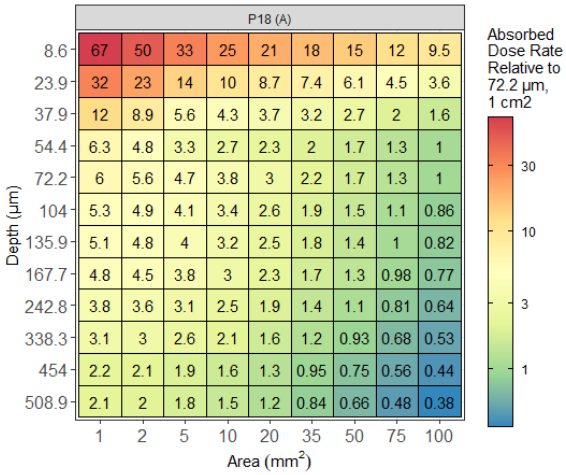
P18 (A)
Depth (µm)
8.6 67 50 33 25 21 18 15 12 9.5
23.9 32 23 14 10 8.7 7.4 6.1 4.5 3.6
37.9 12 8.9 5.6 4.3 3.7 3.2 2.7 2 1.6
54.4 6.3 4.8 3.3 2.7 2.3 2 1.7 1.3 1
72.2 6 5.6 4.7 3.8 3 2.2 1.7 1.3 1
104 5.3 4.9 4.1 3.4 2.6 1.9 1.5 1.1 0.86
135.9 5.1 4.8 4 3.2 2.5 1.8 1.4 1 0.82
167.7 4.8 4.5 3.8 3 2.3 1.7 1.3 0.98 0.77
242.8 3.8 3.6 3.1 2.5 1.9 1.4 1.1 0.81 0.64
338.3 3.1 3 2.6 2.1 1.6 1.2 0.93 0.68 0.53
454 2.2 2.1 1.9 1.6 1.3 0.95 0.75 0.56 0.44
508.9 2.1 2 1.8 1.5 1.2 0.84 0.66 0.48 0.38
1 2 5 10 20 35 50 75 100
Area (mm2)
Absorbed Dose Rate Relative to 72.2 µm, 1 cm2
30
10
3
1

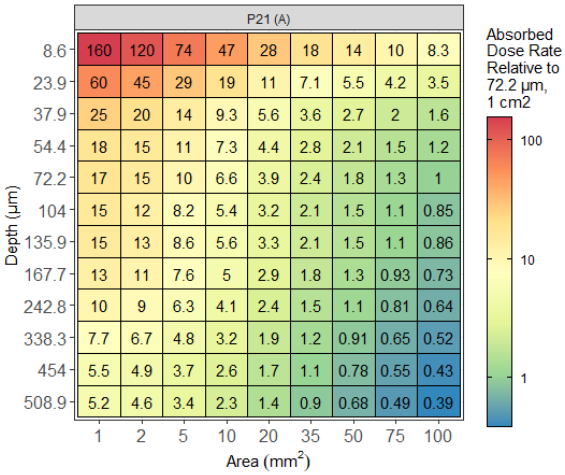
P21 (A)
Depth (µm)
8.6 160 120 74 47 28 18 14 10 8.3
23.9 60 45 29 19 11 7.1 5.5 4.2 3.5
37.9 25 20 14 9.3 5.6 3.6 2.7 2 1.6
54.4 18 15 11 7.3 4.4 2.8 2.1 1.5 1.2
72.2 17 15 10 6.6 3.9 2.4 1.8 1.3 1
104 15 12 8.2 5.4 3.2 2.1 1.5 1.1 0.85
135.9 15 13 8.6 5.6 3.3 2.1 1.5 1.1 0.86
167.7 13 11 7.6 5 2.9 1.8 1.3 0.93 0.73
242.8 10 9 6.3 4.1 2.4 1.5 1.1 0.81 0.64
338.3 7.7 6.7 4.8 3.2 1.9 1.2 0.91 0.65 0.52
454 5.5 4.9 3.7 2.6 1.7 1.1 0.78 0.55 0.43
508.9 5.2 4.6 3.4 2.3 1.4 0.9 0.68 0.49 0.39
1 2 5 10 20 35 50 75 100
Area (mm2)
Absorbed Dose Rate Relative to 72.2 µm, 1 cm2
100
10
1

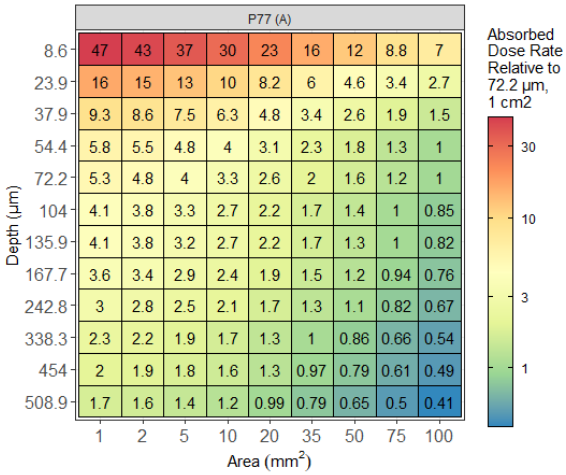
P77 (A)
Depth (µm)
8.6 47 43 37 30 23 16 12 8.8 7
23.9 16 15 13 10 8.2 6 4.6 3.4 2.7
37.9 9.3 8.6 7.5 6.3 4.8 3.4 2.6 1.9 1.5
54.4 5.8 5.5 4.8 4 3.1 2.3 1.8 1.3 1
72.2 5.3 4.8 4 3.3 2.6 2 1.6 1.2 1
104 4.1 3.8 3.3 2.7 2.2 1.7 1.4 1 0.85
135.9 4.1 3.8 3.2 2.7 2.2 1.7 1.3 1 0.82
167.7 3.6 3.4 2.9 2.4 1.9 1.5 1.2 0.94 0.76
242.8 3 2.8 2.5 2.1 1.7 1.3 1.1 0.82 0.67
338.3 2.3 2.2 1.9 1.7 1.3 1 0.86 0.66 0.54
454 2 1.9 1.8 1.6 1.3 0.97 0.79 0.61 0.49
508.9 1.7 1.6 1.4 1.2 0.99 0.79 0.65 0.5 0.41
1 2 5 10 20 35 50 75 100
Area (mm2)
Absorbed Dose Rate Relative to 72.2 µm, 1 cm2
30
10
3
1

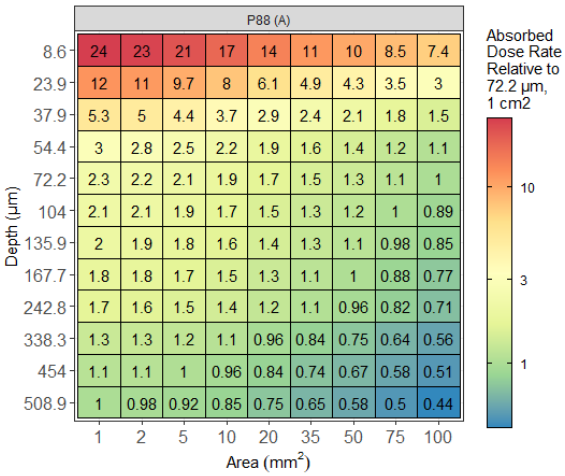
P88 (A)
Depth (µm)
8.6 24 23 21 17 14 11 10 8.5 7.4
23.9 12 11 9.7 8 6.1 4.9 4.3 3.5 3
37.9 5.3 5 4.4 3.7 2.9 2.4 2.1 1.8 1.5
54.4 3 2.8 2.5 2.2 1.9 1.6 1.4 1.2 1.1
72.2 2.3 2.2 2.1 1.9 1.7 1.5 1.3 1.1 1
104 2.1 2.1 1.9 1.7 1.5 1.3 1.2 1 0.89
135.9 2 1.9 1.8 1.6 1.4 1.3 1.1 0.98 0.85
167.7 1.8 1.8 1.7 1.5 1.3 1.1 1 0.88 0.77
242.8 1.7 1.6 1.5 1.4 1.2 1.1 0.96 0.82 0.71
338.3 1.3 1.3 1.2 1.1 0.96 0.84 0.75 0.64 0.56
454 1.1 1.1 1 0.96 0.84 0.74 0.67 0.58 0.51
508.9 1 0.98 0.92 0.85 0.75 0.65 0.58 0.5 0.44
1 2 5 10 20 35 50 75 100
Area (mm2)
Absorbed Dose Rate Relative to 72.2 µm, 1 cm2
10
3
1

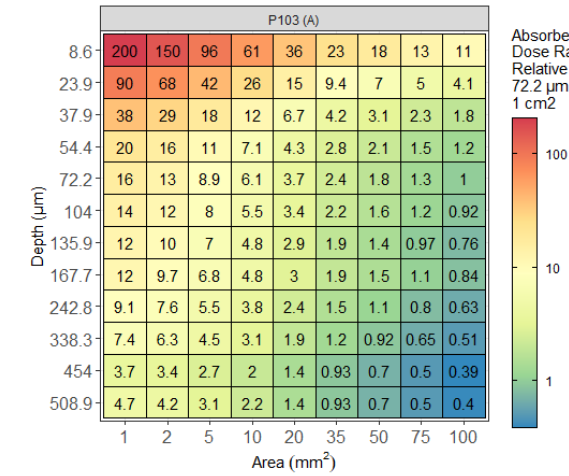
P103 (A)
Depth (µm)
8.6 200 150 96 61 36 23 18 13 11
23.9 90 68 42 26 15 9.4 7 5 4.1
37.9 38 29 18 12 6.7 4.2 3.1 2.3 1.8
54.4 20 16 11 7.1 4.3 2.8 2.1 1.5 1.2
72.2 16 13 8.9 6.1 3.7 2.4 1.8 1.3 1
104 14 12 8 5.5 3.4 2.2 1.6 1.2 0.92
135.9 12 10 7 4.8 2.9 1.9 1.4 0.97 0.76
167.7 12 9.7 6.8 4.8 3 1.9 1.5 1.1 0.84
242.8 9.1 7.6 5.5 3.8 2.4 1.5 1.1 0.8 0.63
338.3 7.4 6.3 4.5 3.1 1.9 1.2 0.92 0.65 0.51
454 3.7 3.4 2.7 2 1.4 0.93 0.7 0.5 0.39
508.9 4.7 4.2 3.1 2.2 1.4 0.93 0.7 0.5 0.4
1 2 5 10 20 35 50 75 100
Area (mm2)
Absorbed Dose Rate Relative to 72.2 µm, 1 cm2
100
10
1

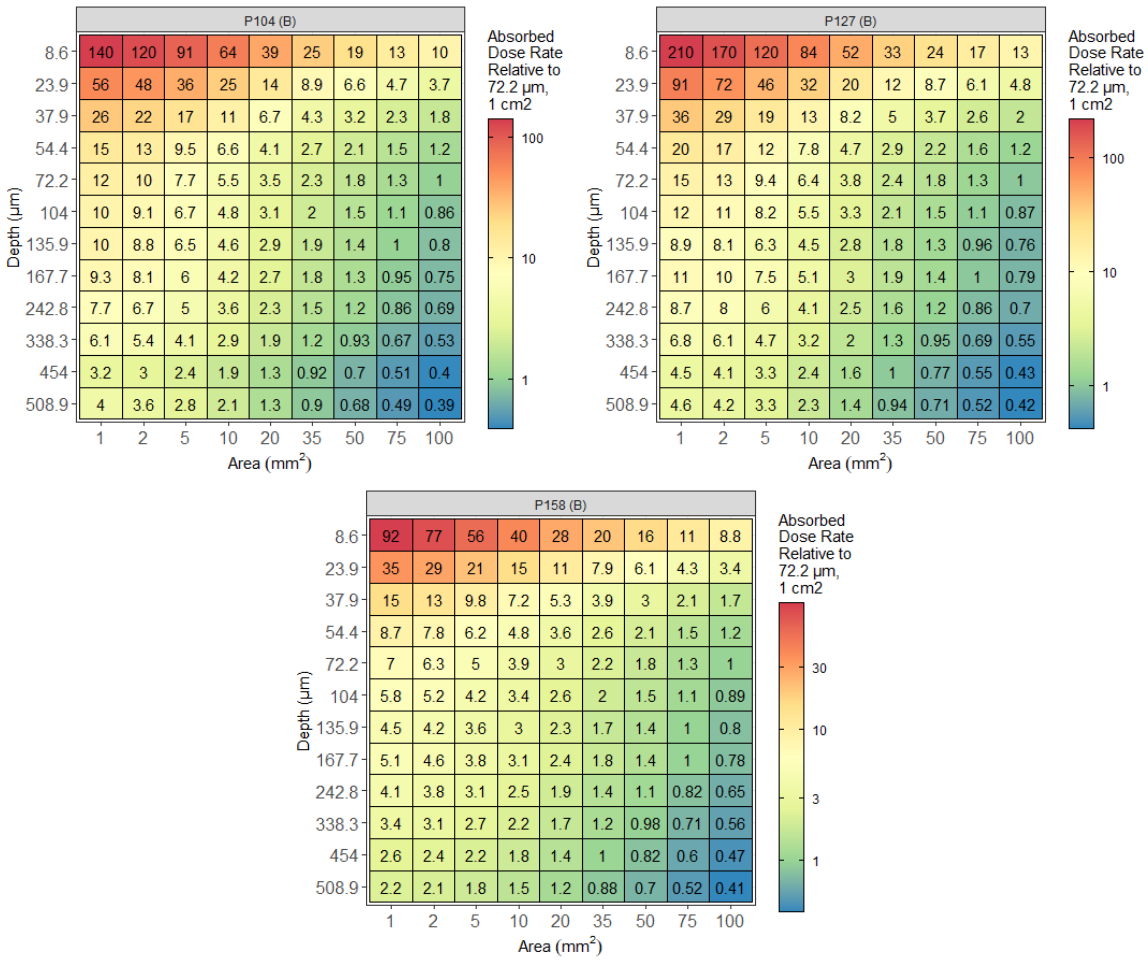

Figure 3.8 Absorbed dose rate for all skin thicknesses and averaging areas relative to the absorbed dose rate at 72.2 µm averaged over 1 cm ^{2} for the nine particles

3.4 Discussion

3.4.1 Variability of absorbed dose rate from Ra-226 particles

The absorbed dose rates at 72.2 µm skin thickness averaged over 1 cm ^{2} highlighted some important considerations for dosimetry and the assessment of skin dose. Firstly, the variable absorbed dose rates from the particles required RCF exposure times to be optimised to ensure the exposures were within the calibrated dose range (0.2 – 10 Gy). It is an important consideration for radioactive particle dosimetry as the exposure times required in this study varied greatly, ranging from 5 minutes to 72 hours, depending on the particle and the simulated skin thickness. Also, absorbed dose rates of at least two different orientations are required due to the potential for the activity within radioactive particles to be heterogeneously distributed.

The variability of the absorbed dose rates has implications for the assessment of skin dose as the time to reach the threshold dose for harmful tissue reactions will be different

depending on the particle. A particle needs to stay in stationary contact with the skin for a sufficient length of time to cause a harmful tissue reaction, but there is a lack of data on what might be a reasonable length of time on which to base an assessment. Furthermore, there is a lack of data on the physical size of particle that would be amenable to prolonged contact with the skin. It seems reasonable to assume that the smaller particles in this study would be more amendable to prolonged contact with the skin, and perhaps the main concern regarding the larger particles is if they could deliver sufficiently high doses over short exposure times. But in the absence of data to substantiate this reasoning, it is difficult to limit the scope of an assessment, hence the inclusion of particles of a range of physical sizes in this study.

Absorbed dose rate per unit activity (MBq) can be used to approximate the absorbed dose rate of other particles but this research has shown it to be variable. In the work undertaken to assess the existing exposure situation at Dalgety Bay, it was assumed that a 1 MBq Ra-226 particle would have an absorbed dose rate of approximately 1 Gy hr^{-1}, although it was recognised this may be an underestimate (Brown and Oatway, 2012; Dale, 2013). However, this research has shown that this could be an over- or under-estimate as the absorbed dose rate per unit activity can vary by a factor between 0.6 and 2.5. It is important this is considered in any dose assessment, especially as it was the lowest activity particle in this study that had the highest absorbed dose rate per unit activity. This demonstrates that particle size is important and particles with higher activities might not necessarily pose the greatest hazard.

Lastly, care must be taken when considering peak absorbed dose rates as, whilst significantly higher than averaged absorbed dose rates, they are not necessarily relevant to radiological protection. The area from which peak absorbed dose rates are taken is dependent on the scanning resolution used when processing the RCF. The 1200 dpi scanning resolution used in this study produces 0.0004 mm^2 pixels. Although there is not an agreed lower limit on the size of the irradiated area when preventing deterministic effects, it is unlikely that doses to an area of this size would be of negligible radiological concern.

3.4.2 Assessment of absorbed dose rate for different skin thicknesses

A key consideration for the dosimetry of Ra-226 particles is whether the alpha emissions can penetrate skin thicknesses relevant to radiological protection. This study has shown that the alpha emissions from Ra-226 particles have a relatively short range in skin reaching a maximum depth of 54.4 µm. Even under the optimal conditions presented by the Am-214 source, where self-absorption is minimal, only 0.009 % of the alpha

emissions reached 54.4 µm relative to the surface dose. However, it should be noted that there are 5 alpha-emitting radionuclides in the Ra-226 decay chain that will all be contributing to the alpha dose at shallow skin depths: Ra-226 (4.8 MeV), Rn-222 (5.5 MeV), Po-218 (6.0 MeV), Po-214 (7.7 MeV), and Po-210 (5.3 MeV). The energy of the highest yield Am-241 alpha emission is 5.5 MeV, which provides an appropriate representation of the Rn-222, as well as the Ra-226 and Po-210, albeit perhaps a slight overestimate of how far the alpha emissions can travel in skin from these radionuclides given their energies are lower. However, alpha emissions from Po-218 and Po-214 are of higher energy and likely capable of penetrating further in skin than the 5.5 MeV alpha emissions of Am-241. There is some evidence of this from the physically smaller particles in this study, which had relative absorbed dose rates of 1.2 Gy hr^{-1} at 54.4 µm, but it should be noted that a proportion of this increasing absorbed dose rate will be due to an increasing beta dose rate therefore not solely driven by alpha emissions.

The measurement of absorbed dose rate from Ra-226 particles at different skin thicknesses indicates that although the reference 70 µm skin thickness is arbitrary, it is likely to be appropriate for the prevention of ADU in adults, and perhaps children. As the fibroblast and endothelial cells involved in ADU are found at ~ 100 – 150 µm in adults, the use of the reference 70 µm skin thickness can be considered conservative for the assessment of adults. This study has shown that the absorbed dose rate at these depths will be lower than at 70 µm and the contribution from alpha emissions is effectively zero. In children, the fibroblast and endothelial cells are found at ~ 64 – 96 µm, therefore the use of the reference 70 µm skin thickness could be considered realistic for the assessment of children. This study has shown that the absorbed dose rate at these depths will be lower at the deeper end of the range, and slightly higher at the shallow end of the range, but the contribution from alpha emissions is effectively zero. However, it could be argued that there are equality issues associated with an assessment based on 70 µm given that the level of conservatism is lower for children than for adults. If the same level of conservatism were to be maintained across all age groups, a thinner skin thickness should be used for the prevention of ADU in children.

For AEN, the target cells are the suprabasal cells that are found at ~ 50 µm in adults and ~ 32 µm in children. This study has shown there is a contribution from alpha emissions at skin depths up to 54.4 µm and the absorbed dose rate could be higher by up to a factor of 2 at 37.9 µm, raising the possibility that AEN could be seen before ADU in adults and children. Furthermore, for radioactive particles dominated by alpha emitters, such as the alpha-rich particles from Sellafield (Brown and Etherington, 2011), AEN may be

the sole harmful tissue reaction. Further research is required to establish whether AEN or ADU is seen first from exposure to mixed alpha/beta radioactive particles, as well as to establish whether AEN is seen from alpha-only radioactive particles.

Lastly, care must be taken when considering absorbed dose rates at other skin depths as the skin cells at these depths are not involved in the harmful tissue reactions. The shallowest skin depth of interested to radiological protection in this study is 37.9 µm as this approximates to the depth of suprabasal cells in the youngest ICRP age group (i.e., new-born), the exposure of which could result in AEN. The higher absorbed dose rates seen in this study at < 37.9 µm are not necessarily relevant to radiological protection but are useful in understanding the potential range of alpha emissions. Likewise, the deepest skin depth of interest to radiological protection in this study is 167.7 µm as this approximates to the depth of fibroblasts and endothelial cells in the oldest ICRP age group (i.e., adults), the exposure of which could result in ADU. The lower absorbed dose rates seen in this study at > 167.7 µm are not necessarily relevant to radiological protection but are useful in understanding potential skin cell survival at deeper depths that could help with skin repair in the event of a harmful tissue reaction.

3.4.3 Assessment of absorbed dose rate for different averaging areas

The measurement of absorbed dose rate from Ra-226 particles over different skin averaging areas indicates that the use of the nominal 1 cm^2 averaging area may not be appropriate for particles of the range of physical sizes in this study. The difference between the range of relative absorbed doses found in this study (2.3 to 17 Gy hr^{-1}) and the study on the skin of pigs by Baum and Kaurin (42 to 80 Gy hr^{-1}) indicates that the effect of dose averaging is variable. This difference is likely due to the Ra-226 particles irradiating a larger area than the physically smaller sources used in the pig skin exposures, and therefore less sensitive to averaging. However, since it is known that the threshold dose changes with changes in the size of the irradiated area, it raises the question of whether the dose threshold, which was derived from sources < 2 mm in diameter, is applicable to particles that irradiate areas > 2 mm in diameter. Further research is required to establish the threshold doses for physically larger particles that irradiate areas > 2 mm in diameter to fully understand whether the 1 Gy (70 µm, 1 cm^2) threshold dose is appropriate for the range of physical sizes of radioactive particles found in the environment.

However, it should be noted that if the irradiated area is > 5 mm in diameter, the reaction of concern is MD. P88 was the physically largest particle used in this study and it irradiated a significant proportion of the 20 mm^2 averaging area (i.e., ~ 5 mm in

diameter). It is not likely that a particle of this physical size would remain in stationary contact with the skin for a prolonged length of time, so the concern from physically larger particles is likely limited to those that could deliver high doses over short periods of time. The dose rate from P88 is too low to cause MD in any reasonable timescale, but there have been a few particles recovered from Dalgety Bay that may have had sufficiently high dose rates. The highest activity particle had an estimated Ra-226 activity of 76 MBq, which could have had a dose rate of ~ 46 to 190 Gy hr^{-1} (72.2 µm, 1 cm^{2}) based on the range of absorbed dose rates per unit activity measured in this study. The physical size of this particle was ~ 40 by ~ 80 mm therefore likely capable of irradiating an area much larger than 5 mm in diameter to cause MD within a timescale of minutes. Furthermore, the dose rate for children would be higher due the basal cells of the epidermis being at 45 µm with a likely contribution from alpha particles.

3.5 Conclusions

This research was the first to study the impact of both skin thickness and averaging area in the assessment of absorbed dose rate from inadvertent skin contact with Ra-226 particles. The absorbed dose rates from Ra-226 particles were highly variable exhibiting wide ranges for the size of the irradiated area, the time to reach the threshold dose, and the absorbed dose rate per unit activity. There was also evidence that activity is heterogeneously distributed within the particles that exhibited uneven lateral dose distributions, peak dose rates that were offset from the centre, and an absorbed dose rate increase of up to a factor of 3.4 when changing orientation.

The use of the reference 70 µm skin thickness is likely to be appropriate for the prevention of ADU in adults and children due to the depth of the fibroblasts and endothelial cells. However, if the level of conservatism were to be kept the same across different age groups, a thinner skin thickness should be used in the assessment of absorbed dose to the skin of children. For the prevention of AEN, the 70 µm skin thickness may not be appropriate due to the potential for an alpha contribution to the absorbed dose at the depth of the suprabasal cells. Further research is required to establish whether ADU or AEN is seen first from exposure to mixed alpha/beta radioactive particles, as well as to establish whether AEN is seen from alpha-only radioactive particles.

The use of the nominal 1 cm^{2} averaging area may not be appropriate for the assessment of skin dose from particles with physical sizes different to the radioactive sources used in the studies from which the threshold dose has been approximated. The absorbed dose

rates over 1 mm^2 relative to 1 cm^2 varied across the particles and were lower than the relative absorbed dose rates of the radioactive sources used in the studies from which the threshold dose was approximated. Further research is required to establish the threshold doses for physically larger particles that irradiate areas > 2 mm in diameter to fully understand whether the 1 Gy (70 µm, 1 cm^2) threshold dose is appropriate for the range of physical sizes of radioactive particles found in the environment.

Chapter 4

Bioaccessibility of Ra-226 Particles from Legacy Contamination and Assessment of Ingestion Dose

4 Bioaccessibility of Ra-226 Particles from Legacy Contamination and Assessment of Ingestion Dose

4.1 Introduction

Radioactive particles are physically discrete sources of radioactivity that have been released into the environment due to past accidents, incidents, and practices (IAEA, 2011), and can present a hazard to members of the public by inadvertent ingestion. The historical use of radium in the luminising of aircraft components, and the subsequent decommissioning of those aircraft and associated waste disposal practices, has left a legacy of contamination on former military sites. One such site is Dalgety Bay in Scotland, which was host to United Kingdom Ministry of Defence air force activities between 1917 and 1959, leaving behind legacy contamination in the form of Ra-226 radioactive particles (Dale, 2013). One of the challenges for radiological protection of the public is in the assessment of the committed effective doses from the inadvertent ingestion of radioactive particles (McGuire *et al.*, 2020).

4.1.1 Ingestion in Radiological Protection

For assessing the committed effective dose from ingested radionuclides, the ICRP maintains a set of ingestion dose coefficients that describe how many sieverts would be received per becquerel of a given radionuclide through ingestion (ICRP, 1995, 2012). The ingestion dose coefficients were calculated based on the 1990 ICRP Recommendations (ICRP, 1991). These are currently subject to a process of review and being updated based on the 2007 ICRP Recommendations (ICRP, 2007).

The ingestion dose coefficients were derived using a model of the alimentary tract and reference physiological parameters to describe how material moves through the body (ICRP, 1979), biokinetic models to describe radionuclide absorption, distribution, retention, and excretion from the body (ICRP, 1981, 1993), and dosimetric models and nuclear decay data to describe the energy deposition whilst the radionuclides are retained in body tissues (ICRP, 1983, 1990). Dose coefficients were derived for environmental exposure of the public to take account of age-dependent radiosensitivity and the form in which radionuclides are typically found in the environment, such as incorporated into foodstuffs. Dose coefficients were also derived for occupational exposure of workers to take account of an adult-only population and the radionuclides typically found in the workplace.

The fraction of an ingested radionuclide that is released from the ingested material into the gastrointestinal fluids (i.e., the fraction that is bioaccessible) and absorbed across the gastrointestinal wall into systemic circulation (i.e., the fraction that is bioavailable) is described by the fractional absorption (f_1) value. It is important to note that the body does not necessarily absorb everything that is released into the gastrointestinal fluids, in other words, just because a radionuclide is bioaccessible doesn't mean it is bioavailable. Table 4.1 shows the ingestion dose coefficients and associated f_1 values for Ra-226 and its daughter radionuclides across the ICRP public age groups; infant, 1 -, 5 -, 10 -, 15 - years, and adults. The assessment of committed effective dose is the product of the dose coefficients, which have the f_1 values embedded, and the activity of the ingested material.

Table 4.1 Committed effective dose coefficients and f_1 values for the ingestion of Ra-226 and daughter radionuclides[a] by members of the public (Sv Bq^{-1}) (ICRP, 1995, 2012)

Nuclide	f_1[b]	Infant	f_1[c]	1 y	5 y	10 y	15 y	Adult
Ra-226	0.6	4.7E-06	0.3[d]	9.6E-07	6.2E-07	8.0E-07	1.5E-06	2.8E-07
Pb-214	0.6	2.7E-09	0.4[d]	1.0E-09	5.2E-10	3.1E-10	2.0E-10	1.4E-10
Bi-214	0.1	1.4E-09	0.05	7.4E-10	3.6E-10	2.1E-10	1.4E-10	1.1E-10
Pb-210	0.6	8.4E-06	0.4[d]	3.6E-06	2.2E-06	1.9E-06	1.9E-06	6.9E-07
Bi-210	0.1	1.5E-08	0.05	9.7E-09	4.8E-09	2.9E-09	1.6E-09	1.3E-09
Po-210	1.0	2.6E-05	0.5	8.8E-06	4.4E-06	2.6E-06	1.6E-06	1.2E-06

The public ingestion dose coefficients were derived using higher f_1 values than for workers to take account of the potentially more soluble organic forms typical of public exposure, such as radionuclides in the environment incorporated into foodstuffs (RIFE-27, 2022), as well as age-dependent differences in physiology and biokinetics. However, as radioactive particles are not incorporated into foodstuffs and are not a typical public exposure, it is appropriate to consider the applicability of the ICRP dose coefficients, specifically their embedded f_1 values, to the inadvertent ingestion of radioactive particles.

[a] ICRP does not publish ingestion dose coefficients for Rn-222, Po-218, and Po-214.
[b] Apply to infants only.
[c] Apply to all other age groups.
[d] For adults, f_1 is 0.2.

4.1.2 Bioaccessibility and Bioavailability of Radioactive Particles

A few studies have been published that have measured the *in vitro* bioaccessibility, and in some cases the *in vivo* bioavailability, of radioactive particles found in the environment. The main *in vitro* bioaccessibility method that has been used was developed by Professor David Taylor of the University of Heidelberg, Germany, for the simulated gastrointestinal digestion of radioactive particles from the former research reactor establishment at Dounreay, on the north coast of Scotland (Stewart, A; Cook, GT; MacKenzie, 2003 - NB. The 'Taylor' method is included as Appendix 1 of this report). The method includes a stomach compartment and a small intestine compartment simulated by synthetic gastrointestinal fluids. Samples are first digested in the simulated stomach fluid for 2 hours, after which it is converted to the conditions of the small intestine by the addition of a simulated small intestine fluid and digested for a further 4 hours. The method was derived principally from literature and computer simulations but does not appear to have gone through any further validation or quality control. Furthermore, it was somewhat tailored to actinide and lanthanide chemistry by the omission of gastrointestinal fluid constituents thought not to be important for the digestion of Dounreay radioactive particles (e.g., amino acids, bile acids, and some digestive enzymes were not included in the simulated gastrointestinal fluids). Nevertheless, this is the method that has been used in the few studies on the ingestion of radioactive particles.

Radioactive particles derived from irradiated nuclear fuel containing Cs-137 Sr-90, Am-241, and Pu-238/239/240 from Dounreay were the first to be digested by the 'Taylor' method. The digestion of 11 particles found that bioaccessibility was low for Cs-137 and Sr-90 (≤ 0.3 %) and higher for the actinides ranging from 0.1 to 7.1 %. One particle was significantly different with bioaccessibilities ranging from 40.5 to 59.4 % across the radionuclides. Although, 8 different particles were administered to adult rats to study *in vivo* bioavailability and found it to be considerably lower than the *in vitro* bioaccessibility results. However, validation was difficult given the small sample sizes and that different particles were used in the *in vitro* and *in vivo* studies (Harrison *et al.*, 2005).

Subsequently, alpha-rich particles containing Pu-238/239/230 and Am-241 that have arisen from Sellafield were digested *in vitro* based on the 'Taylor' method and *in vivo* using rats. The *in vitro* digestion used the same gastrointestinal fluid composition as the detailed in the 'Taylor' method, but the digestion timings were modified to 4 hours in the stomach and 2 hours in the small intestine. The *in vitro* digestion of 8 particles found that bioaccessibility ranged from 0.04 to 0.97 % across the radionuclides, whereas the *in vivo* digestion using 5 different particles found that bioavailability was very low ranging from

10^{-8} to 10^{-5} %. To reconcile this discrepancy, 5 fresh particles were first subject to *in vivo* digestion followed by *in vitro* digestion, but validation proved difficult given the particles would have been modified by the *in vivo* treatment prior to the *in vitro* treatment (Brown and Etherington, 2011).

Radioactive particles containing plutonium and americium isotopes dispersed by nuclear weapons testing undertaken by the former Soviet Union at the Semipalatinsk Nuclear Test Site in Kazakhstan have also been digested using the 'Taylor' method. Six particles were digested in the stomach solution for 2 hours, two of which were also subject to digestion in the small intestine solution for 4 hours. The study found the bioaccessibility of the particles was considerably less than the ICRP f_1 values for these radionuclides (Conway et al., 2009). It was recommended the measured bioaccessibility should be used instead of the ICRP f_1 values in the assessment of committed effective dose.

Bioaccessibility of Ra-226 Particles

There are limited data available on the bioaccessibility, and no data available on the bioavailability, of Ra-226 particles as only one study has been published on the *in vitro* bioaccessibility of Ra-226 particles (Tyler *et al.*, 2013). Simulated gastrointestinal digestion was undertaken on 60 particles from Dalgety Bay using the 'Taylor' method. A wide range of gastrointestinal solubility (1 – 35 % of particle activity) was found. However, the particles used in this study had not been physically or chemically characterised, limiting the interpretation of the chemical and physical characteristics that might influence the observed solubilities. Furthermore, the application of this method to the Ra-226 particles had some notable differences, namely that the digestion times were extended to 8 hours for both the stomach and the small intestine compartments, and the two fluids were kept separate rather than converting the conditions of the stomach to those of the small intestine. Here, the approach taken to the assessment of committed effective dose was to apply the ICRP ingestion dose coefficients, with their embedded f_1 values, to the sum of the activities released into the stomach and small intestine fluids.

The differences observed between the ICRP f_1 values and the measured bioaccessibilities of radioactive particles highlights the importance of bioaccessibility studies for assessing ingestion dose. However, the lack of method validation and inconsistency with reference physiological parameters, such as digestion time and mixing of gastrointestinal fluids, will affect the robustness of ingestion dose assessments. Also, the lack of pre-digestion particle characterisation has limited the understanding of why radioactive particle bioaccessibility exhibits such wide variation.

4.1.3 The BARGE Unified Bioaccessibility Method

Given the lack of validation and variable application of the 'Taylor' *in vitro* bioaccessibility method to radioactive particles, and the validation and ethical issues of *in vivo* bioavailability studies, the application of a standard, validated approach to *in vitro* bioaccessibility could improve the assessment of committed effective doses from inadvertent ingestion of radioactive particles. A method that offers this opportunity is the Bioaccessibility Research Group of Europe (BARGE) Unified Bioaccessibility Method (UBM).

BARGE is a network of international research institutes and research groups for the collaborative study of the bioaccessibility of soil contaminants in the human gastrointestinal tract. The main aim of BARGE is to harmonise the use of *in vitro* bioaccessibility methods to provide robust and defensible bioaccessibility data for use in public risk assessments. The work of BARGE focused on the evaluation of the *in vitro* bioaccessibility method developed by the Dutch National Institute for Public Health and the Environment (RIVM) (Oomen *et al.*, 2003) to establish how it could be adopted as a general method applicable to a range of contaminants and ingested matrices.

Oomen *et al.* recognised that public risk assessments are often based on toxicity studies in which ingested contaminants are incorporated into liquid or food matrices. However, the inadvertent ingestion of contaminated soil is also a pathway of exposure, as is the inadvertent ingestion of radioactive particles. Differences in bioaccessibility of contaminants incorporated into different ingested matrices could have a significant impact on public risk assessments. To address this issue, Oomen *et al*. developed the RIVM method, which is a physiologically based *in vitro* bioaccessibility method designed to be independent of the ingested matrix. The RIVM method was derived using physiologically relevant parameters including distinct gastrointestinal compartments, body temperature, digestion fluid ratios, digestion fluid composition, concentration and pH, and transit times for material movement through the gastrointestinal tract.

Due to its physiological relevance, BARGE adopted the RIVM method as the starting point in their work to harmonise *in vitro* bioaccessibility methods. The UBM was derived by modifying the RIVM method to ensure adequate conservatism and applicability to different soil types, and then evaluated and refined by means of an international interlaboratory comparison exercise (Wragg *et al.*, 2011). Furthermore, the UBM was validated against *in vivo* bioavailability data for arsenic (As), antimony (Sb), cadmium (Cd), and lead (Pb) using a juvenile swine model. Relative bioavailability of As, Sb, Cd, and Pb was measured for a variety of different contaminated soils and assessed against

the bioaccessibility of those soils using the UBM. The study found that the bioaccessibility data from the UBM were suitable to act as analogues for the bioavailability of As, Cd, and Pb, but not for Sb (Denys *et al.*, 2012). Subsequently, the UBM was published as a standard method, ISO 17924:2018, by the International Organisation for Standardisation (ISO, 2018) and has been used in a number of studies to measure the bioaccessibility of a range of contaminants in soils (Broadway *et al.*, 2010; Juhasz, Weber and Smith, 2011; Appleton *et al.*, 2013; Cave *et al.*, 2015).

4.1.4 Aim and Objectives

As the inadvertent ingestion of radioactive particles is not a typical public exposure, it is important to consider the applicability of the ICRP ingestion dose coefficients, specifically the f_1 values, in the assessment of committed effective dose. Furthermore, a lack of method validation, inconsistency with reference physiological parameters, and lack of pre-digestion characterisation has limited the understanding of the hazard from the inadvertent ingestion of radioactive particles. The aim of this research was to investigate whether the nominal f_1 values are appropriate for the assessment of committed effective dose from inadvertent ingestion of Ra-226 particles by the public and investigate the particle characteristics that influence bioaccessibility. This aim was achieved through the following objectives:

I. Measure the *in vitro* bioaccessibility of Ra-226 particles using the BARGE UBM.

II. Assess the committed effective doses from inadvertent ingestion of Ra-226 particles using bioaccessibility data.

III. Investigate the relationships between Ra-226 particle characteristics and *in vitro* bioaccessibility.

4.2 Materials and Methods

4.2.1 Sample Selection

The Ra-226 sample inventory from Dalgety Bay collected by SEPA was made available for this research. A total of 162 samples (~ 10 % of the inventory) were selected from the inventory comprising 160 Ra-226 particles (P1 – P160) and two Ra-226 artefacts (A1 and A2). The artefacts were identifiable aircraft components, where A1 was a partially intact dial and A2 was a flick switch. These samples have been physically, chemically, and radiologically characterised as reported in Chapter 2.

4.2.2 Ra-226 Particle Digestion

The UBM considers three compartments in simulating the human digestive system: the mouth; the stomach; and the small intestine. Using synthetic digestive fluids to represent the compartments, unknown samples, controls, and blanks are digested and the leachates collected for analysis to measure how much of the contaminant(s) has been made bioaccessible. Two leachates are produced by the UBM: the gastric (GC) leachate and the gastro-intestinal (GC – INT) leachate. The GC leachate is collected after digestion in the mouth and stomach compartments whereas the GC – INT leachate is collected after digestion in the mouth, stomach, and small intestine. The following method describes how the UBM was applied to the Ra-226 particles and artefacts, including any modifications to the original UBM.

Sample Preparation

The UBM was developed primarily for the digestion of soil, which can be sampled, dried, homogenised, and divided into aliquots. The original UBM uses two aliquots, one to produce the GC leachate, and a separate aliquot to produce the GC – INT leachate. However, the samples digested in this research were discrete objects from which aliquots could not be taken. The UBM was modified to accommodate this by taking a sub-sample of the leachate after digestion in the mouth and stomach compartments, but then continuing the same digestion through to the small intestine compartment. Figure 4.1 shows the modified UBM as applied to Ra-226 particles and artefacts. The blanks and controls were treated as per the original UBM.

The control was a guidance material produced by the British Geological Survey (BGS), described as a ferritic brown earth soil from North Lincolnshire, England, containing a range of naturally occurring contaminants including arsenic and lead. Its supporting documentation provides guidance values for the bioaccessible mass fractions of lead (GC = 13.0 ± 6.0 mg kg^{-1}) and arsenic (GC – INT = 5.4 ± 2.4 mg kg^{-1}) based on the international inter-laboratory study undertaken during the UBM validation (British Geological Survey, 2020).

One batch of digestions was performed per day and included nine digestions: five samples, the BGS-102 control (GC and GC – INT), and the blanks (GC and GC – INT). On the day prior to digestion, each sample was placed in a single 50 ml polypropylene centrifuge tube. Two 0.5 g aliquots of BGS-102 were weighed and placed in two separate centrifuge tubes for the GC and GC – INT controls. A further two separate centrifuge tubes were prepared for the GC and GC – INT blanks.

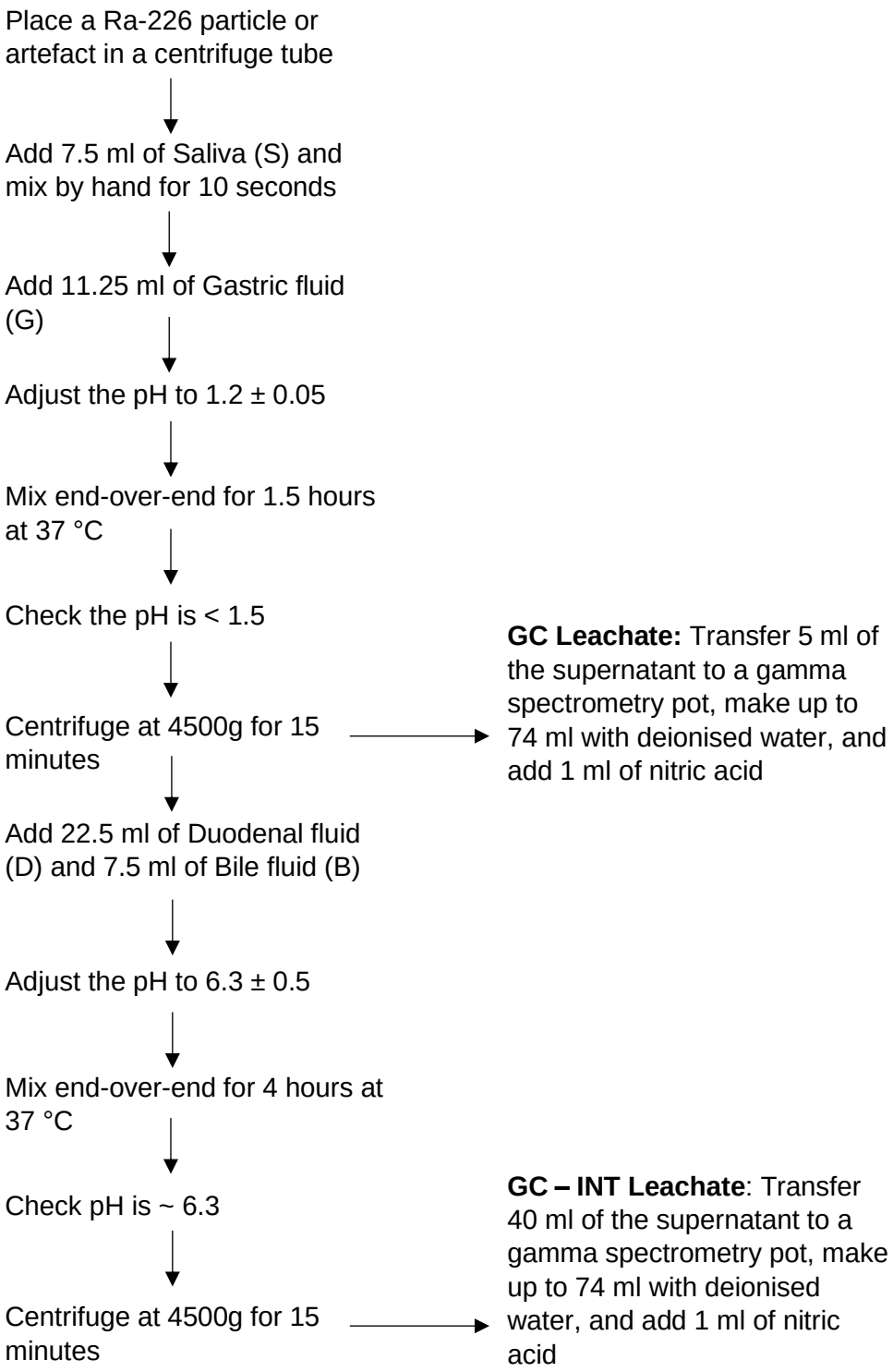

Figure 4.1 The BARGE Unified Bioaccessibility Method modified for the digestion of Ra- 226 particles and artefacts

Preparation of Digestive Fluids

Four separate digestive fluids were prepared: saliva (S) for the mouth compartment; gastric fluid (G) for the stomach compartment; and duodenal fluid (D) and bile (B) for the small intestine compartment. Each digestive fluid was a combination of three components: an inorganic solution, an organic solution, and enzymes. The reagents used in making each of the three components for each of the four digestive fluids are detailed in Appendix A. The quantities specified are for making a total volume of 500ml of each digestive fluid.

On the day prior to digestion, each digestive fluid was prepared by making their respective inorganic and organic solutions, which were subsequently combined, followed by the addition of the enzymes. Proportionate adjustments were made to the reagent quantities to prepare only the volume required for the batch of digestions taking place the following day. Now complete, the four digestive fluids were placed under magnetic agitation for 3 hours and then stored at room temperature overnight for use the following day.

Sample Digestion

On the day of digestion, the four digestive fluids were placed in a water bath at 37°C for 1 hour. The pH of each digestive fluid was measured with a pH meter against the following tolerances: 6.5 ± 0.5 (S); 1.1 ± 0.1 (G); 7.4 ± 0.2 (D); and 8.0 ± 0.2 (B). Adjustments to the pH were made using HCl (37%) or NaOH (1M), if required. The pH meter was calibrated using buffers of pH 4.0 (Phthalate, CAS No. 877-24-7) and pH 7.0 (Phosphate, CAS No. 7732-18-5) traceable to NIST standards.

Starting with the mouth compartment, 7.5 ml of saliva was added to each tube and mixed by hand for 10 seconds. To simulate the movement of material into the stomach compartment, 11.25 ml of gastric fluid was added to each tube. The pH of each tube was measured with a pH meter to ensure the mixture of saliva and gastric fluid was 1.20 ± 0.05. Adjustments to the pH were made using HCl (37%) or NaOH (1M), if required. The tubes were then placed under end-over-end agitation in a water bath at 37°C for 1.5 hours. The original UBM specifies 1 hour for the stomach compartment, but 1.5 hours was used in this study for consistency with the recommendations of the ICRP. In its current recommendations, the ICRP specify a stomach transit time of 1 hour for males and 1.5 hours for females.

At the end of the 1.5 hours, the tubes were removed from the water bath and the pH checked using pH paper. The pH of the GC leachate must be > 1.2 and < 1.50 to be

valid. The samples, plus the GC control and GC blank, were centrifuged for 15 minutes at 4500 rpm. For the samples, 5 ml of the supernatant was extracted to form the GC leachate, with the remaining 13.75 ml plus the sample being taken forward into the small intestine compartment. For the control and blank, 15 ml of the supernatant was extracted to form the GC leachate, with the remaining being discarded. The GC leachates were transferred to a polypropylene pot, made up to 74 ml with deionised water, and acidified with 1 ml nitric acid (70 %).

To simulate the movement of material into the small intestine compartment, the five samples, plus the GC – INT control and GC – INT blank had 22.5 ml of duodenal fluid and 7.5 ml of bile added to each tube. The pH of each tube was measured with a pH meter to ensure the mixture of saliva, gastric, duodenal, and bile fluids was 6.30 ± 0.5. Adjustments to the pH were made using HCl (37 %) or NaOH (1M), if required. The tubes were then placed under end-over-end agitation in a water bath at 37°C for 4 hours. At the end of the 4 hours, the tubes were removed from the water bath and the pH checked using pH paper. The samples, plus the GC – INT control and GC – INT blank, were centrifuged for 15 minutes at 4500 rpm. Due to having had 5 ml removed, 40 ml of the supernatant was extracted to form the GC – INT leachates of the samples, whereas 45 ml was extracted to form the GC – INT leachates of the control and blank. The GC – INT leachates were transferred to a polypropylene pot, made up to 74 ml with deionised water, and acidified with 1 ml nitric acid (70 %).

Digestion Leachate Analysis

The sample and blank leachates were analysed by gamma spectrometry using Ortec Gamma-X (GMX) N-Type High Purity Germanium (HPGe) Coaxial Photon Detectors linked to Ortec Gamma Vision Software for spectrum analysis. The leachates were analysed in the 74 ml polypropylene pots, the efficiency of which was calibrated using a multi-nuclide standard solution (Eckert & Ziegler, Cat. No. 7503, Source No.2115-94-1) containing 11 radionuclides covering an energy range from 46 keV to 1.8 MeV. The activity in the leachates was measured for Ra-226 and Pb-210, but not Pb-214 and Bi-214 due to their short physical half-lives relative to the analytical timings required by the UBM. The measured activities in the 5 ml GC leachate sub-samples were corrected to give the total activity that would have been present in the 18.75 ml GC fluid. The measured activities in the 40 ml GC – INT leachate aliquots were corrected to give the total activity that would have been present in the 48.75 ml GC – INT fluid, including a correction for the activity removed in the 5 ml GC leachate sub-sample.

The control and blank leachates were analysed using a Thermo Scientific iCAP Series 6000 Inductively Coupled Plasma – Optical Emission Spectrometer (ICP – OES). Lead and arsenic concentrations were measured for comparison with the BGS-102 guidance bioaccessible mass fraction values (mg kg^{-1} ± 1σ) (British Geological Survey, 2020). The ICP – OES was calibrated using certified reference materials including a multi-element standard solution containing Pb (Sigma-Aldrich, Product No. 54704) and an As standard solution (Fisher Scientific, Product No. 11468619). The BGS-102 bioaccessible mass fraction guidance value for Pb in the GC leachate is 13.0 ± 6.0 mg kg^{-1}. The bioaccessible mass fraction for Pb measured in this study was 22.3 ± 4.6 mg kg^{-1}, which is within the expected range. The BGS-102 bioaccessible mass fraction guidance value for As in the GC – INT leachate is 5.4 ± 2.4 mg kg^{-1}. The bioaccessible mass fraction for As measured in this study was 3.1 ± 0.5 mg kg^{-1}, which is within the expected range.

Calculation of Bioaccessibility

Bioaccessibility is expressed as the percentage of the contaminant in the sample that is released into the gastrointestinal fluids, as described by the following equation:

$$\text{Bioaccessibility (\%)} = \left(\frac{\text{Activity of radionuclide in leachate (Bq)}}{\text{Activity of radionuclide in particle (Bq)}}\right) \text{x } 100$$

Bioaccessibility was calculated for the GC leachates and the GC – INT leachates using the Ra-226 and Pb-210 leachate activities reported in this chapter and the Ra-226 and Pb-210 particle activities reported in Chapter 2. For instances where activities in the leachates were below limits of detection, the limit of detection was treated as a positive value as is done in other public dose assessments (RIFE-27, 2022).

4.2.3 Assessment of committed effective dose

Committed effective dose was assessed for both the GC and GC – INT leachates using the ICRP ingestion dose coefficients and their f_1 values as shown in Table 4.1. The committed effective dose was calculated for each particle and artefact including contributions from Ra-226 and Pb-210, as well as Po-210, as these radionuclides account for ≥ 99.91 % of the committed effective dose per Bq across all ICRP age groups. Table 4.2 shows the relative contribution of the Ra-226 decay chain to committed effective dose calculated using the ICRP ingestion dose coefficients. The greatest contribution is from Po-210 across all age groups except 15 years, but as an alpha emitter it is not measurable by gamma spectrometry. In the absence of Po-210 data, the Pb-210 data were used as analogues as has been done in other assessments (Brown and Oatway, 2012; Dale, 2013).

Table 4.2 Relative contribution of the Ra-226 decay chain to committed effective dose (e, Sv Bq^{-1})

Radionuclide	Age					
	3 months	**1 year**	**5 years**	**10 years**	**15 years**	**Adult**
Ra-226	12.01%	7.18%	8.58%	15.08%	29.99%	12.89%
Pb-214	0.007%	0.007%	0.007%	0.006%	0.004%	0.006%
Bi-214	0.004%	0.006%	0.005%	0.004%	0.003%	0.005%
Pb-210	21.47%	26.92%	30.45%	35.83%	37.99%	31.77%
Bi-210	0.04%	0.07%	0.07%	0.05%	0.03%	0.06%
Po-210	66.46%	65.81%	60.89%	49.02%	31.99%	55.26%
Total = Ra-226 + Pb-210 + Po-210	**99.95%**	**99.91%**	**99.92%**	**99.94%**	**99.96%**	**99.93%**

4.2.4 Relationships with Ra-226 particle characteristics

Exploratory data analysis was undertaken to establish whether there were any relationships between bioaccessibility and particle characteristics, as measured and reported in Chapter 2. The characteristics studied were particle activity, mass, density, equivalent circular diameter (ECD), shape factor, sphericity, and surface elemental composition. Due to the sensitivity of the ECD and density to particle shape, only particles classed as “volume” were included in the analysis of these characteristics.

4.3 Results

4.3.1 Bioaccessibility of Ra-226 particles

The digestion of the Ra-226 particles released varying amounts of activity and the data are highly skewed to the right as shown in Figure 4.2. The Ra-226 activity in the GC leachates ranged from a minimum of 1.95 Bq to a maximum of 4,658 Bq with a median of 66 Bq (IQR = 183 Bq). Similarly, the Pb-210 activity in the GC leachate ranged from a minimum of 0.6 Bq to a maximum of 4,722 Bq with a median of 76 Bq (IQR = 187 Bq). However, the activities in the GC – INT leachates were significantly lower. The Ra-226 activity in the GC – INT leachates ranged from a minimum of 0.4 Bq to a maximum of 2,679 Bq with a median of 29 Bq (IQR = 82 Bq). Similarly, the Pb-210 activity in the GC – INT leachates ranged from a minimum of 0.2 Bq to a maximum of 2,880 Bq with a median of 23 Bq (IQR = 73 Bq).

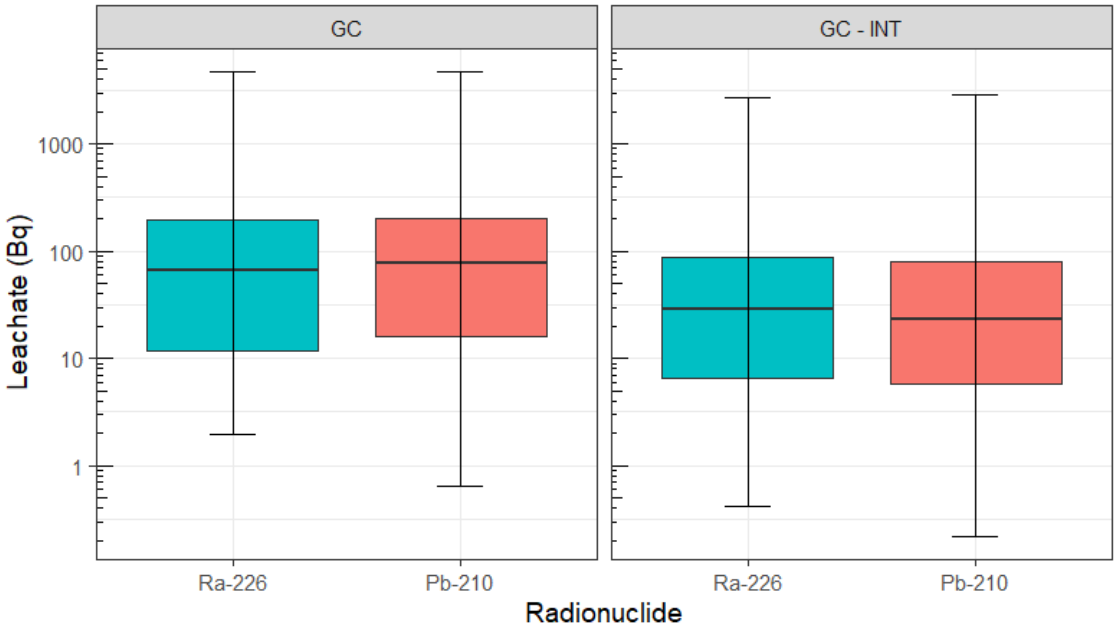

Figure 4.2 The activity of Ra-226 and Pb-214 in the GC and GC – INT leachates

The bioaccessibility varied widely and the data are highly skewed to the right as shown in Figure 4.3. The Ra-226 bioaccessibility in the GC leachates ranged from a minimum of 0.017 % to a maximum of 44 % with a median of 1.11 % (IQR = 3.97 %). Similarly, the Pb-210 bioaccessibility in the GC leachates ranged from a minimum of 0.023 % to a maximum of 60 % with a median of 1.83 % (IQR = 6.72 %). However, the bioaccessibilities in the GC – INT leachates were significantly lower. The Ra-226 bioaccessibility in the GC – INT leachates ranged from a minimum of 0.005 % to a maximum of 30.8 % with a median of 0.58 % (IQR = 1.88 %). Similarly, the Pb-210 bioaccessibility in the GC – INT leachates ranged from a minimum of 0.004 % to a maximum of 30.5 % with a median of 0.62 % (IQR = 2.08 %).

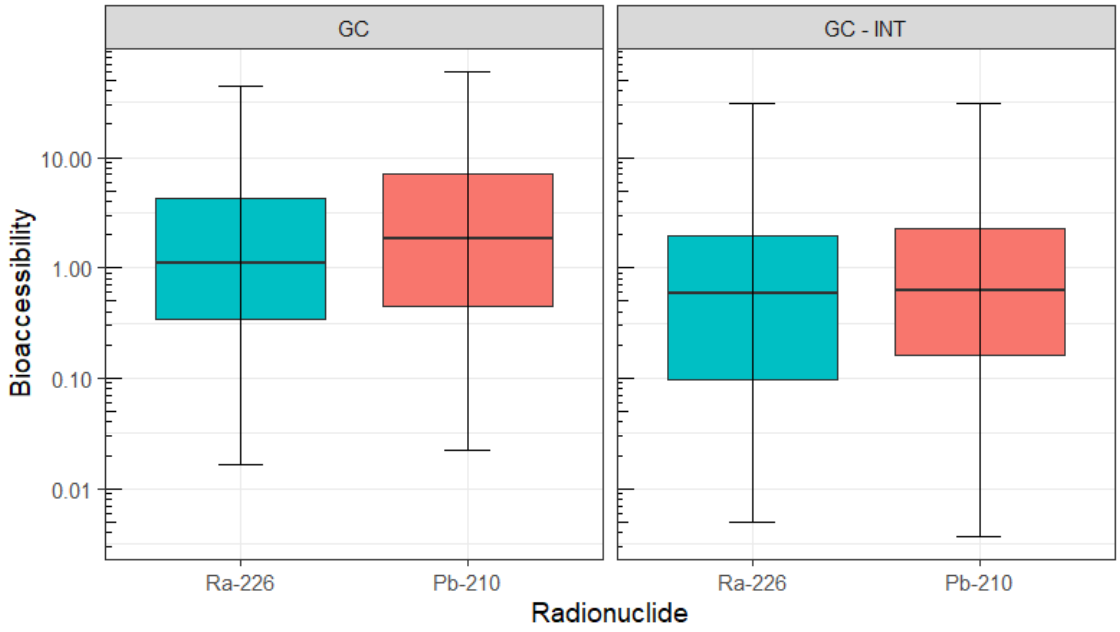

Figure 4.3 The bioaccessibility of Ra-226 and Pb-210 in the GC and GC – INT leachates

Artefact A1, the aircraft dial, behaved in a similar way with bioaccessibilities for Ra-226 and Pb-210 of 4.59 % and 4.98 % in the GC leachate that reduced to 0.62 % and 0.08 % in the GC – INT leachate. However, artefact A2, the aircraft switch, behaved differently as the bioaccessibility of Ra-226 in the GC leachate was 2.43 % and increased to 16.5 % in the GC – INT leachate. The same was not observed for Pb-210 with a bioaccessibility of 11.5 % in the GC leachate that reduced to 3.41 % in the GC – INT leachate.

4.3.2 Committed effective dose from inadvertent ingestion of Ra-226 particles

The total committed effective doses from Ra-226, Pb-210, and Po-210 in the GC and GC – INT leachates for the ICRP age groups for members of the public are shown in Figure 4.4. The highest doses were seen for the 3 - month age group ranging from 0.03 to 184 mSv with a median of 2.9 mSv (IQR = 7.01 mSv) from the GC leachate. Doses were lower in the GC – INT leachate ranging from 0.01 to 108 mSv with a median of 0.95 mSv (IQR = 3.2 mSv). The lowest doses were seen for the adult age group ranging from 0.002 to 10.2 mSv with a median of 0.16 mSv (IQR = 0.39 mSv) in the GC leachate. Again, doses were lower in the GC – INT leachate ranging from 0.0005 mSv to 6 mSv with a median of 0.053 mSv (IQR = 0.18 mSv).

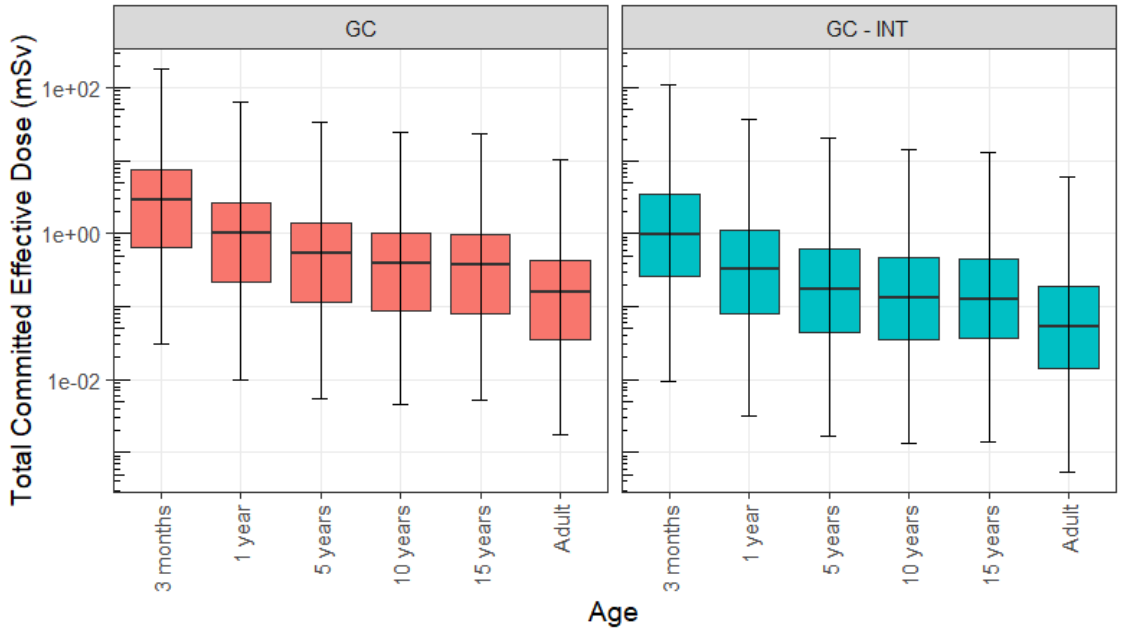

Figure 4.4 Total committed effective dose from Ra-226, Pb-210, and Po-210 in the GC and GC – INT leachates for the ICRP age groups for members of the public

The contributions to committed effective dose from the three individual radionuclides in the GC and GC – INT leachates for the ICRP age groups for members of the public are shown in Figure 4.5. Using the median for comparison, Po-210 was the highest contribution for most age groups, followed by Pb-210 and then Ra-226. For the 3 - month age group, the contribution from Po-210 in the GC leachate was 1.98 mSv compared to 0.64 and 0.31 mSv for Pb-210 and Ra-226. The same was observed for the GC – INT leachate but with lower doses. The only exception to this is the 15 - year age group, where Pb-210 was the highest contributor to dose (0.15 mSv) in the GC leachate followed by Po-210 (0.12 mSv) and Ra-226 (0.098 mSv). A different pattern was seen for the GC – INT leachate for the 15 - year age group where Pb-210 was still the highest contributor (0.045 mSv) but was followed by Ra-226 (0.043 mSv) then Po-210 (0.038 mSv).

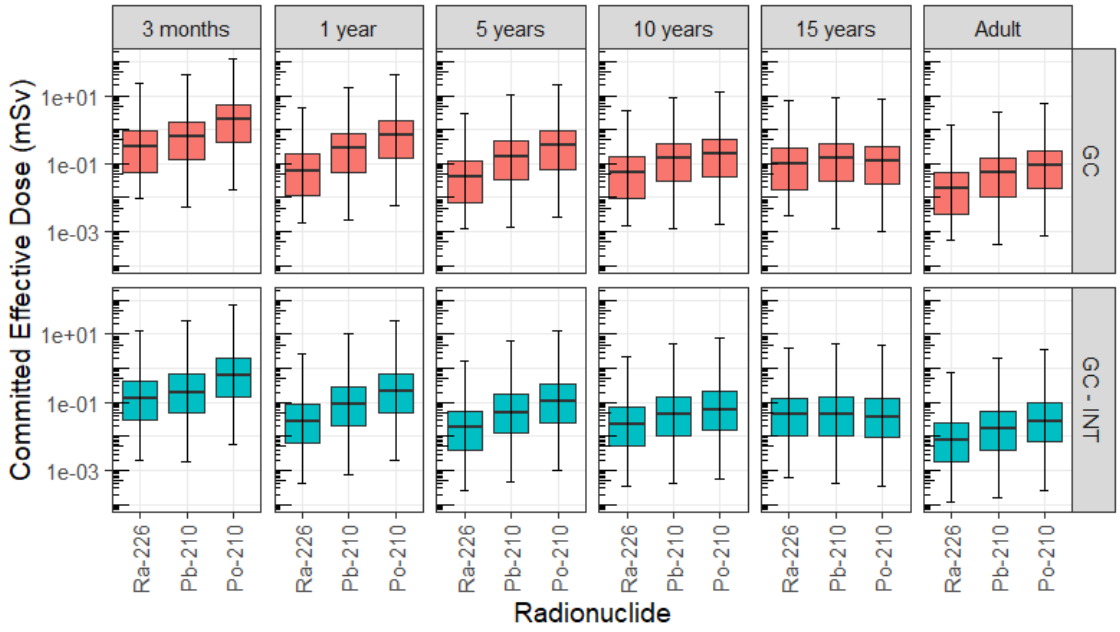

Figure 4.5 Contribution to committed effective dose from Ra-226, Pb-210, and Po-210 in the GC and GC – INT leachates for the ICRP age groups for members of the public

4.3.3 Effect of Ra-226 particle characteristics on bioaccessibility

Exploratory data analysis provided very little evidence of any linear or non-linear relationships between bioaccessibility and the particle characteristics reported in Chapter 2. The greatest amount of the observed variation was explained by the ECD and bioaccessibility in the GC – INT leachate, as shown in Figure 4.6, where there appears to be a negative relationship where bioaccessibility decreases as the physical size of the particles increases. However, the R^2 values were low (Ra-226 = 0.18, Pb-210 = 0.15) indicating that much of the variation in the data remains unexplained and there are likely other determinants controlling this variation. Regression analysis showed very little of the observed variation could be explained by particle activity, mass, density, shape factor, sphericity, and surface chemical composition (plots for 5 of the 23 elements detected across the particles are presented as examples: Al, Cu, Fe, Si, and Zn) as summarised in Appendix B.

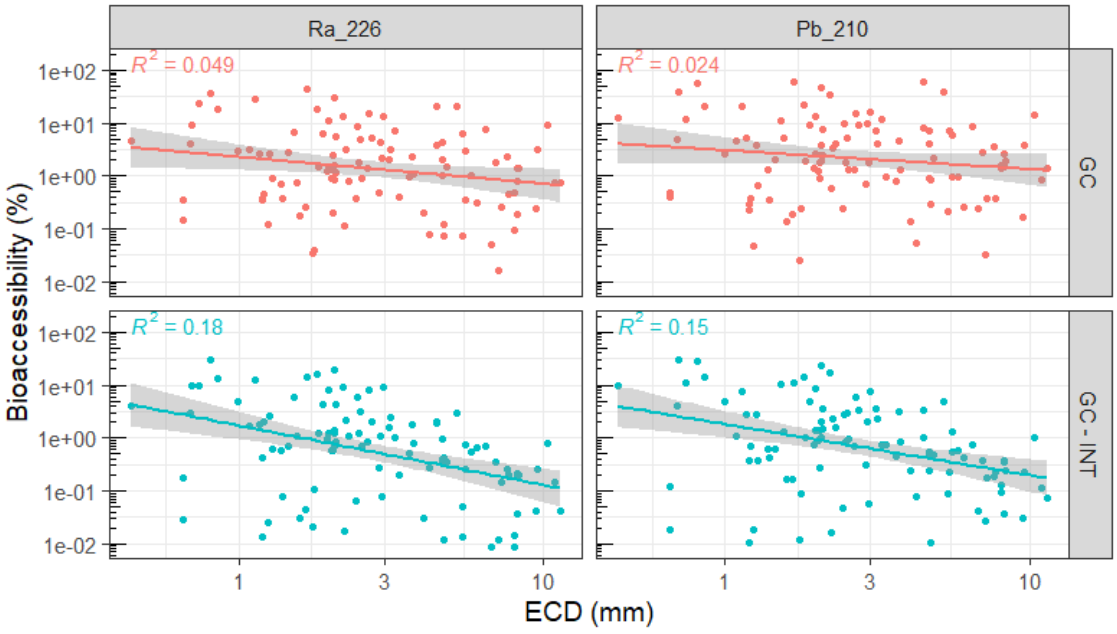

Figure 4.6 The observed variation between bioaccessibility (%) and ECD (mm)

4.4 Discussion

4.4.1 Variability of Ra-226 and Pb-210 bioaccessibility

The wide variation in bioaccessibility suggests that the f_1 value is not suitable for the assessment of committed effective dose from Ra-226 particles. In the assessment of committed effective dose, the ingestion dose coefficients, with their embedded f_1 values, are applied to the activity of the ingested material. Applying the dose coefficients to the Ra-226 particle activities would significantly overestimate the dose in most cases. For example, the f_1 value for the adult age group for Ra-226 is 0.2 (i.e., 20 %), but the bioaccessibility of Ra-226 for most particles was significantly less than 20 %. For the particles with a Ra-226 bioaccessibility > 20 %, there is the possibility that the f_1 value could underestimate the dose. Although, this is not certain as the amount that is bioaccessible is not necessarily all bioavailable (i.e., the body doesn't necessarily absorb everything that is released into the gastrointestinal fluids). It is not recommended to apply the ingestion dose coefficients directly to the ingested material in the case of ingestion of Ra-226 particles.

The similarity between the bioaccessibilities of Ra-226 and Pb-210 in both the GC and GC – INT leachates suggests their chemistry in the simulated gastrointestinal solutions is similar. However, the difference between the bioaccessibilities in the GC and GC – INT leachates for both radionuclides suggests the chemistry of the simulated gastrointestinal

solutions significantly affects bioaccessibility. The lower bioaccessibility in the GC – INT leachate suggests the change from the conditions of the stomach to the small intestine results in a precipitative effect. This is an important observation for the application of bioaccessibility methods to radioactive particles, and any subsequent dose assessment, as other studies could not have seen this effect due to the method used. In the study that digested Ra-226 particles using the 'Taylor' method, the stomach and small intestine solutions were kept separate meaning that the activity released into the stomach solution never transitioned into the small intestine solution and so the precipitative effect could not have been observed (Tyler *et al.*, 2013). Solubility experiments have been conducted on bulk soil/sand samples from Kosovo and Kuwait known to be contaminated with depleted uranium particles, but the method used 0.16 M HCl to simulate the gastrointestinal tract therefore did not include the conditions of the small intestine (Lind *et al.*, 2009). It is recommended that for measuring the bioaccessibility of radioactive particles, the method used should include the conditions of the small intestine and should simulate the movement of the stomach contents into the small intestine so that any effect of the change in conditions can be studied.

It is notable that the artefacts did not have the highest bioaccessibilities as the artefacts were likely to have offered the best opportunity for interaction with the simulated gastrointestinal fluids, given they would have been painted with radium paint on their surface and the radionuclides are presumably still located on, or close to, the surface. This suggests factors other than proximity of the activity to the gastrointestinal fluids are influencing bioaccessibility. Waste treatment and disposal practices were known to be diverse at Dalgety Bay including burning at incineration temperatures and incomplete burning at lower temperatures under uncontrolled conditions, as well as direct disposal into pits (Patton, 2013). It could be that these waste treatment and disposal practices transformed the original radium paint into different chemical forms that can have bioaccessibilities that are higher or lower than the original material. Such transformations could also be responsible for the different behaviour of A2 where its Ra-226 bioaccessibility increased in the GC – INT leachate. It is recommended that a large sample size should be analysed to ensure that the results of bioaccessibility studies are representative given the wide range of bioaccessibilities found in this study.

4.4.2 Using bioaccessibility data in the assessment of committed effective dose

The difference between the bioaccessibility in the GC leachates and the GC – INT leachates shown in this study requires a decision to be taken on which value to use in the assessment of committed effective dose. As absorption across the gastrointestinal

tract generally occurs in the small intestine, using the activities in the GC – INT leachates to undertake a physiologically-relevant assessment of committed effective dose is recommended. Due to the observed precipitative effect, the committed effective doses reported using the GC leachates are overestimates but could be useful as a basis for a conservative assessment provided its lack of physiological relevance is acknowledged.

As the ICRP ingestion dose coefficients include the f_1 values, which account for both bioaccessibility and bioavailability, applying the ICRP dose coefficients to the activities in the GC – INT leachates could in effect be accounting for bioaccessibility twice. However, as the ICRP ingestion dose coefficients were derived for radionuclides in relatively soluble forms (i.e., bioaccessible forms), it is likely that the f_1 values are driven more by bioavailability than bioaccessibility. On this basis, applying the ingestion dose coefficients, with their embedded f_1 values, to the GC – INT leachates was the approach taken in this study. Further research would be beneficial to establish what proportion of what is bioaccessible is actually bioavailable. An alternative could be to take the quotient of the committed effective dose and the f_1 value, in effect assuming the complete absorption of the activity in the GC – INT leachate. Taking this approach would avoid the potential double accounting for bioaccessibility, but it neglects to account for bioavailability and would be an overestimate. Again, it could be useful as a basis for a conservative assessment provided it is acknowledged that the doses would be overestimates.

The assumptions made regarding Po-210 could have a significant impact on dose assessment given that this radionuclide accounts for a large proportion of the committed effective dose. The assumption that the Po-210 activity in the particles is the same as Pb-210 is reasonable as these radionuclides will be in secular equilibrium given the age of the particles. However, the assumption that the bioaccessibility of Po-210 is the same as Pb-210 assumes the chemistry of Po and Pb is similar in the simulated gastrointestinal fluids, which is not known. This assumption was made in the assessments of SEPA and PHE and has also been adopted here in the absence of direct measurements of the bioaccessibility of Po-210. The similarity between the bioaccessibilities of Ra-226 and Pb-210 shown in this study provides an indication that the assumption made for Po-210 might not be unreasonable, but future research for the direct measurement of Po-210 bioaccessibility would be beneficial for refining ingestion dose assessment.

4.4.3 The contribution of the full Ra-226 decay chain to committed effective dose

Although Ra-226, Pb-210, and Po-210 account for ≥ 99.91 % of the committed effective dose per Bq across all ICRP age groups, it is important to acknowledge the other

daughter radionuclides in the decay chain. Firstly, Bi-210 is not measurable by gamma spectrometry as it is a beta emitter and was not assessed in this study. However, the application of a different analytical technique to measure Bi-210 would be of questionable value considering its negligible contribution to committed effective dose of ≤ 0.07 % across all ICRP age groups.

Secondly, Pb-214 and Bi-214 present challenges due to their physical half-lives of t ½ = 26.8 min and t ½ = 19.7 min, respectively. Decay correction is challenging as their physical half-lives are short relative to the analytical timings required in this study. A significant number of half-lives will have elapsed during the digestion (1.5 hrs in the stomach and 4 hrs in the small intestine), the post-digestion sample preparation time (~ 1 hr), and the gamma spectrometry measurement of the leachates (~ 5 hrs for the GC leachate and ~ 19 hrs for the GC – INT leachate). Furthermore, it is not possible to determine a time to which decay correction should be calculated as the biokinetics of the release of Pb-214 and Bi-214 into the simulated gastrointestinal fluids are not known. For example, the activity could be released at a constant rate, peak early and tail off, or peak late after a lag. Simulated digestion of radioactive particles from the Semipalatinsk Nuclear Test Site in Kazakhstan demonstrated that the rate of release of activity from the particles is variable, with 3 – 27 % of the total alpha activity extracted during the first 2 hours of digestion (Conway *et al.*, 2009). Additionally, Pb-214 and Bi-214 will be growing in due to the decay of their parent radionuclides that will depend in part on the amount of dissolved Rn-222 present in the leachates, which is not known. Any decay/ingrowth correction would have a significant impact on the estimated activities of Pb-214 and Bi-214. Nevertheless, as their contributions to committed effective dose are ≤ 0.007 % across all ICRP age groups, the lack of Pb-214 and Bi-214 data is of negligible radiological significance.

Lastly, Po-218, Po-214, and Rn-222 do not have their own dose coefficients and were not assessed in this study. Due to their short physical half-lives, Po-218 (t ½ = 3.05 min) and Po-214 (t ½ = 0.16 ms) make negligible contributions to committed effective dose, and the ICRP does not publish ingestion dose coefficients for these radionuclides. As a rule, the ICRP only publishes ingestion dose coefficients for radionuclides with physical half-lives > 10 minutes. Rn-222 does not have an ingestion dose coefficient due to being gaseous, however the ICRP intends to publish ingestion dose coefficients for radon as part of its ongoing work to update the dose coefficients to reflect the 2007 ICRP Recommendations (ICRP, 2010). Updated ingestion dose coefficients have been published for occupational intakes of radionuclides by workers, to be followed by updated

ingestion dose coefficients for the public. The new occupational ingestion dose coefficient for Rn-222 is 6.9 E^{-10} Sv Bq^{-1} (ICRP, 2017) which is comparable to the current public adult ingestion dose coefficients for Pb-214, Bi-214, and Bi-210, and therefore likely to be of similar negligible radiological significance in the inadvertent ingestion of Ra-226 particles. Although these three radionuclides do not have their own ingestion dose coefficients, their impact as daughter radionuclides formed in body issues is embedded in the ingestion dose coefficients of their parent radionuclides (ICRP, 1995, 2012).

Considering the full Ra-226 decay chain, it is sufficient to include only Ra-226, Pb-210, and Po-210 in the assessment of committed effective doses from the inadvertent ingestion of Ra-226 particles. Future research into the bioaccessibility of Po-210 from Ra-226 particles would provide valuable data for refining dose assessments.

4.4.4 No strong relationships between particle characteristics and bioaccessibility

It appears the particle characteristics assessed here cannot explain the wide range of bioaccessibility found in this study as, except for the ECD, they all exhibited either a very weak relationship with bioaccessibility, or no relationship at all. The weak negative relationship with ECD could be due to an increasing amount of the particle activity becoming inaccessible to the gastrointestinal fluids as a higher proportion of the activity could be located within the body of larger particles. However, as highlighted in Chapter 2, some particles exhibited heterogeneity in their activity distribution, which could at least partly explain why the relationship between bioaccessibility and the ECD is weak. The lack of any strong relationships between bioaccessibility and particle characteristics highlights the importance of the direct measurement of bioaccessibility, using a method that is representative of human physiology and adequately validated, such as the UBM.

4.5 Conclusions

This research was the first to study the bioaccessibility of Ra-226 particles using the UBM and has highlighted important considerations in the application of bioaccessibility methods to radioactive particles and for the assessment of committed effective dose. The Ra-226 particles and artefacts exhibited a wide range of bioaccessibilities, from close to zero up to 60 %. Consequently, the ingestion dose coefficients with their embedded f_1 values are not suitable for the assessment of committed effective dose of the ingested material in the case of Ra-226 particles. Ra-226 and Pb-210 chemistry is similar in the simulated gastrointestinal fluids, but the different conditions presented by

the stomach and small intestine compartments has a significant effect on bioaccessibility. The change from the stomach to the small intestine conditions appears to cause precipitation of some of the activity released in the stomach resulting in lower bioaccessibility in the small intestine. It is recommended that for measuring the bioaccessibility of radioactive particles, the method used should include the conditions of the small intestine and should simulate the movement of the stomach contents into the small intestine so that any effect of the change in conditions can be studied.

The difference between the bioaccessibility in the stomach and the small intestine requires a decision to be made on the data on which to base an assessment of committed effective dose. As absorption across the gastrointestinal tract generally occurs in the small intestine, using the activities in the small intestine is recommended for undertaking a physiologically relevant assessment of committed effective dose. Furthermore, considering the full Ra-226 decay chain, it is sufficient to include only Ra-226, Pb-210, and Po-210 in the assessment of committed effective doses from the inadvertent ingestion of Ra-226 particles.

Although there appears to be some explanation of the variation in bioaccessibility by particle ECD (i.e., 15 % for Pb-210 and 18 % Ra-226 in the GC – INT), none of the particle characteristics studied here were able to adequately explain the wide range of bioaccessibility values. Considering this, the importance of the direct measurement of bioaccessibility of radioactive particles is highlighted, that should use an appropriate method that is representative of human physiology and is adequately validated, such as the BARGE UBM.

Chapter 5

General Discussion

5 General Discussion

The overall aim of this thesis was to advance the current understanding of the characteristics of Ra-226 particles found in the environment and improve the assessment of radiation doses via inadvertent skin contact and inadvertent ingestion by members of the public. This general discussion summarises the key findings from this research and how they apply to radioactive particles more generally as well as identifying areas for further research.

5.1 Characterisation of Radioactive Particles

The research presented in Chapter 2 was the first to study a large sample of Ra-226 particles from legacy contamination and has revealed a population that diverse in their physical, chemical, and radiological properties. The widespread use of Ra-226 in military applications raises the possibility of a similar contaminant profile as at Dalgety Bay being present at many other sites. The analytical techniques used in this study are equally applicable to Ra-226 particles from other sites, and the insights provided by this research may help with future Ra-226 particle characterisation. It is important to use a suite of analytical techniques to gather complimentary datasets and analyse a sufficiently large sample size to capture the potential variety of particles that may be present on a Ra-226 legacy site.

The highly heterogeneous characteristics of the particles may have implications for the assessment of doses due to skin contact and inadvertent ingestion. Comparisons of the particles with the two artefacts potentially indicates that the original material has undergone significant alteration, meaning it may not be appropriate to make assumptions during dose assessment based on knowledge of the original material, if available. It is not possible to say whether the characteristics and diversity seen in the Dalgety Bay particles is typical of Ra-226 contamination from past military applications, due to the general lack of data available on Ra-226 particles from legacy contamination. Until data from other sites become available, site-specific characterisation studies will be required to understand the hazard from Ra-226 particles for the radiological protection of the public.

Further research is recommended into particle friability and the impact of heterogeneously distributed activity. For example, none of the particles in this research were small enough to inhale, but if left to physically breakdown in the environment, could be inhalable in future. This is particularly important for particles with heterogeneously

distributed activity where there is the possibility of the activity being unequally distributed between the breakdown products. A potential approach to studying this for different environments could be to subject radioactive particles to a simulated estuarine environment, like at Dalgety Bay, under laboratory conditions using sediment, salt water, and mechanically induced water and sediment movement. A terrestrial environment could be simulated by placing radioactive particles in soil mesocosms and monitoring their changes over time. Such data could help in decision making regarding remediation where a case could be made to remediate sooner rather than later to avoid a potentially higher hazard in future.

5.2 Dosimetry of Radioactive Particles

The research presented in Chapter 3 was the first to study the impact of both skin thickness and averaging area in the assessment of absorbed dose rate from inadvertent skin contact with Ra-226 particles. The absorbed dose rates from Ra-226 particles were highly variable exhibiting wide ranges for the size of the irradiated area, the time to reach the threshold dose, and the absorbed dose rate per unit activity. There was also evidence that activity is heterogeneously distributed within the particles that exhibited uneven lateral dose distributions, peak dose rates that were offset from the centre, and an absorbed dose rate increase of up to a factor of 3.4 when changing orientation.

The use of the reference 70 µm skin thickness is likely to be appropriate for the prevention of ADU in adults and children due to the depth of the fibroblasts and endothelial cells. However, if the level of conservatism were to be kept the same across different age groups, a thinner skin thickness should be used in the assessment of absorbed dose to the skin of children. For the prevention of AEN, the 70 µm skin thickness may not be appropriate due to the potential for an alpha contribution to the absorbed dose at the depth of the suprabasal cells. The use of the nominal 1 cm^2 averaging area may not be appropriate for the assessment of skin dose from particles with physical sizes different to the radioactive sources used in the studies from which the threshold dose has been approximated. The absorbed dose rates over 1 mm^2 relative to 1 cm^2 varied across the particles and were lower than the relative absorbed dose rates of the radioactive sources used in the studies from which the threshold dose was approximated.

Further research is recommended to establish whether ADU or AEN is seen first from exposure to mixed alpha/beta particles and whether AEN is seen from alpha-only particles, as well as threshold doses for physically larger particles that irradiate areas

> 2 mm in diameter. A technique that may be suitable in helping answer these questions is the use of *in vitro* skin cells and organotypic skin models. The human skin HaCaT cell line has been used extensively in toxicity studies such investigating the toxicity of hair dye on human skin cells (Zanoni *et al.*, 2014). HaCaT cells are cultured as a monolayer of cells but organotypic skin models offer the opportunity for *in vitro* studies on a three-dimensional skin structure. A study investigating the impact of ionising radiation on the skin of astronauts during manned space missions used an organotypic skin model composed of epidermal keratinocytes and dermal fibroblasts arranged in multiple layers (von Neubeck *et al.*, 2015). As ADU, AEN, and MD are all the result of skin cell death, the use of these *in vitro* techniques could offer the opportunity to study the death of skin cells at different skin thicknesses and over different areas. This could provide the data required to answer these questions without using *in vivo* techniques such as the pigs used in previous studies.

5.3 Bioaccessibility of Radioactive Particles

The research presented in Chapter 4 was the first to study the bioaccessibility of Ra-226 particles using the UBM and has highlighted important considerations in the application of bioaccessibility methods to radioactive particles and for the assessment of committed effective dose. The Ra-226 particles and artefacts exhibited a wide range of bioaccessibilities, from effectively zero to over 50 %, greater than has previously been observed (Tyler *et al.*, 2013). Consequently, the ingestion dose coefficients with their embedded f_1 values are not suitable for the assessment of committed effective dose of the ingested material in the case of Ra-226 particles. Ra-226 and Pb-210 chemistry is similar in the simulated gastrointestinal fluids, but the different conditions presented by the gastric and intestinal compartments has a significant effect on bioaccessibility. The change from the gastric to the intestinal conditions causes a precipitative effect resulting in lower bioaccessibility in the small intestine. It is recommended that for measuring the bioaccessibility of radioactive particles, the method used should include the conditions of the small intestine and should simulate the movement of the stomach contents into the small intestine so that any effect of the change in conditions can be studied.

The difference between the bioaccessibility in the stomach and the small intestine necessitates a decision to be made on the data on which to base an assessment of committed effective dose. As absorption across the gastrointestinal tract and into blood generally occurs in the small intestine, using the activities in the small intestine is recommended for undertaking a physiologically relevant assessment of committed effective dose. Furthermore, considering the full Ra-226 decay chain, it is sufficient to

include only Ra-226, Pb-210, and Po-210 in the assessment of committed effective doses from the inadvertent ingestion of Ra-226 particles. Although there appears to be a weak relationship between bioaccessibility and the particle ECD, none of the particle characteristics studied here were able to adequately explain the wide range of bioaccessibility values. Considering this, the importance of the direct measurement of bioaccessibility of radioactive particles is highlighted, that should use an appropriate method that is representative of human physiology and is adequately validated, such as the BARGE UBM.

Further research is recommended to establish the bioaccessibility of Po-210. Such data would be useful for either validating the assumption that Po-210 and Pb-210 chemistry in simulated gastrointestinal fluids is not significantly different or provide the necessary data for refining ingestion dose assessments using measured Po-210 bioaccessibility values. A sub-sample of 16 particles from this research were selected for Po-210 analysis but the data were not suitable for use. Briefly, the GC and GC – INT leachates were spiked with a Po-208 tracer for calculating the efficiency of polonium recovery for each sample, dissolved in aqua regia, evaporated to almost dryness, resuspended in 0.5M HCl, and sent to an external laboratory for analysis by alpha spectrometry. Unfortunately, the peak of the Po-208 tracer on the alpha spectrum was obscured by the Po-210 peak due to the relatively high activity concentration of Po-210 in the leachates, meaning the results could not be calculated to take into account the sample recoveries. Reference recoveries were derived from the blank GC and GC – INT leachates as they were also spiked with the Po-208 tracer, but the results were considered unreliable as the Po-210 activity concentrations were so low that they didn't even account for the amount of Po-210 that should have grown-in to the leachates from the Pb-210 present.

Further research is recommended to establish the relative contribution of bioaccessibility and bioavailability to committed effective dose. A potential method to achieve this could be to couple an *in vitro* bioaccessibility method, such as the UBM, with an *in vitro* bioavailability method. The human intestinal Caco-2 cell line has been used extensively to study the transport of drugs and nutrients across the gastrointestinal tract (Etcheverry, Grusak and Fleige, 2012). Radioactive particles could be digested by a physiologically relevant method, such as the UBM, followed by exposure of a Caco-2 cell culture to the GC – INT leachates to measure how much of the radionuclides released into the gastrointestinal fluids cross the intestinal barrier. Such data would be useful in determining whether it is appropriate to apply the ICRP ingestion dose coefficients, with their embedded f_1 values, to the activities in the GC – INT leachate.

5.4 Definition of Radioactive Particles

This research has shown there are radioactive particles that can deliver radiation doses of concern for radiological protection that do not meet the current definitions as discussed in section 1.1.1, as well as particles that do meet the definitions but cannot deliver radiation doses of concern for radiological protection. All the radioactive particles in this research met the IAEA definition, but some of them had low skin dose rates or low bioaccessibility and would not be a concern for radiological protection. Some particles met the US DoE definition due to high localised dose rates, but others that did not meet it would have been capable of delivering high committed effective doses through inadvertent ingestion. About half of the particles were < 3,000 µm therefore met the US NCRP definition, but some of the larger particles irradiated a smaller area of skin than their size would suggest due to heterogeneously distributed activity. Lastly, most particles did not meet either the ICRP or the NRC definitions as they had dimensions greater than 1 mm. However, some particles where friable and, if left to persist in the environment, could breakdown into smaller particles that could meet the definition in future. In addition to the further research identified for particle characterisation, dosimetry and bioaccessibility, a useful piece of international collaboration would be to work towards a unified definition for radioactive particles that is focused on hazard, both now and in the future, to improve the radiological protection of the public.

Chapter 6

General Conclusions

6 General Conclusions

The research presented in this thesis characterised and assessed the greatest number of Ra-226 particles of any study and has found that many standard assumptions used in radiological protection may not appropriate for Ra-226 particles. The diversity of Ra-226 particle characteristics and the wide range of potential radiation doses highlights the need for site-specific characterisation and assessment studies. The recommendations from this thesis will provide a valuable input into future studies, helping to improve the radiological protection of the public from radioactive particles.

The characterisation of Ra-226 particles presented here was the first to study a large sample of Ra-226 particles from legacy contamination and has revealed a population that is physically, chemically, and radiologically diverse. A key recommendation from this research is that the diversity of Ra-226 particle characteristics necessitates the analysis of a large sample size and the use of complementary analytical techniques for gathering data for a range of particle characteristics. Special attention should be given to the extent of secular equilibrium achieved in Ra-226 particles as this research has shown that in some cases Rn-222 is likely to be escaping, and in many cases the Pb-210 activities are lower than expected due to self-absorption and heterogeneity of activity distribution within the particles.

The dosimetry of Ra-226 particles presented here was the first to study the impact of both skin thickness and averaging area in the assessment of absorbed dose rate from inadvertent skin contact with Ra-226 particles. It was found that the ICRP reference 70 µm skin thickness and the nominal 1 cm^2 averaging area are not appropriate for preventing all deterministic effects in all ICRP age groups for members of the public. A key recommendation from this research is that the use of the reference 70 µm skin thickness is likely to be appropriate for the prevention of ADU in adults and children due to the depth of the fibroblasts and endothelial cells. However, if the level of conservatism were to be kept the same across different age groups, a thinner skin thickness should be used in the assessment of absorbed dose to the skin of children.

The bioaccessibility of Ra-226 particles presented here was the first to study the bioaccessibility of Ra-226 particles using the UBM and has highlighted important considerations in the application of bioaccessibility methods to radioactive particles and for the assessment of committed effective dose. Ra-226 particle bioaccessibility was found to have a very wide range and was dependent on the gastrointestinal conditions, with lower bioaccessibilities found in the simulated small intestine. A key

recommendation from this research is that bioaccessibility methods applied to radioactive particles must include the conditions of the small intestine, and the bioaccessibility of the small intestine should be used for a physiologically relevant assessment of ingestion dose.

Lastly, the future research areas identified to study particle friability and heterogeneity, acute epidermal necrosis at skin thicknesses < 70 µm, dose thresholds for irradiated areas of skin > 2 mm in diameter, the bioaccessibility of Po-210, and the relationship between bioaccessibility and bioavailability, coupled with a unified definition for radioactive particles focused on hazard, will provide further improvements in the radiological protection of the public from radioactive particles.

7 References

Alnawaf, H., Yu, P. K. N. and Butson, M. (2012) 'Comparison of Epson scanner quality for radiochromic film evaluation', *Journal of Applied Clinical Medical Physics*, 13(5), pp. 314–321. doi: 10.1120/JACMP.V13I5.3957.

Appleton, J. D. *et al.* (2013) 'Lead bioaccessibility in topsoils from lead mineralisation and urban domains, UK', *Environmental Pollution*, 178, pp. 278–287. doi: 10.1016/J.ENVPOL.2013.03.028.

Aragón, A. *et al.* (2008) 'Characterization of radioactive particles from the Palomares accident.', *Journal of Environmental Radioactivity*, 99(7), pp. 1061–7. doi: 10.1016/j.jenvrad.2007.12.014.

Aydarous, A. S., Charles, M. W. and Darley, P. J. (2008) 'Dose distribution measurements and calculations for Dounreay hot particles', *Radiation Protection Dosimetry*, 128(2), pp. 146–158. doi: 10.1093/rpd/ncm328.

British Geological Survey (2020) *BGS 102 Certificate of Analysis*. Available at: https://www.bgs.ac.uk/download/bgs-igf-102-certificate-of-analysis/.

Broadway, A. *et al.* (2010) 'Determination of the bioaccessibility of chromium in Glasgow soil and the implications for human health risk assessment', *Science of The Total Environment*, 409(2), pp. 267–277. doi: 10.1016/J.SCITOTENV.2010.09.007.

Brown, J. and Etherington, G. (2011) *Health Risks from Radioactive Objects on Beaches in the Vicinity of the Sellafield Site*.

Brown, J. and Oatway, W. (2012) *Scoping Health Risk Assessment for Beach Users at Dalgety Bay to Support Advice to Scottish Government Given in February 2012*, *Health Protection Agency*. Health Protection Agency.

Cave, M. *et al.* (2015) 'Measuring the solid-phase fractionation of lead in urban and rural soils using a combination of geochemical survey data and chemical extractions', *Environmental Geochemistry and Health 2015 37:4*, 37(4), pp. 779–790. doi: 10.1007/S10653-015-9697-9.

Charles, M. W. and Gow, C. (2010) *Skin dose from Dalgety Bay Ra-226 contamination : Dose rate measurements for ten selected samples*, *University of Birmingham*.

Clacher, A. (2010) *Analysis of Beach Monitoring Finds - Second Tranche: Report to Sellafield Limited*, *Serco*.

Clacher, A. (2011) *Analysis of Beach Monitoring Finds – Third Tranche: Report to Sellafield Limited*, *Serco*.

COMARE (2014) *Committee on Medical Aspects of Radiation in the Environment: Fifteenth Report*.

Conway, M. *et al.* (2009) 'In-vitro analysis of the dissolution kinetics and systemic availability of plutonium ingested in the form of "hot" particles from the Semipalatinsk NTS.', *Applied Radiation and Isotopes*, 67(5), pp. 884–8. doi: 10.1016/j.apradiso.2009.01.051.

Cowper, M. (2009) *Analysis of Beach Monitoring Finds – Final Report Issue 1: Report to Sellafield Ltd*, *Serco*.

Dale, P. (2013) *Dalgety Bay Radioactive Contaminated Land Risk Assessment*, *Scottish Environment Protection Agency*.

Dale, P., Robertson, I. and Toner, M. (2008) 'Radioactive particles in dose assessments.', *Journal of Environmental Radioactivity*, 99(10), pp. 1589–95. doi: 10.1016/j.jenvrad.2008.06.005.

Danesi, P. R. *et al.* (2003) 'Depleted uranium particles in selected Kosovo samples', *Journal of Environmental Radioactivity*, 64(2–3), pp. 143–154. doi: 10.1016/S0265-931X(02)00045-0.

Denys, S. *et al.* (2012) 'In vivo validation of the unified BARGE method to assess the bioaccessibility of arsenic, antimony, cadmium, and lead in soils', *Environmental Science and Technology*, 46(11), pp. 6252–6260. doi: 10.1021/ES3006942/SUPPL_FILE/ES3006942_SI_001.PDF.

Devic, S., Tomic, N. and Lewis, D. (2016) 'Reference radiochromic film dosimetry: Review of technical aspects.', *Physica Medica*, 32(4), pp. 541–56. doi: 10.1016/j.ejmp.2016.02.008.

DPAG (2006) *Dounreay Particles Advisory Group Third Report*, *DPAG*.

Eakins, J. S., Hager, L. G. and Tanner, R. J. (2016) 'Calibration of thermoluminescence and film dosemeters for skin doses from high-activity microparticles', *Radiation*

Protection Dosimetry, 170(1–4), pp. 173–176. doi: 10.1093/rpd/ncv437.

Eriksson, M. *et al.* (2005) 'Source term identification of environmental radioactive Pu/U particles by their characterization with non-destructive spectrochemical analytical techniques', *Spectrochimica Acta Part B: Atomic Spectroscopy*, 60(4), pp. 455–469. doi: 10.1016/j.sab.2005.02.023.

Etcheverry, P., Grusak, M. A. and Fleige, L. E. (2012) 'Application of in vitro bioaccessibility and bioavailability methods for calcium, carotenoids, folate, iron, magnesium, polyphenols, zinc, and vitamins B(6), B(12), D, and E', *Frontiers in Physiology*, 3, p. 317. doi: 10.3389/fphys.2012.00317.

EU (2013) 'Council Directive 2013/59/Euratom of 5 December 2013 laying down basic safety standards for protection against the dangers arising from exposure to ionising radiation'.

Futagami, F. *et al.* (2020) 'Isolation, characterization and source analysis of radiocaesium micro-particles in soil sample collected from vicinity of Fukushima Dai-ichi nuclear power plant', *Journal of Environmental Radioactivity*, 223–224, p. 106388. doi: 10.1016/J.JENVRAD.2020.106388.

Handley-Sidhu, S. *et al.* (2010) 'A review of the environmental corrosion, fate and bioavailability of munitions grade depleted uranium', *Science of the Total Environment*, pp. 5690–5700. doi: 10.1016/j.scitotenv.2010.08.028.

Harrison, J. D. *et al.* (2005) *Health Implications of Dounreay Fuel Fragments : Estimates of Doses and Risks*, *Health Protection Agency*.

Hopewell, J. W. (2000) 'Biological Effects of Radioactive Hot Particles on the Skin', *Radiation Protection Dosimetry*, 92(1–3), pp. 145–149. Available at: http://rpd.oxfordjournals.org/content/92/1-3/145.abstract.

IAEA (2011) *Radioactive particles in the Environment: Sources, Particle Characterization and Analytical Techniques*, *International Atomic Energy Agency*.

IAEA (2014) *Radiation Protection and Safety of Radiation Sources: International Basic Safety Standards*.

ICRP (1979) 'Limits for Intakes of Radionuclides by Workers. ICRP Publication 30 (Part 1)', *Annals of the ICRP*.

ICRP (1981) ‘Limits of Intakes of Radionuclides by Workers. ICRP Publication 30 (Part 2)’, *Annals of the ICRP*.

ICRP (1983) ‘Radionuclide Transformations - Energy and Intensity of Emissions. ICRP Publication 38’, *Annals of the ICRP*.

ICRP (1990) ‘Age-Dependent Doses to Members of the Public from Intake of Radionuclides (Part 1). ICRP Publication 56’, *Annals of the ICRP*.

ICRP (1991) *The 1990 Recommendations of the International Commission on Radiological Protection. ICRP Publication 60.*, *Annals of the ICRP*.

ICRP (1992) *The Biological Basis for Dose Limitation in the Skin. ICRP Publication 59*, *Annals of the ICRP*.

ICRP (1993) ‘Age-Dependent Doses to Members of the Public from Intake of Radionuclides (Part 2). ICRP Publication 67’, *Annals of the ICRP*.

ICRP (1995) *Age-dependent Doses to the Members of the Public from Intake of Radionuclides - Part 5 Compilation of Ingestion and Inhalation Coefficients. ICRP Publication 72.*, *Annals of the ICRP*.

ICRP (2002) *Basic Anatomical and Physiological Data for Use in Radiological Protection Reference Values. ICRP Publication 89.*, *Annals of the ICRP*.

ICRP (2007) *The 2007 Recommendations of the International Commission on Radiological Protection. ICRP Publication 103.*, *Annals of the ICRP*.

ICRP (2010) ‘Lung Cancer Risk from Radon and Progeny and Statement on Radon. ICRP Publication 115’, *Annals of the ICRP*. Available at: https://www.icrp.org/publication.asp?id=ICRP Publication 115.

ICRP (2012) ‘Compendium of Dose Coefficients based on ICRP Publication 60. ICRP Publication 119’, *Annals of the ICRP*. Available at: https://www.icrp.org/publication.asp?id=ICRP Publication 119.

ICRP (2017) *Occupational Intakes of Radionuclides: Part 3. ICRP Publication 137*, *Annals of the ICRP*. Available at: https://www.icrp.org/publication.asp?id=ICRP Publication 137.

ISO (2018) ‘Soil quality — Assessment of human exposure from ingestion of soil and

soil material — Procedure for the estimation of the human bioaccessibility/bioavailability of metals in soil (ISO 17924:2018)'.

IXPRC (1928) 'International Recommendations for X-ray and Radium Protection'.

Jernström, J. *et al.* (2006) 'Characterization and source term assessments of radioactive particles from Marshall Islands using non-destructive analytical techniques', *Spectrochimica Acta Part B: Atomic Spectroscopy*, 61(8), pp. 971–979. doi: 10.1016/j.sab.2006.09.002.

Jiménez-Ramos, M. C. *et al.* (2006) 'Presence of plutonium contamination in soils from Palomares (Spain).', *Environmental Pollution*, 142(3), pp. 487–92. doi: 10.1016/j.envpol.2005.10.030.

Juhasz, A. L., Weber, J. and Smith, E. (2011) 'Influence of saliva, gastric and intestinal phases on the prediction of As relative bioavailability using the Unified Bioaccessibility Research Group of Europe Method (UBM)', *Journal of Hazardous Materials*, 197, pp. 161–168. doi: 10.1016/J.JHAZMAT.2011.09.068.

Kashparov, V. *et al.* (2019) 'Environmental behaviour of radioactive particles from chernobyl', *Journal of Environmental Radioactivity*, 208–209, p. 106025. doi: 10.1016/J.JENVRAD.2019.106025.

Kaurin, D G; Baum, J. W. (1997) *Effects of Radioactive Hot Particles on Pig Skin*.

Lind, O. C. *et al.* (2005) 'Characterization of uranium and plutonium containing particles originating from the nuclear weapons accident in Thule, Greenland, 1968.', *Journal of Environmental Radioactivity*, 81(1), pp. 21–32. doi: 10.1016/j.jenvrad.2004.10.013.

Lind, O. C. *et al.* (2007) 'Characterization of U/Pu particles originating from the nuclear weapon accidents at Palomares, Spain, 1966 and Thule, Greenland, 1968.', *Science of the Total Environment*, 376(1–3), pp. 294–305. doi: 10.1016/j.scitotenv.2006.11.050.

Lind, O. C. *et al.* (2009) 'Solid state speciation and potential bioavailability of depleted uranium particles from Kosovo and Kuwait', *Journal of Environmental Radioactivity*, 100(4), pp. 301–307. doi: 10.1016/j.jenvrad.2008.12.018.

Lind, O. C., Tschiersch, J. and Salbu, B. (2020) 'Nanometer-micrometer sized depleted uranium (DU) particles in the environment', *Journal of Environmental Radioactivity*, 211, p. 106077. doi: 10.1016/j.jenvrad.2019.106077.

Lukashenko, S. *et al.* (2020) ‘Radioactive particles released from different sources in the Semipalatinsk Test Site’, *Journal of Environmental Radioactivity*, 216, p. 106160. doi: 10.1016/j.jenvrad.2020.106160.

McGuire, C. *et al.* (2020) ‘Characterising radium-226 particles from legacy contamination to support radiation dose assessments’, *Journal of Environmental Radioactivity*, 212, p. 106127. doi: 10.1016/J.JENVRAD.2019.106127.

NCRP (1999) ‘Biological Effects and Exposure Limits for “Hot Particles” - NCRP Report No.130’, *National Council on Radiationi Protection and Measurements*.

von Neubeck, C. *et al.* (2015) ‘The effect of low dose ionizing radiation on homeostasis and functional integrity in an organotypic human skin model.’, *Mutation Research*, 775, pp. 10–18. doi: 10.1016/j.mrfmmm.2015.03.003.

Oomen, A. G. *et al.* (2003) ‘Development of an in vitro digestion model for estimating the bioaccessibility of soil contaminants’, *Archives of Environmental Contamination and Toxicology*, 44(3), pp. 281–287. doi: 10.1007/s00244-002-1278-0.

Patton, N. (2013) *Dalgety Bay Appropriate Person Report*, *Scottish Environment Protection Agency*.

Peel, D. M. *et al.* (1984) ‘Nonstochastic Effects of Different Energy β Emitters on Pig Skin’, *Radiation Research*, 99(2), pp. 372–382.

Prăvălie, R. (2014) ‘Nuclear Weapons Tests and Environmental Consequences: A Global Perspective’, *Ambio*, 43(6), pp. 729–744. doi: 10.1007/s13280-014-0491-1.

R Core Team (2022) ‘R: A language and environment for statistical computing’, *R Foundation for Statistical Computing*. Vienna, Austria. Available at: https://www.r-project.org/.

RIFE-27 (2022) *Radioactivity in Food and the Environment Report*. Available at: https://www.sepa.org.uk/media/594536/rife-27.pdf.

Sajih, M. *et al.* (2010) ‘Physicochemical characterisation of depleted uranium (DU) particles at a UK firing test range’, *Science of the Total Environment*, 408(23), pp. 5990–5996. doi: 10.1016/j.scitotenv.2010.07.075.

Salbu, B. *et al.* (2003) ‘Oxidation states of uranium in DU particles from Kosovo’, *Journal of Environmental Radioactivity*, 64(2–3), pp. 167–173. doi: 10.1016/S0265-

931X(02)00047-4.

Salbu, B. *et al.* (2005) ‘Oxidation states of uranium in depleted uranium particles from Kuwait’, *Journal of Environmental Radioactivity*, 78(2), pp. 125–135. doi: 10.1016/j.jenvrad.2004.04.001.

Salbu, B. *et al.* (2018) ‘Challenges associated with the behaviour of radioactive particles in the environment’, *Journal of Environmental Radioactivity*, 186, pp. 101–115. doi: 10.1016/J.JENVRAD.2017.09.001.

Schindelin, J. *et al.* (2012) ‘Fiji: An open-source platform for biological-image analysis’, *Nature Methods*. Nature Publishing Group, pp. 676–682. doi: 10.1038/nmeth.2019.

Scottish Government (2010) ‘The Radioactive Contaminated Land (Scotland) Regulations 2007 Statutory Guidance’.

Stewart, A; Cook, GT; MacKenzie, A. (2003) ‘Simulation of Human Stomach and Intesting Leaching of Dounreay Hot Particles’. Available at: https://www.sepa.org.uk/regulations/radioactive-substances/guidance-and-reports/.

Török, S. *et al.* (2004) ‘Characterization and speciation of depleted uranium in individual soil particles using microanalytical methods’, *Spectrochimica Acta - Part B Atomic Spectroscopy*, 59(5), pp. 689–699. doi: 10.1016/j.sab.2004.02.003.

Tyler, A. N. *et al.* (2013) ‘The radium legacy: Contaminated land and the committed effective dose from the ingestion of radium contaminated materials.’, *Environment International*, 59, pp. 449–55. doi: 10.1016/j.envint.2013.06.016.

US DoE (2011) ‘Radiation Protection Programs Guide for use with Title 10, Code of Federal Regulations, Part 835, Occupational Radiation Protection’, *United States Department of Energy*.

US NRC (1990) ‘Information Notice No. 90-48: Enforcement Policy for Hot Particle Exposures’, *United States Nuclear Regulator Commission*.

Wilson, C. A. *et al.* (2013) ‘Characterising the morphological properties and surface composition of radium contaminated particles: a means of interpreting origin and deposition.’, *Environmental science. Processes & impacts*, 15(10), pp. 1921–9. doi: 10.1039/c3em00141e.

Wragg, J. *et al.* (2011) ‘An inter-laboratory trial of the unified BARGE bioaccessibility

method for arsenic, cadmium and lead in soil', *Science of the Total Environment*, 409(19), pp. 4016–4030. doi: 10.1016/j.scitotenv.2011.05.019.

Zanoni, T. B. *et al.* (2014) 'Basic Red 51, a permitted semi-permanent hair dye, is cytotoxic to human skin cells: Studies in monolayer and 3D skin model using human keratinocytes (HaCaT).', *Toxicology Letters*, 227(2), pp. 139–49. doi: 10.1016/j.toxlet.2014.03.007.

8 Appendix A

Table 8.1 Reagents used in the preparation of the simulated gastrointestinal fluids (ISO, 2018)

Component	Reagents	CAS No.	Units	Saliva (S)	Gastric (G)	Duodenal (D)	Bile (B)
Inorganic	Potassium chloride	7447-40-7	mg	448	412	282	188
	Sodium phosphate	13472-35-0	mg	444	133	0	0
	Potassium thiocyanate	333-20-0	mg	100	0	0	0
	Sodium sulphate	7757-82-6	mg	285	0	0	0
	Sodium chloride	7647-14-5	mg	149	1376	3506	2630
	Calcium chloride dihydrate	10035-04-8	mg	0	200	0	0
	Ammonium chloride	12125-02-9	mg	0	153	0	0
	Sodium hydrogen carbonate	144-55-8	mg	0	0	2803.5	2893
	Potassium dihydrogen phosphate	7778-77-0	mg	0	0	40	0
	Magnesium chloride hexahydrate	7791-18-6	mg	0	0	25	0
	Sodium hydroxide (1M)	1310-73-2	ml	0.9	0	0	0
	Hydrochloric acid (37%)	7647-01-0	ml	0	4.15	0.09	0.09
	Deionised Water	N/A	ml	250	250	250	250
Organic	Urea	57-13-6	mg	100	42.5	50	125
	D + Glucose	50-99-7	mg	0	325	0	0
	D - Glucuronic acid	6556-12-3	mg	0	10	0	0
	D - Glucosamine hydrochloride	66-84-2	mg	0	165	0	0
	Deionised Water	N/A	ml	250	250	250	250
Enzymes	Alpha amylase (Bacillus)	9000-90-2	mg	72.5	0	0	0
	Mucin (Porcine)	84082-64-4	mg	25	1500	0	0
	Uric acid	69-93-2	mg	7.5	0	0	0
	Bovine serum albumin	9048-46-8	mg	0	500	500	900
	Pepsin (Porcine)	9001-75-6	mg	0	500	0	0

Component	Reagents	CAS No.	Units	Saliva (S)	Gastric (G)	Duodenal (D)	Bile (B)
	Calcium chloride dihydrate	10035-04-8	mg	0	0	100	111
	Pancreatin (Porcine)	8049-47-6	mg	0	0	1500	0
	Lipase (Porcine)	9001-62-1	mg	0	0	250	0
	Bile (Bovine)	8008-63-7	mg	0	0	0	3000
Total volume			ml	500	500	500	500
pH			N/A	6.5 ± 0.5	1.1 ± 0.1	7.4 ± 0.2	8.0 ± 0.2

9 Appendix B

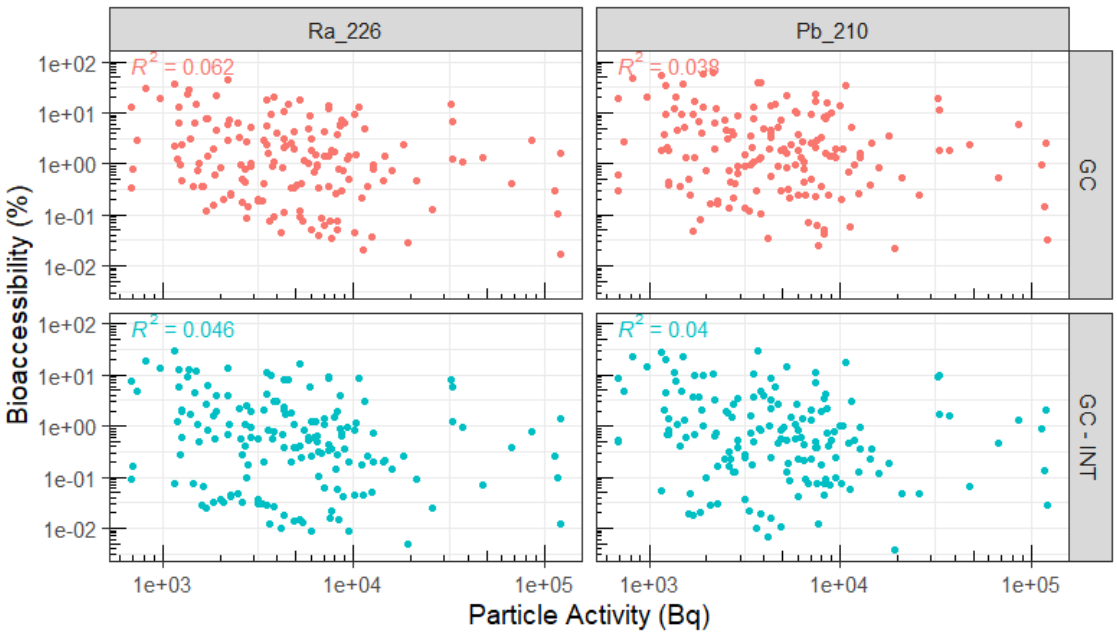

Figure 9.1 No relationship between bioaccessibility (%) and particle activity (Bq)

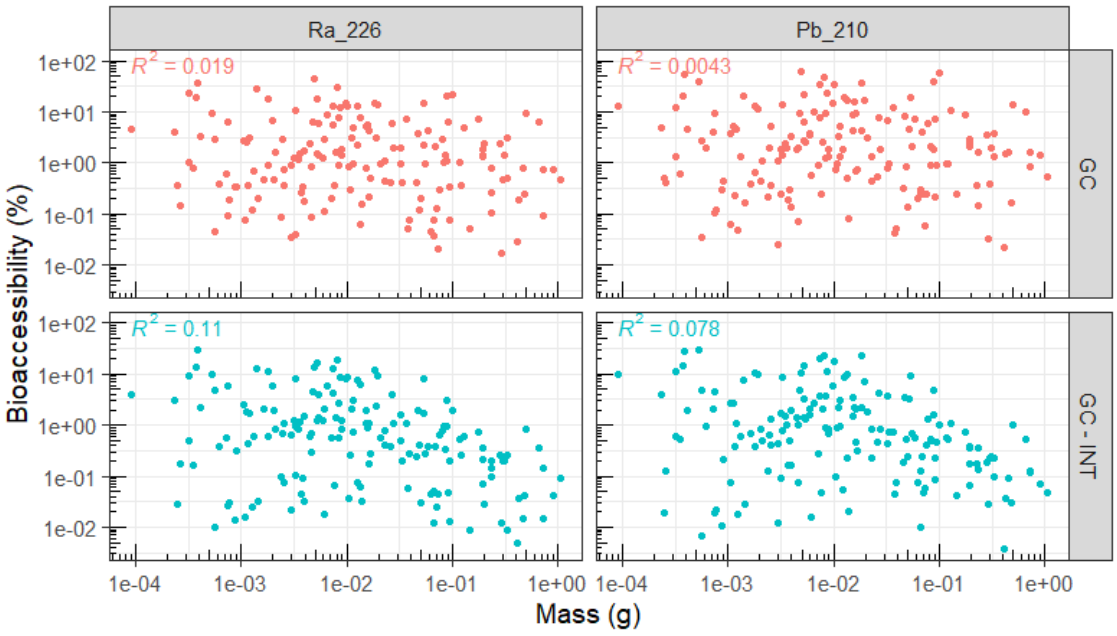

Figure 9.2 No relationship between bioaccessibility (%) and particle mass (g)

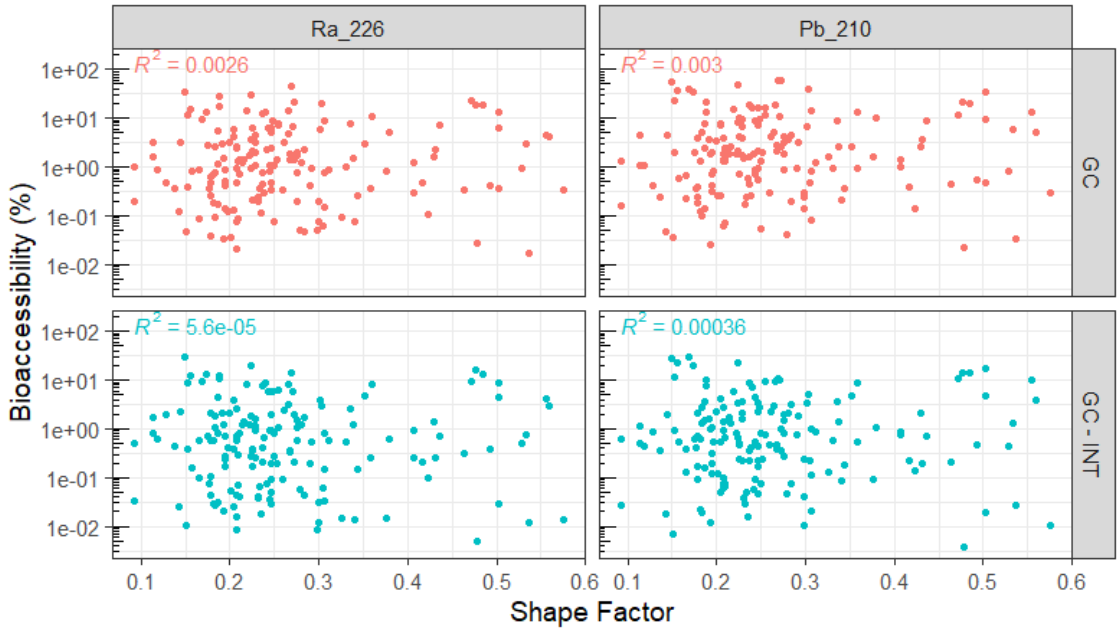

Figure 9.3 No relationship between bioaccessibility (%) and shape factor

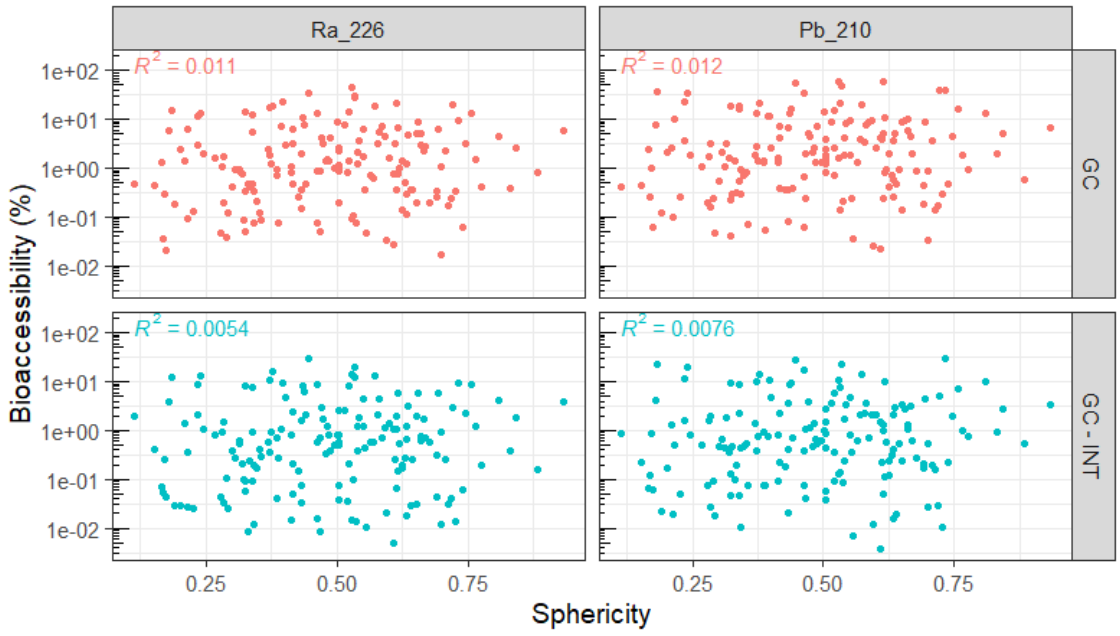

Figure 9.4 No relationship between bioaccessibility (%) and sphericity

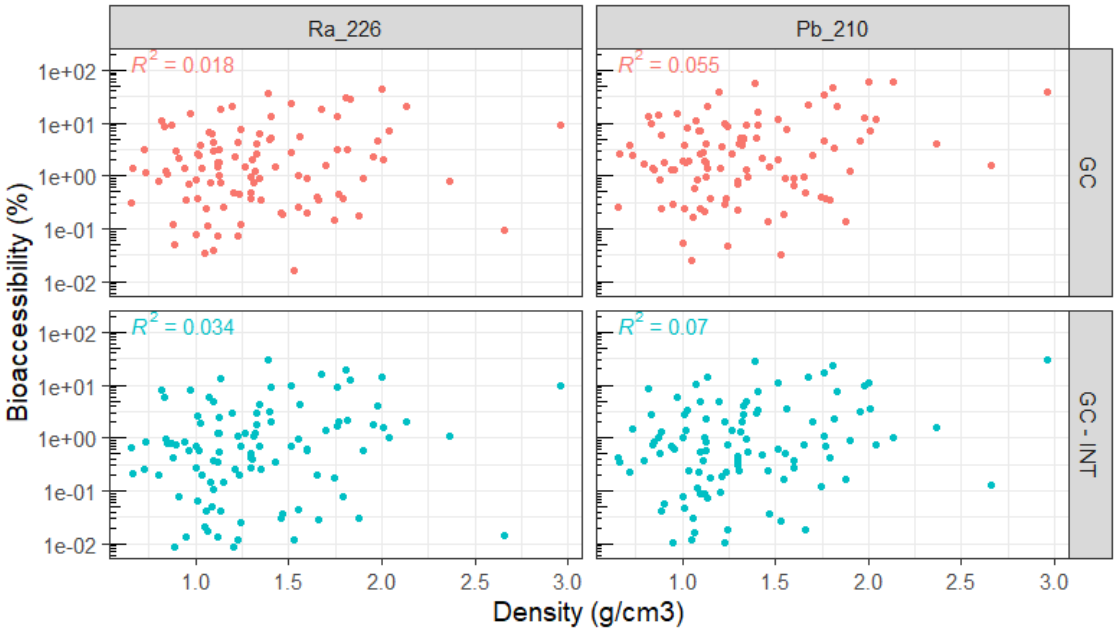

Figure 9.5 No relationship between bioaccessibility (%) and particle density (g/cm^3)

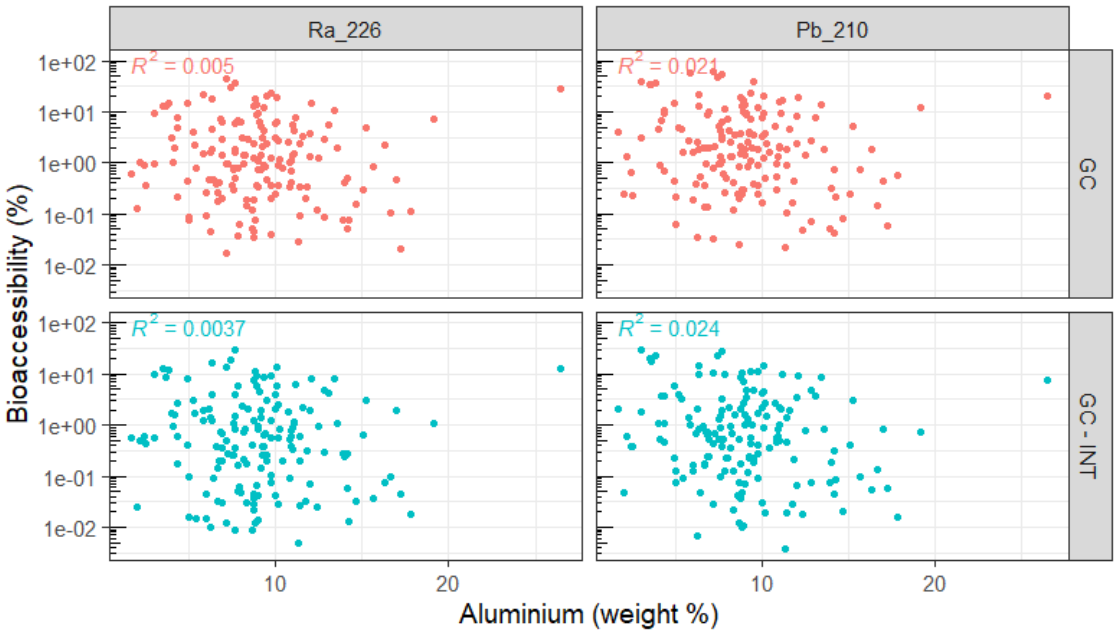

Figure 9.6 No relationship between bioaccessibility (%) and aluminium (weight %)

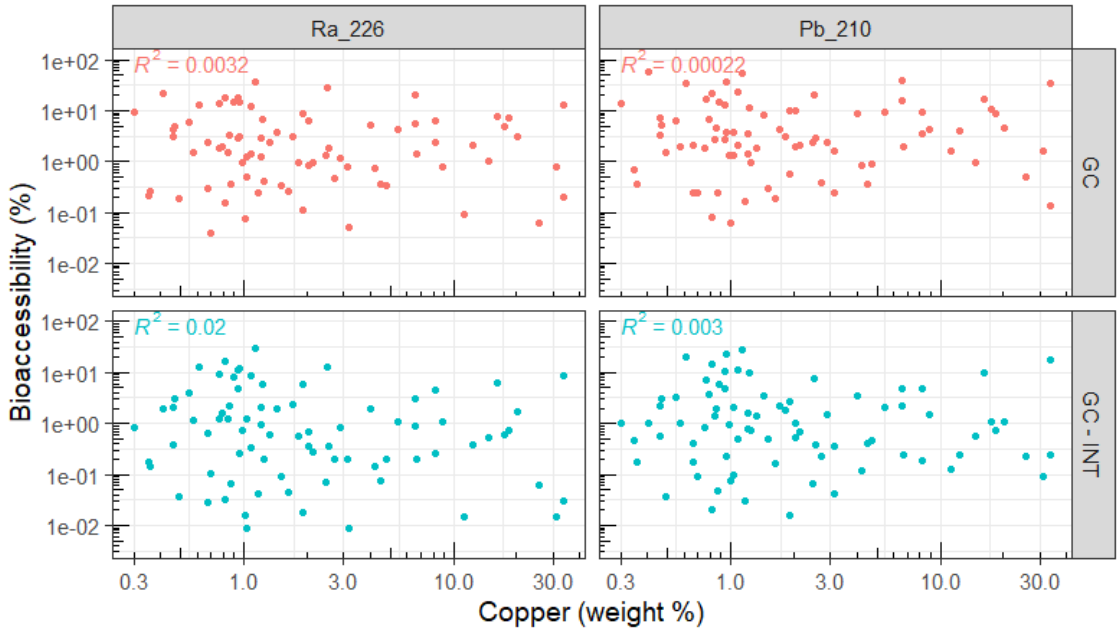

Figure 9.7 No relationship between bioaccessibility (%) and copper (weight %)

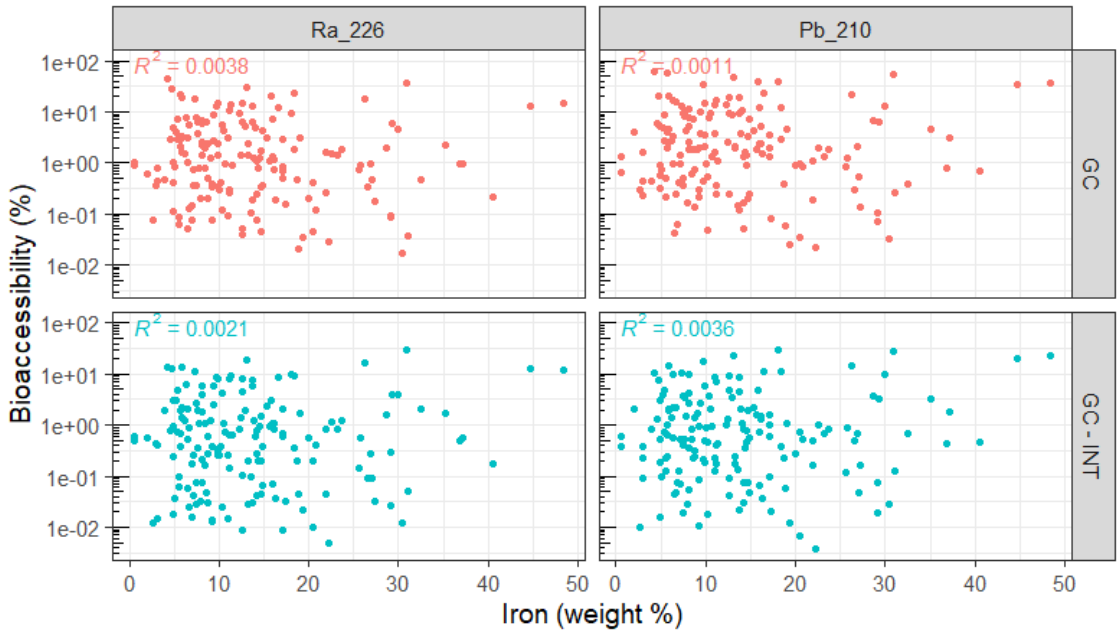

Figure 9.8 No relationship between bioaccessibility (%) and iron (weight %)

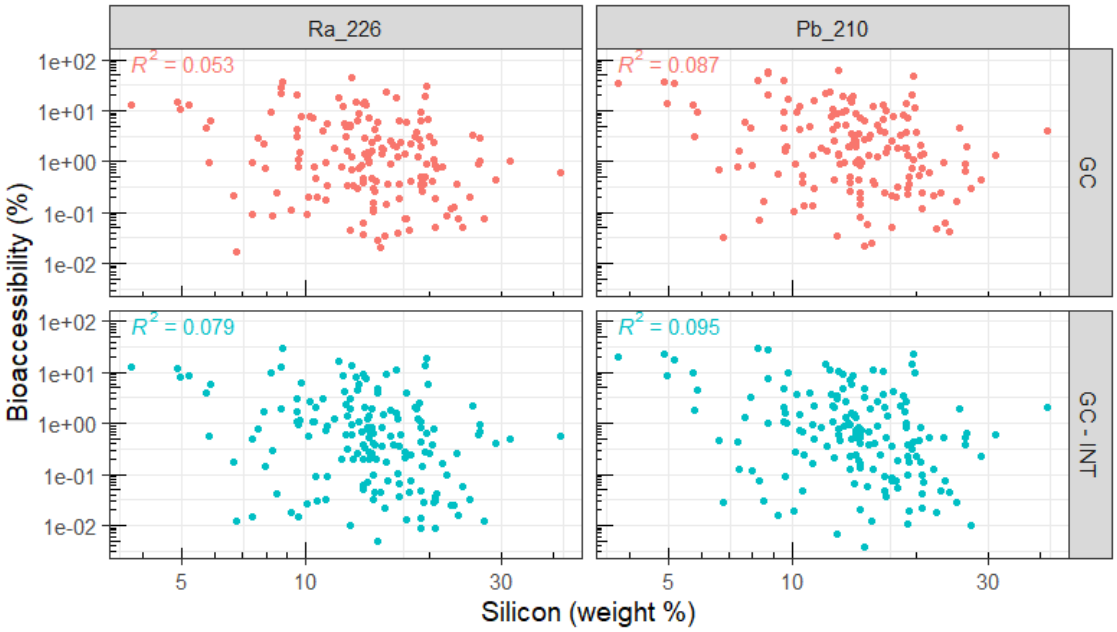

Figure 9.9 No relationship between bioaccessibility (%) and silicon (weight %)

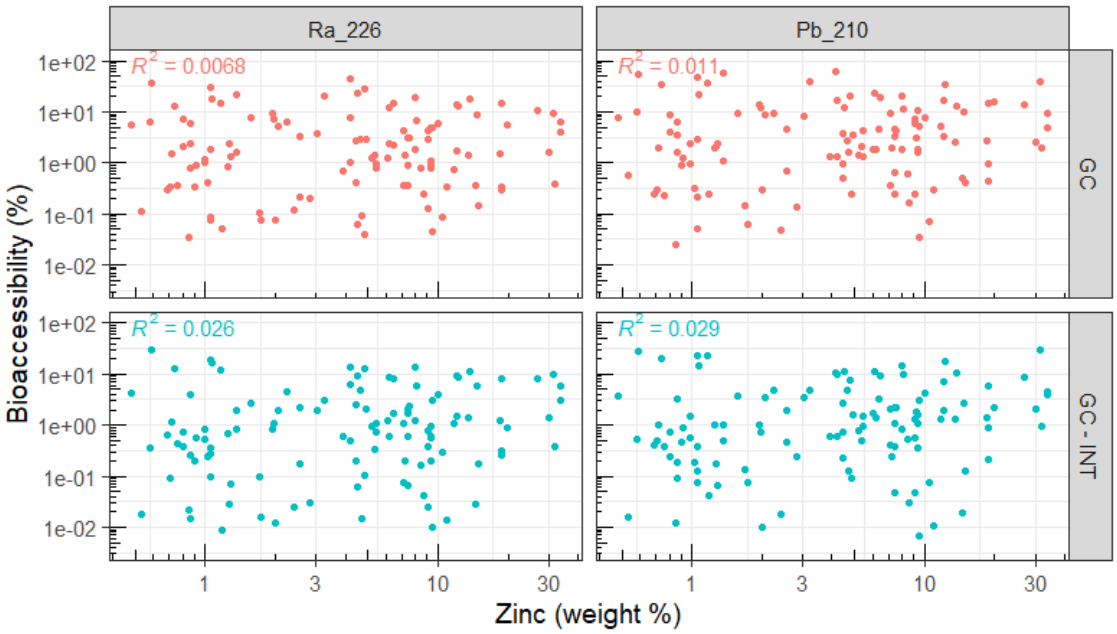

Figure 9.10 No relationship between bioaccessibility (%) and zinc (weight %)